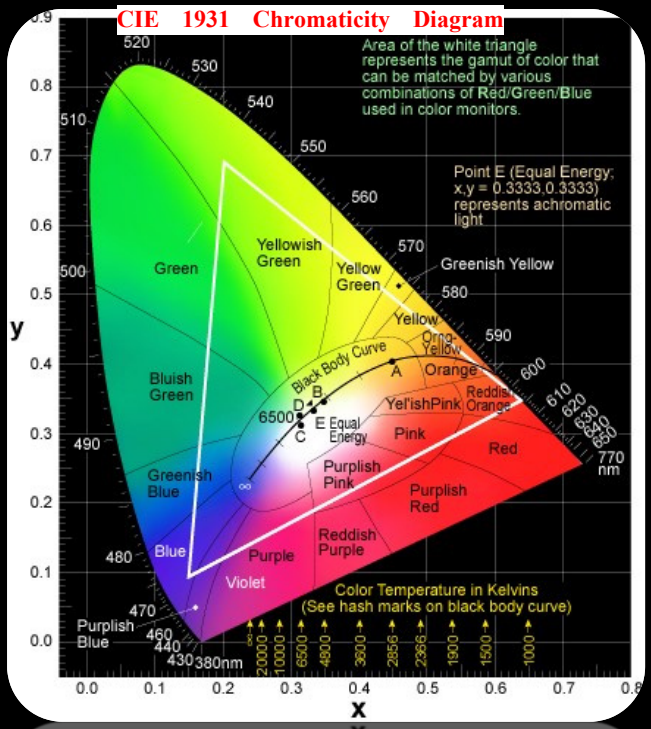

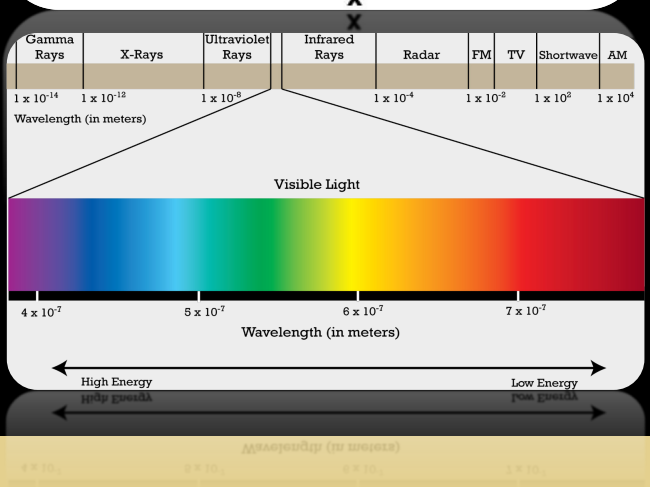

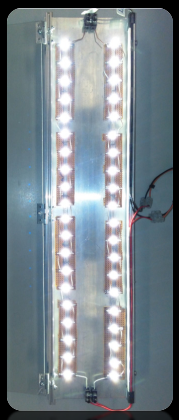

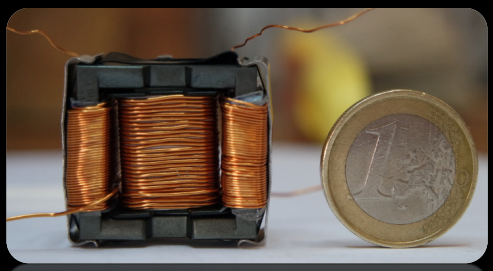

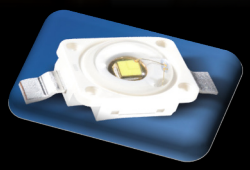

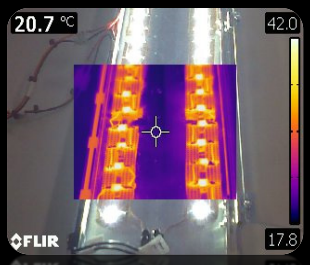

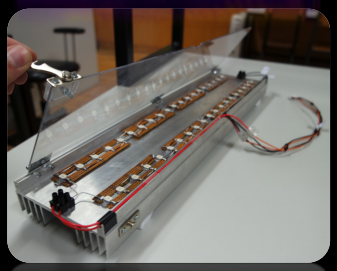

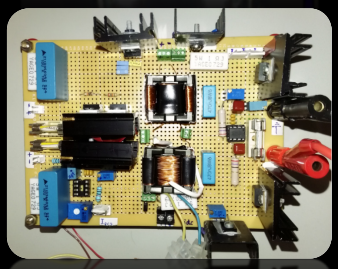

Marco André Cunha Martins

LED Lamp Driver Based on a Resonant Switched Capacitor Converter with a Variable Resonant Tank

Master of Science Degree Thesis

Electrical and Computer Engineering

Specialization in Energy

March 2015

• U C •

FCTUC FACULDADE DE CIÊNCIAS
E TECNOLOGIA
UNIVERSIDADE DE COIMBRA

Departamento de Engenharia Eletrotécnica e de Computadores

Mestrado Integrado em Engenharia Eletrotécnica e de Computadores

Dissertação de Mestrado – Área de Especialização em Energia

Controlo de lâmpadas LED baseado num conversor de condensadores comutados com circuito ressonante variável

Autor:

Marco André Cunha Martins

Júri:

Professora Doutora Maria do Carmo Raposo de Medeiros (Presidente)

Professor Doutor Tony Richard de Oliveira de Almeida (Vogal)

Professor Doutor André Manuel dos Santos Mendes (Orientador)

Professora Doutora Marina Mendes Sargento Domingues Perdigão (Coorientadora)

Coimbra, Março de 2015

To my wife, and family,
for their strong support and encouragement.

Acknowledgements

Foremost, I would like to express my deepest gratitude to my two supervisors, Prof. André Mendes and Prof. Marina Perdigão. Their patience, guidance, wise and invaluable advice, and help were key motivations throughout this work. I wish to thank Prof. Marina for her positive thinking and for making everything seem simple. I am also indebted to Prof. André who persuasively conveyed an interest in my work, and shared with me is immense knowledge and the value of discipline in pursuing objectives.

I wish to thank my colleagues from the Department of Electrical and Computers Engineering, University of Coimbra. Particularly those who worked with me in Laboratório de Eletrónica de Potência. I am grateful to them for their help, support and valuable hints.

I also would like to thank my fellows from the Department of Electrical and Computers Engineering, University of Coimbra, for their truly support, collaboration and encouragement.

In addition, I would like to express a special gratitude to my wife, sister and my parents for their patience and support, but especially to my wife, for her strength and belief.

Finally, I would like to thank my closest friends, for their support, encouragement and good times.

The financial support from the Instituto de Telecomunicações is also gratefully acknowledged.

Resumo

As fontes de luz artificial desempenham um papel indispensável no quotidiano de qualquer ser humano na sociedade moderna. No entanto tem-se verificado uma tendência crescente pela procura de sistemas de iluminação mais flexíveis, versáteis e facilmente controláveis. Para além disso, a procura mundial de energia elétrica, está a aumentar a um ritmo elevadíssimo, devido não só ao aumento da população, mas também à necessidade de um maior nível de conforto que resulta, por exemplo, na existência de habitações cada vez maiores, novos serviços como a internet ou equipamentos móveis que proporcionam lazer, etc.

Desta forma, as medidas que visam promover a eficiência energética desempenham um papel vital, por permitir mitigar as alterações climáticas, e por garantir a sustentabilidade dos recursos de energia, já que na maioria dos casos estão associadas a um vasto leque de fatores como a redução significativa de custos monetário, redução das emissões de CO_2 associadas, e aumento da segurança e fiabilidade dos próprios sistemas de energia elétrica. Outro fator preponderante, que abre a porta para novos tipos de iluminação, mais eficientes e com uma vida útil muito superior como a iluminação LED, é o processo gradual que visa banir do mercado as lâmpadas incandescentes, e que entrou em vigor um pouco por todo mundo, e particularmente em 2009 na União Europeia. De igual forma, relativamente a lâmpada de halogéneo, está previsto o mesmo processo, a partir de 2020.

Durante a última década tem-se assistido ao aumento com um ritmo surpreendente do desempenho dos LEDs, nomeadamente no que toca à fiabilidade, eficiência, eficácia luminosa e qualidade de luz. No entanto, visto que é uma tecnologia relativamente recente, torna-se imprescindível continuar a apostar e investir na sua pesquisa e desenvolvimento para as lâmpadas LED tirem o máximo proveito possível do aumento da desempenho e eficácia luminosa que os LEDs apresentam hoje em dia.

Em suma, a necessidade da regulação de fluxo luminoso, aliada com a necessidade de sistemas de iluminação mais eficientes e flexíveis com os benefícios da tecnologia de iluminação LED, requer, inevitavelmente, um driver adequado e fiável, com alto desempenho e de baixo custo. Desta forma, o trabalho desenvolvido nesta dissertação incidiu no estudo e desenvolvimento de um novo driver de baixo custo para alimentar lâmpadas LED, e a implementação de uma nova técnica de regulação de fluxo luminoso – dimming que vise aumentar a poupança energética.

A estrutura desta dissertação é brevemente apresentada a seguir: no capítulo 1 são explicados os objetivos principais deste trabalho bem como a sua motivação. Em seguida é dado uma pequena introdução sobre iluminação moderna. O capítulo 2 inicia-se com uma breve introdução à iluminação LED é posteriormente é apresentada uma breve descrição dos mecanismos mais utilizados para gerar luz branca com LEDs. De seguida, são introduzidos alguns dos protocolos de comunicação mais vulgarmente utilizados em iluminação. Para finalizar este capítulo, é feita a introdução de drivers para LEDs, onde são apresentados os métodos de regulação de fluxo luminoso e métodos para equalização de corrente em lâmpadas LED multiarray. Na parte final deste capítulo são ainda apresentados algumas técnicas de modelação de LEDs. No capítulo 3 é introduzido o conceito de indutância variável e o seu princípio de operação. No capítulo 4 é apresentado o conversor ressonante de condensadores e sua operação é analisada. No capítulo 5, é analisado o modelo de simulação desenvolvido para simular tanto o conversor como a indutância variável e alguns dos resultados obtidos com a simulação. Finalmente, no capítulo 6, são introduzidas as principais diretrizes e os resultados obtidos com a implementação prática. O trabalho descrito neste capítulo visa validar toda a análise teórica e de simulação.

Palavras-chave: *iluminação, eficiência energética, lâmpadas LED, eficácia luminosa, driver de LEDs, dimming.*

Abstract

Artificial light sources play an indispensable role in daily life of any human being in actual and modern society. However, current trends vacillate for more efficient, flexible, versatile and controllable lighting systems. Moreover, world's energy demand is rapidly increasing, not only due to the increase of population, but also to a higher degree of basic comfort and level of amenities: larger homes, new services and new appliances and equipment, etc.

Thereby, energy-efficiency measures play a vital role in achieving a sustainable energy future and socio-economic development while mitigating climate changes, ever since, in most of cases, they are highly cost-effective, feature CO_2 emission reduction, and offer a worthy opportunity to increase security and reliability of energy supplies. Furthermore, the worldwide gradual phase-out of incandescent lamps (incandescent lamp ban policy), which started in the EU in 2009, and the future halogen lamp ban foreseen to 2020, opens the door for high-efficiency and long-life light sources such as LED lamps.

For the last decade, LED efficacy, reliability and light quality have been constantly increasing with an amazing pace. However, because it is a very recent technology it is mandatory to increase research efforts and investment so that the efficacy of LED lamps takes advantage of the increase in luminous efficacy that LEDs feature nowadays.

In summary, the highly needed dimming features, allied with the necessity for more efficient and flexible lighting systems, and with the benefits of LED lighting technology, leads to the inevitable requirement of a proper, high performance and cost-effective LED lamp driving/control system. Therefore, the work developed on this dissertation is focused on the research of a new and cost-effective LED lamp driver, and a new dimming technique which could potentially increase energy savings.

The structure of the dissertation is briefly presented below:

In **Section** Erro! A origem da referência não foi encontrada., the motivation and main goals for this work are listed and briefly explained. Afterwards, a brief introduction to this work is given. In **Section 2**, firstly LED lighting is briefly introduced, and then Light-Emitting Diodes (LEDs) are presented with a brief description of the mechanisms available to generate white light. Then, the most commonly employed communication protocols are introduced. And finally, LED drivers are introduced, where dimming and current sharing methods are covered prior to introducing LED modelling techniques. In **Section 3**, the concept of variable inductor, main operation principle and features are introduced. In **Section 4**, the resonant switched-capacitor converter is introduced and

its operation is analysed. In **Section 5**, the full simulation model of both the converter and the variable inductor as a first step to validate theoretical statements is described. Afterwards, simulation results are shown. In **Section 6**, are introduced the main guidelines and results obtained regarding practical implementation, its retrieved results and their comparison with simulation results to validate the effectiveness and the efficiency of variable inductor control, and the resonant switched-capacitor converter topology.

Keywords: *Lighting, energy-efficiency, LED lamps, luminous efficacy, LED driver, dimming.*

Index

List of Figures

List of Tables

List of Acronyms

AC	*Alternating-Current*
AM	*Amplitude Modulation*
ANSI	*American National Standards Institute*
ASCII	*American Standard Code for Information Exchange*
CAD	*Computer-Aided Design*
CAN	*Controller Area Network*
CCT	*Correlated Colour Temperature*
CIE	*International Commission on Illumination*
CO_2	*Carbon Dioxide*
CRI	*Colour Rendering Index*
CT	*Colour Temperature*
DALI	*Digital Addressable Lighting Interface*
DC	*Direct Current*
EFD	*Type of magnetic core structure*
emf	*Electromotive Force*
EMI	*Electromagnetic Interferences*
ESL	*Equivalent Series Inductance*
ESR	*Equivalent Series Resistance*
ETSI	*European Telecommunications Standards Institute*
EU	*European Union*
GaAsP	*Gallium arsenide phosphide*
GaP	*Gallium Phosphide*
HB-LED	*High-Brightness Light Emitting Diode*
HVAC	*Heating, Ventilation, and Air Conditioning*
IC	*Integrated Circuit*
IEC	*International Electrotechnical Commission*
InGaAlP	*Indium Gallium Aluminium Phosphorus*
InGaN	*Indium gallium nitride*
IR	*Infrared*
KNX	*Worldwide standard for Home and Building Control*
L70	*70% Lumen Maintenance*
LED	*Light Emitting Diode*

LIN	*Local Interconnect Network*
LtL	*Light-to-Light System*
LVDC	*Low Voltage Direct Current*
LVI	*Linear Variable Inductor/Inductance*
MIDI	*Musical Instrument Digital Interface*
mmf	*Magnetomotive force*
MPPT	*Maximum power point tracking*
OLED	*Organic Light Emitting Diode*
PDA	*Personal Digital Assistants*
PEL	*Permanent Emergency Lamp*
PFC	*Power Factor Correction*
PLC	*Power Line Communication*
P-LED	*Power Light Emitting Diode*
PRS-LED	*Photon Recycling Semiconductor – Light Emitting Diode*
PSIM	*Power Electronics Simulation Software*
PV	*Photovoltaic*
PWL	*Piecewise Linear Modelling*
PWM	*Pulse-Width Modulation*
RDM	*Remote Device Management*
RGB	*Additive colour model based on red, green and blue light mixture*
RSCC	*Resonant Switched-Capacitor Converter*
SCC	*Switched-Capacitor Converter*
SELV	*Safety Extra Low Voltage*
SI	*International System of Units*
SMPS	*Switched-Mode Power Supplies*
SMPTE	*Society of Motion Picture and Television Engineers*
TCP/IP	*Transmission Control Protocol and Internet Protocol*
UPS	*Uninterruptible Power Supply*
USA	*United States of America*
USB	*Universal Serial Bus*
VI	*Variable Inductor/Inductance*
VLC	*Visible Light Communication*
XML	*eXtensible Markup Language*
ZCS/ZVS	*Zero-Current-Switching/ Zero-Current-Switching*

List of Symbols

$\boldsymbol{A}$	*Surface area [m^2]*
$\boldsymbol{A_e}$	*Effective magnetic core cross section* $[m^2]$
$\boldsymbol{A_w}$	*Winding occupation area [m^2]*
$\boldsymbol{B}$	*Magnetic flux density [T]*
$\boldsymbol{\vec{B}}$	*Magnetic flux density vector*
$\boldsymbol{B_{max}}$	*Maximum magnetic flux density [T]*
$\boldsymbol{B_n}$	*LED branch/string n*
$\boldsymbol{B_{sat}}$	*Saturation flux density [T]*
$\boldsymbol{C}$	*Capacitor of the integrator circuit [F]*
$\boldsymbol{C_{fi}}$	*IC bootstrap capacitor [F]*
$\boldsymbol{C_i}$	*Constant*
$\boldsymbol{C_o}$	*Converter output capacitor [F]*
$\boldsymbol{C_{o_n}}$	*Output capacitor of the output n [F]*
$\boldsymbol{C_r}$	*Resonant capacitor [F]*
$\boldsymbol{C_{r_n}}$	*Resonant capacitor of the output n [F]*
$\boldsymbol{C_{rt}}$	*IC Oscillator timing capacitor [F]*
$\boldsymbol{D1_n}$	*Diode 1 of the output n*
$\boldsymbol{D2_n}$	*Diode 2 of the output n*
$\boldsymbol{d_{ac}}$	*Diameter of the main winding's wire [m]*
$\boldsymbol{d_{dc}}$	*Diameter of the bias winding's wire [m]*
$\boldsymbol{Dn}$	*Diode n*
$\boldsymbol{dS}$	*Surface element*
$\boldsymbol{\overrightarrow{dS}}$	*Area element or vector with the direction normal to the surface element* dS *[m^2]*
$\boldsymbol{E_v}$	*Illuminance [lux]*
$\boldsymbol{f_r}$	*Resonant frequency [Hz]*
$\boldsymbol{\mathcal{F}}$	*Magnetomotive force [A]*
$\boldsymbol{f_s}$	*Switching/operation frequency [Hz]*
$\boldsymbol{g}$	*Air gap of the variable inductor cores assembly [m]*
$\boldsymbol{H}$	*Magnetic field intensity [A/m]*

$\vec{H}$	*Magnetic field vector*
i	*Current flowing through a winding [A]*
i_{Co}	*Output capacitor current [A] – instantaneous value*
$i_{Co}(t)$	*Output capacitor current [A] – time varying*
I_{dc}	*Variable inductor bias/control winding current [A] – average value*
I_{dc_mac}	*Maximum current in the bias/control winding of the variable inductor [A]*
I_{Dn}	*Diode n current [A]*
I_{DSn}, I_{Mn}	*Mosfet n drain-source current [A]*
I_f	*LED forward current [A] – average value*
I_{F_n}, I_{fn}	*LED forward current corresponding to the threshold voltage n of the LED piecewise linear model [A] – average value*
i_{LEDs}	*LEDs string current [A] – instantaneous value*
I_{LEDs}	*LEDs string current [A]*
I_{LEDs_avg}, I_o	*LEDs string current [A] – average value*
$I_{LEDsn_{avg}}$	*LED string n current [A] – average value*
I_{Lr_pp}, i_{ac_pp}	*Resonant inductor current [A] – peak-to-peak value*
$i_r(t), i(t)$	*Resonant tank/variable inductor current [A] – time varying*
$i_{rn}(t)$	*Resonant tank/variable inductor current during stage n [A] – time varying*
I_r, I_{Lr}	*Resonant tank/variable inductor current [A]*
$I_{r_{avg}}$	*Resonant inductor current during half switching cycle [A]– average value*
$I_{r_{max}}, I_{ac\_max}$	*Maximum Resonant inductor current [A]*
$I_{supply_{max}}$	*IC maximum recommended supply current [A]*
k	*Constant*
$k.B_{sat}$	*Flux density in the external path of the core of the variable inductor, for maximum control current and zero current in the main winding [T]*
K_u	*Core Window utilization/fill factor*
l	*Magnetic path length [m]*
l_e	*Effective magnetic path length of the variable inductor's magnetic core* [m]
L	*Secant inductance [H]*
L_{ac}	*Inductance of the main winding of the variable inductor [H]*
L_{ac_max}	*Maximum inductance of the variable inductor's main winding [H]*
L_{ac_min}	*Minimum inductance of the variable inductor's main winding [H]*
L_{dc}	*Inductance of the bias winding of the variable inductor [H]*

L_f	*Differential Inductance [H]*
L_r	*Inductance of the resonant inductor [H]*
L_{r_n}	*Inductance of the variable inductor n [H]*
M_n	*Mosfet n*
N	*Number of turns of a winding*
N_{ac}	*Number of turns of the main winding of the variable inductor*
N_{dc}	*Number of turns of each bias winding of the variable inductor*
$P_{DC_{losses}}$	*Power handled by thee bias winding of the variable inductor [W]*
$P_{LEDs_{avg}}$	*LED strings power [W] – average value*
$P_{in_{avg}}$	*LED driver input power [W] – average value*
$\mathcal{P}$	*Permeance [Wb.A^{-1}]*
r_{ac}	*Radius of the main winding's wire [m]*
r_{dc}	*Radius of the bias winding's wire [m]*
r_n	*Dynamic resistance n of the LED piecewise linear model [Ω]*
$\mathcal{R}$	*Global reluctance of the magnetic circuit as seen from the VI's main winding [A/Wb]*
$\mathcal{R}_{ext}$	*Reluctance of the external path of the core [A/Wb]*
R	*Resistance of the integrator circuit [Ω]*
R_D	*LED dynamic resistance [Ω]*
R_{DC}	*Variable Inductor DC winding resistance [Ω]*
R_{eq}	*LED static equivalent resistance at a given operating point [Ω]*
R_f	*Equivalent resistance of the LED in its piecewise linear model [Ω]*
R_{Gn}	*Mosfet n gate driving resistor [Ω]*
R_{LEDs}	*LED string static equivalent resistance at a given operating point [Ω]*
R_{Li}	*IC supply current limiting resistor [Ω]*
R_{rt}	*IC Oscillator timing resistor [Ω]*
s^{-1}	*Laplace Integrator*
S	*Wire cross section [m^2]*
$\tan\alpha$	*Tangent at the LED operating point in the I-V curve [1/Ω]*
T_s	*Switching period [s]*
v_C	*Voltage on the capacitor of the integrator circuit [V] – instantaneous value*
v_{C_pp}	*Voltage on the capacitor of the integrator circuit [V] – peak to peak value*
V_{cc}	*Supply voltage pin of the IC which drives the Mosfets*

$v_{Cr}(t)$	*Resonant capacitor voltage [V]- time varying*
$v_{C_{rn}}$	*Resonant capacitor voltage during stage n [V] – instantaneous value*
$v_{C_{rn}}(t)$	*Resonant capacitor voltage during stage n [V] – time varying*
V_{Cr}	*Resonant capacitor voltage [V]*
V_{Cr_avg}, $\overline{V_{C_r}}$	*Resonant capacitor voltage [V] – average value*
V_{Cr_min}	*Minimum resonant capacitor voltage [V]*
V_{Cr_max}	*Maximum resonant capacitor voltage [V]*
$\overline{V_{Cr_{3,4}}}$	*Resonant capacitor voltage during stages 3 and 4 [V] - – average value*
V_{DSn}	*Mosfet n drain-source voltage [V]*
V_f	*LED forward Voltage [V] – average value*
V_{F_n}	*Threshold voltage n of the LED piecewise linear model [V] – average value*
$v_i(t)$	*Inductive voltage [V] – time varying*
V_{in}	*Converter input voltage [V] – average value*
$V_{LEDsn_{avg}}$	*LED string n voltage [V] – average value*
V_{LED}	*LED forward voltage in the linear equivalent model [V]*
V_{LEDs}	*LED string voltage [V]*
V_{LEDs_avg}, $\overline{V_{LEDs}}$	*LED string voltage [V] – average value*
V_{Lr}	*Resonant inductor voltage [V]*
v_{LEDs}	*LED string voltage [V] – instantaneous value*
v_{Ln}	*Resonant inductor voltage for the stage n [V] – instantaneous value*
$v_{Ln}(t)$	*Resonant inductor voltage for the stage n [V] – time varying*
$V_{out_{ideal}}$	*Ideal output voltage of a step-up switched-capacitor converter [V] – average value*
V_γ	*LED threshold voltage in the linear equivalent model [V]*
X_c	*Reactance of the capacitor of the integrator circuit [Ω]*
W_a	*Core window area [m^2]*
Z_c	*Resonant tank characteristic impedance [Ω]*
Z_r	*Resonant tank impedance [Ω]*
δ	*Current density [A/m^2]*
ΔB	*Magnetic flux density swing [T]*
ΔI_f	*LED forward current swing in the linear equivalent model [A]*
ΔV_{Cr}	*Resonant capacitor voltage ripple [V]*
ΔV_{LED}	*LED forward voltage swing in the linear equivalent model [A]*

Δt_n	*Time interval lasting during stage n [s]*
ε	*Error in the linear equivalent model approximation to the real I-V curve*
η	*Efficiency [%]*
μ	*Permeability [H/m]*
μ_0	*Air magnetic permeability ≈ vacuum magnetic permeability [H/m]*
$\mu_{B_{sat}}$	*Permeability of the core of the variable inductor for maximum control current and zero current in the main winding [T]*
μ_r	*Relative permeability [H/m]*
ϕ	*Magnetic flux [Wb]*
ϕ_{ac}	*Magnetic flux produced by the main winding of the variable inductor [Wb]*
$\phi_{ac,pp}$	*Magnetic flux produced by the main winding of the variable inductor [Wb] – peak-to-peak value*
ϕ_{dc}	*Magnetic flux produced by the bias winding of the variable inductor [Wb]*
ϕ_v	*Luminous flux [lm]*
$\Psi(t)$	*Linkage flux [Wb]*
Ψ_{ac}	*Linkage flux produced by the main winding of the variable inductor [Wb]*
$\Psi_{ac,pp}$	*Linkage flux produced by the main winding of the variable inductor [Wb] – peak-to-peak value*
ω	*Switching angular frequency [rad/s]*
ω_o	*Resonant angular frequency [rad/s]*

Glossary

Binning	*Methodical process of segregating LEDs according to a set of standard determined and/or measured parameters* [19]
Blackbody or Planckian Radiator	*"Ideal thermal radiator that absorbs completely all incident radiation, whatever the wavelength, the direction of incidence of the polarization; a blackbody has, for any wavelength and any direction, the maximum spectral concentration of radiance for a thermal radiator in thermal equilibrium at a given temperature"* [9]
CIE Diagram	*Also known as 'CIE colour space', is a diagram that does a 'quantitative' link between physical colours in the electromagnetic visible spectrum and physiological colours perceived by the human eye* [20]. *Generally this diagram is divided into x, y coordinates.*
Colour Rendering Index (CRI)	*Also known as Colour Rendition Index, is a measure of the ability of a light source to show object colours realistically or naturally compared to a reference source, typically sunlight or incandescent lamp light, or by another words, the ability to reproduce colours of an object faithful as seen under an ideal white-light source (or Blackbody) such as sun light. The CRI values are typically comprised between 0 and 100 [9] and the higher the value, the better the degree of the colour's reproduction of any object. The CRI is predominantly used in lighting industry and may be found in most of commercial lamps packaging, thus, in terms of light quality evaluation it can be used as follows [10]:* ➢ *Poor, CRI < 60* ➢ *Good, 60 < CRI < 80* ➢ *Very Good, 80 < CRI <90* ➢ *Excellent, 90 < CRI < 100*
Colour Temperature	*Parameter which is defined as the temperature of a Blackbody that emits radiation of the same chromaticity of the light source within the visible spectrum. Or by another words, any light source whose chromaticity coordinates fall directly on the Blackbody curve (or Planckian locus) has a colour temperature equal to the Blackbody temperature with those coordinates. Colour Temperature is usually expressed in Kelvin [K] and it*

	is a notion which is typically used to characterize incandescent lamps or the sun for the reason that they possess characteristics to consider them a Blackbody, namely their quasi-Blackbody spectrum throughout the visible spectrum region [16].
Correlated Colour Temperature	*Temperature of the Blackbody source which is the closest to the chromaticity of the light source in the colour space, usually expressed in Kelvin [K]. It is a concept used to characterize light sources which do not have chromaticity coordinates that fall exactly on the Planckian locus but do lie near it* [2], *such as fluorescent lamps, LED lamps, along with others (all lamp types with exception of incandescent). It is also an essential metric used in general lighting industry to specify the perceived colour of such light sources and, of course, according to European and US norms it is a parameter which is obligatorily present in every certified manufacturer's lamp packaging. For instance, according to the norm DIN 5035, this metric classify light sources into three different types* [10]*:* ➢ *Warm white*, $T_c < 3300$ K ➢ *Neutral or natural white*, $3300\ K < T_c < 5000$ K ➢ *Cool white*, $T_c > 5000$ K 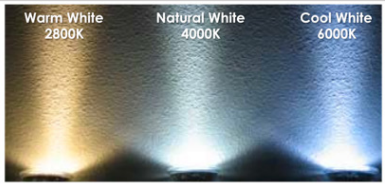
Dichromatic Source	*Optical device which generates light with two particular wavelengths*
Dimming	*Regulation of the Luminous Flux level*
Illuminance	*Total luminous flux incident on a surface per unit area. In SI derived units illuminance is expressed in [lux] (lx) which is equivalent to lumens per square meter* (lm/m^2) [11]*; Recommended illuminance levels are tabled according to the visual needs, for a specific task and/or place, in European norms such as EN 12464 (2002), DIN 5035 (1990) and ISO 8995 (2002).*
LCR Meter	*Equipment used to measure inductance, capacitance and resistance*
Life Span	*Period of time elapsed corresponding to the lumen maintenance concept: "period of time until a light source does not satisfy the operation requirements, typically a 70% lumen maintenance of its rated lumen output" for LED lamps – L70* [2].
Light-to-light system	*System whose aim is to directly convert sun light into artificial light*

Lumen	"*Luminous Flux emitted in unit solid angle (steradian) by a uniform point source having a Luminous Intensity of 1 cd"* or equivalently *"luminous flux of a beam of monochromatic radiation whose frequency is* $540*10^{12}$ *Hz and whose radiant flux is 1/683 W"* [12]
Lumen Maintenance	*Luminous flux output remaining at any selected elapsed operating time, generally expressed as percentage of the initial luminous flux output* [17]. *This metric is simply used to compare the amount of light produced from a light source or luminaire when it is brand new to the amount of light output at a specific time in the future* [18]. *Generally, in LED light industry, tests to determine lumen maintenance are realized under the standard ISE LM-80-2008* [17] *and the most common lumen maintenance factor employed is the L70, which stands for a 70% luminous flux output remaining after a determined operating time.*
Luminous Efficacy	*"Quotient of the luminous flux emitted by the power consumed by the source"* [9], *expressed in [lm/W]. This parameter, and given its importance, is a measure of the efficiency which a light source provides visible light from electric power or, by another words, the ability of a light source to produce a visual sensation in the human eye* [13].
Luminous Flux	*"Quantity derived from Radiant Flux by evaluating the radiation according to its action upon the CIE 084-1989 standard photometric observer"* [14], *expressed in lumen [lm]. Or, by another words, it is the measure of the useful/perceived power emitted by a light source per second* [10] *and it is correlated to the differing sensitivity of the human eye to light with different wavelengths* [15]. *It is typically measured in Lumen [lm], SI unit and it is a parameter given on the packaging of most commercial light lamps.*
Luminous Intensity	*"Quotient of the luminous flux, leaving the source and propagated in the element of solid angle, containing the given direction, by the element of solid angle"* [9], *expressed in candela [cd].*
Pentachromatic Source	*Optical device which generates light with five particular wavelengths*
Piecewise Linear Modelling	*Modelling method which consists on breaking down a complex signal/curve behaviour into several linear segments (or discrete data sets).*
Radiant Flux	*"Power emitted, transmitted or received in the form of radiation [W]"* [9]

Tetrachromatic Source	*Optical device which generates light with four particular wavelengths*
Thermal radiation	*"Emission of electromagnetic radiation due to the thermal motion of electrons caused by the material temperature"*[9]
Trichromatic Source	*Optical device which generates light with three particular wavelengths, i.e. red, green and blue (RGB) light*

1 Motivation and Main Objectives

The work developed during this dissertation resides on the pursuit of three main objectives:

- ✓ The main one: to design a 48 V DC-supplied LED driver based on a magnetic-control technique - the *variable inductor*. With this technique the driver will be capable to perform luminous flux regulation (dimming) on a 44 W LED lamp as shown in Fig. 1.1.

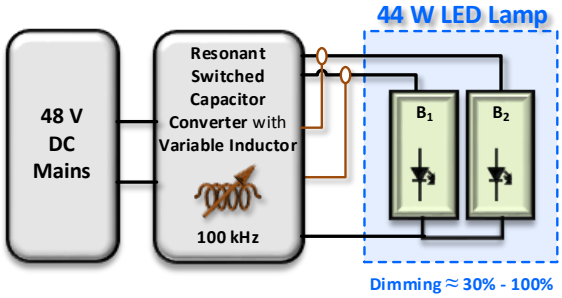

Fig. 1.1 - Proposed DC-Supplied Single Stage Topology

- ✓ The second goal: implement a 100 kHz LED driver based on a resonant switched-capacitor converter, to supply the LED lamp (formed by two strings of 20 LEDs each) and perform dimming in a range of ≈ 30% to 100%, by means of variable inductance control, imposed by the limits of current given by the manufacturer (0.1 A to 0.35 A).

- ✓ Finally, the third goal: to investigate the proposed variable inductor control technique to perform current sharing (also known as current equalization) on a multi-array (strings) based LED lamps.

The main factors that motivated the work efforts to accomplish the previous objectives is the fact that so far, there are not any commercially available LED systems based on resonant-switched capacitor converters neither LED lamps controlled via the variable inductor technique. Moreover, in literature it was not found any proposal of this specific converter topology for LED driving purposes. Therefore, the present converter topology proposed, together with variable inductor control, shall be considered a new and consequently innovative technique. It features high potential for further investigation and development, due, not only to its novelty, but also to its inherent low power losses (might even be negligible when compared to the whole system power handled).

1.1 Introduction

Current trends vacillate for more efficient, flexible, versatile and controllable lighting systems. The world's energy demand is rapidly increasing, thus, taking a look on a few recent lighting statistics is therefore rather interesting and important:

- Lighting in Portugal accounts for 13,6% of the total electric energy consumption in the domestic sector [1]
- In Spain 25% of electric energy is assumed to be consumed by lighting appliances [2]
- In the USA, lighting accounts for 17% of the total electric energy consumed in residential and commercial sector [3]
- Lighting represents around 20% of global electric energy consumption [4-7] and 14% in the EU [4]
- Worldwide, is estimated that lighting accounts for 35% of the whole energy consumption in offices [8]

These stats, allied with an increasing global awareness of environmental protection and energy conservation, has brought the rise of energy-efficient lighting solutions for the past few years, such has smart lamps, smart meters and mobile equipment (i.e. smartphones), and communication protocols, which allow households to be a key part of smart grids, and provide energy savings through the use of indispensable features such as dimming.

LED technology has advanced at a remarkable pace in recent years and it has proven to be a viable alternative to conventional light sources with ongoing improvements in their features. However, most of the residential lighting systems use so far non-efficient incandescent, halogen and fluorescent technologies. In addition, natural sunlight is, frequently, not properly used to complement artificial light, resulting in excessive illumination during daylight hours. Furthermore, lighting systems quite often remain switched on unintentionally, even when nobody is in a particular place, which leads to severe energy inefficiencies. Consequently, lighting systems should be, obligatorily, able to perform dimming of artificial light, for instance based on light sensor information. This is one of the most promising research fields: the development of smart dimming techniques for light usage by means of luminous flux control, to ensure that the illumination levels correspond to the actual needs in any kind of application.

Clearly, with new energy efficiency regulations becoming more demanding and tighter, it becomes mandatory to increase research efforts and investment so that the efficacy of LED lamps takes advantage of the increase in luminous efficacy that LEDs feature nowadays. In fact, the luminous efficacy of LEDs has already broken the 300 lm/W barrier [9] which raises them as the most efficient lighting technology presently. Moreover, the LED itself typically does not fail

catastrophically, i.e. it does not fails to emit light, but slowly decreases its light output over time [10] and it has a high lifespan, up to 100,000 hours [11, 12], higher than any other light source technology. Besides, in comparison to other light sources technology, LED lighting has an extremely high degree of flexibility (both in the vast range of possible application and shape/form), it is environment friendly – non-toxic elements, and can have a really fast start-up, i.e. < 2 ms.

Several commercial dimmable LED drivers have a negative feature, which is the non-constant frequency operation [13]. Thereby, to overcome this issue (but not only), it was investigated and developed, in this dissertation, a resonant switched-capacitor converter to drive LED lamps, using a new control technique, based on a different principle: vary the resonant frequency, instead of varying the operating frequency of the converter. This technique is accomplished by means of a variable inductor, which has the advantage of, not only replacing and fulfilling the role of a typical resonant inductor in resonant switched-capacitor converters, but also of controlling the amount of power flowing to LEDs – dimming.

2 LED Lighting and Drivers

The first human attempts to create an artificial light lamp occurred probably around 70 000 years ago, though the first electric lamp (the carbon arc lamp) was developed only in the 19th century, in 1801 [14, 15]. The most remarkable evolution that led to the beginnings of the lighting industry - took place with the appearance of the incandescent bulb in 1874, which was created by Henry Woodward and Mathew Evans. Later they would sell their USA patent to Thomas Edison, who is considered the 'father' of the electric light bulb [16]. In 1879, he patented a new version of the incandescent bulb which would, posteriorly, be the core of a massive mass production of 16 W light bulb that could last 1500 hours [17]. Subsequently, more and more types of light lamps were developed leading to new and more efficient technologies, which are available nowadays. Such technologies are halogen lamps, discharge lamps, fluorescent lamps, and the recent and promising LED lamps. LED lighting, commonly referred to as Solid-State-Lighting (SSL), is the light source type addressed in this work.

2.1 General Lighting Overview

Light is a particular form of electromagnetic radiation travelling in a specific direction, which is able to excite/stimulate the human visual system [18].

As light is a very general concept, it is usually characterized in terms of its performance and physics phenomena according to the following parameters: *Luminous Flux* *Dimming*, *Luminous Efficacy*, *Illuminance*, *CRI* (*Colour Rendition Index*), *CT* (*Colour Temperature* - used to characterize incandescent light sources), *CCT* (*Correlated Colour Temperature* – which characterizes non-incandescent light sources), *Lumen Maintenance/Life span*[1]. Regarding the mechanisms used to produce visible light, the most common are *incandescence*, which is a particular case of thermal radiation, and *luminescence*.

2.2 LEDs – Light Emitting Diodes

LEDs, compared to most of light source types, are solid-state devices where the light is generated by *luminescence*. Essentially, *luminescence* (in opposition to *incandescence* where light results from heat) is a form of cold body radiation, or more specifically, is the mechanism of electromagnetic radiation emission from a body due to electrons excitation produced by a foreign agent [2]. *Luminescence* can be manifested in several types, but the aim of this word is to bring

[1] *More details regarding some of these **parameters/notions**, which may be recalled during this work, can be found in the glossary*

focus on LEDs which are based on the *electroluminescence* mechanism. Roughly speaking, this mechanism consists on the light emission as a result of an electric field applied to a specific substance. The first known report of electroluminescence dates from 1907 and it is claimed that the first LED was invented in 1920, nevertheless, only in 1968 the first mass-production of LEDs would take place by Monsanto Company and introduced by Hewlett Packard [19]. Since then, LEDs have undergone a series of dramatic increases in performance and capability. Initially, LEDs suffered from poor light-generation efficiency and were available only in yellow–green, orange, and red, which restricted their use only to low light applications such as indicator lamps and alphanumeric displays. Only in 1993 the first white-blue high-brightness LEDs (HB LEDs) based on InGaN that could produce light across the entire visible spectrum would appear. It was invented by the Japanese-American Shuji Nakamura who was awarded the Nobel Prize of Physics in 2014 "*for the invention of efficient blue light-emitting diodes, which has enabled bright and energy-saving white light sources*" [20]. Nowadays, most of LEDs are based on InGaAlP and InGaN compound semiconductors.

2.2.1 LEDs – Brief Operation Principle and Structure

In a simple manner, a LED is a diode which is able to produce light and its electric symbol, as well as its typical I-V curve are shown below:

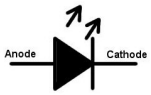

Fig. 2.1 – LED - Light Emitting Diode

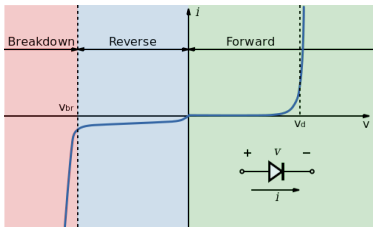

Fig. 2.2 - Typical I-V curve of a diode [21]

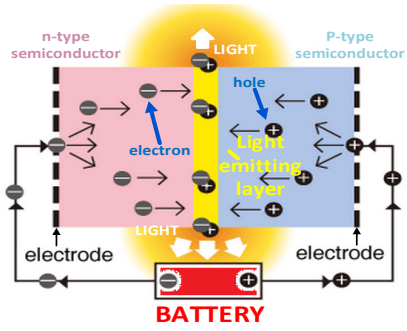

Fig. 2.3 - Light Generation on a LED, adapted from [22]

The 'core' of a LED consists of a chip of semiconductor material doped with impurities to create a p-n junction that allows electric current to flow in only one direction, from the anode to cathode. The electroluminescence featured in LEDs, is basically a radiative recombination of a hole-electron pair through the band gap (in the light emitting layer) of the semiconductor as the p-n junction is excited by the electric current flow (external bias electric field), which results in the release of energy in the form of light - photons [2], as the Fig. 2.3 sketches. In terms of general construction and assembly, most of LEDs feature the same or an approximated complex structure,

which can be observed in Fig. 2.4, where the structure of the HB-LEDs selected to use in this work is presented.

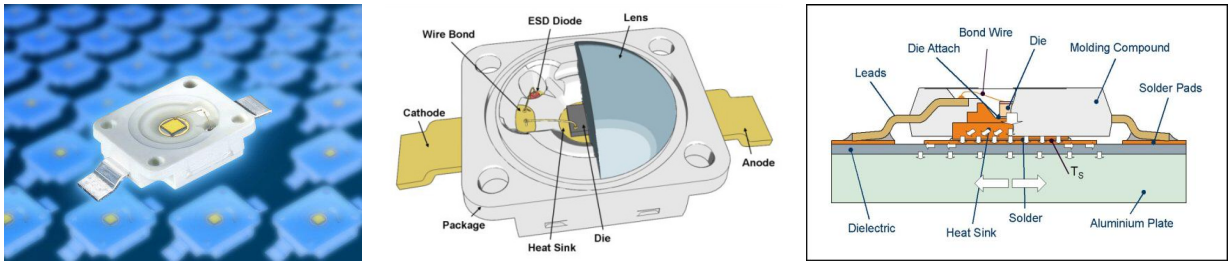

Fig. 2.4 - Golden DRAGON PLUS LCW W5AM [23]

The typical common elements that build-up a single LED are *LED chip or die, thermal materials and heat-sinks, optical elements, mechanical and electrical elements.* Depending on what the LED is made of and how it is configured, the colour of the light produced is different. Truthfully, LEDs available nowadays feature a tremendously high flexibility for numerous applications and thereby they may be categorised based on their nature in: *organic devices* (OLEDs) or *inorganic devices* (non-organic semiconductors). Inorganic LEDs, the most used type, may be classified according to the nominal power or their package as follows [2]:

- *Low and mid-power LEDs* (< 1 W), mostly for non-lighting purposes such as signalling.

- *1 W LEDs* – also known as Power or High Brightness LEDs (P-LEDs or HB-LEDs), mostly used for lighting purposes and the most efficient type so far, up to 303 lm/W [9].

- *High-Power LEDs* (>5W), developed to overcome a well-known issue, namely the relatively high cost per luminous flux due to the large number of single LEDs required in order to fulfil a specific luminous flux, particularly in higher power applications.

- Others: *AC LEDs* (figure of merit by Seoul Semiconductor) which are directly plugged to the AC mains supply [24], and *High Voltage LEDs* that are intended for use in applications in which energy conversion from the mains voltage to a few volts may cause serious efficiency and/or performance limitations [9].

2.2.1.1 White Light - Generation Mechanisms

In this work we are focused only on LEDs used to produce white light and therefore it is important to mention the main mechanisms/techniques used to produce white light. Several approaches to generate white light with LEDs may be employed, but they all feature the same principle which relies on the mixture of different wavelengths to obtain the desired white light

colour [2]. Basically, there are two main strategies to produce white light: *colour mixture* or *wavelength converters* [2, 25, 26].

Colour mixture

Concerning this technique three main approaches may be employed [26]:

- Using *dichromatic sources*, where generally a mixture of two complimentary colours, blue and yellow, is used to result in a perceived white light by the human eye.

- Using *trichromatic* or *RGB sources*, where a mixture of three primary colours is used to create white light

- Using *tetrachromatic* and *pentachromatic sources*, which consist on a mixture of four and five colours respectively and in spite of the fact that their CRI and luminous efficacy are higher than any other type, due to its complexity and cost this solution is barely employed.

Wavelength converters

With regard to this technique, also three main approaches may be employed [26]:

- White LEDs based on *phosphor converters*, where the light emitted with a particular wavelength by the chip is partially absorbed by a phosphor and then re-emitted with a higher wavelength. This is, by far, the most employed technique nowadays, especially in HB-LEDs.

- White LEDs based on *semiconductor converters (PRS-LED[2])*. Analogously to the previous type, a primary excited active region is responsible for emission of light which is posteriorly absorbed by a second excited active area which in turn will re-emit light with a higher wavelength.

- White LEDs based on *dye converters*. In this case LEDs are fabricated using organic dye molecules, instead of phosphors, which can be incorporated in an epoxy encapsulant or in optically transparent polymers. Nonetheless, this technique faces a major drawback, namely the relatively low lifetime of organic dyes, as well as its stability.

[2] ***PRS-LED****: photon-recycling semiconductor LED*

Concerning the future of LED technology, the raise of *Organic LEDs* (OLEDs) performance, utility and flexibility in several applications is spreading worldwide. The term organic is derived from the fact that polymers based on some types of carbon composites are used [27]. This type of LEDs is innovative, not only because of its high simplicity of the manufacturing process, high flexibility, high utility but also due to the fact that its technology is environmentally friendly [27]. Moreover, under laboratory conditions, some impressive numbers about OLEDs, such as luminous efficacy of 120 lm/W, CRI > 90 and useful lifetime of 30 000 h [28] have already been published.

2.2.2 Supplying LEDs from DC Power

DC power distribution buses of -48 V for power telecommunications equipment installations have been in widespread all over the world for many years and have proven to be reliable, safe and cost-effective [29-44]. For such reason this standard voltage level is well defined both by the European Telecommunications Standards Institute (ETSI) and the American National Standards Institute (ANSI) [43].

"*One of the motives behind the universal 48 V DC standard is that it allows work on a live conductor with minimum risk for personal injury and without safety measures. This is a practical advantage when electricians work at a considerable distance from the voltage source and therefore cannot disconnect it*" [43].

In Fig. 2.5 is shown a simple schematic of a traditional telecommunications LVDC power distribution system used widely for many years and still in use nowadays.

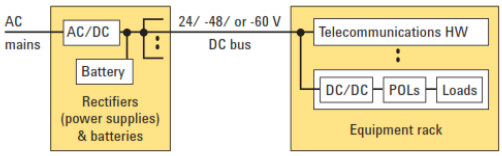

Fig. 2.5 - Typical telecommunications low voltage DC power distribution [29]

Generally AC power from the mains is usually converted by rectifiers into DC power which is generally stored in batteries. These batteries serve as the power source to the DC bus which will further feed all the DC equipment.

In -48 V DC power distribution systems the voltage level is not tightly regulated due to a number of factors, such as the fact that as these buses are nearly always backed up directly with a battery of appropriate voltage, the normal operating voltage limits are determined by the battery's state of charge for normal operation [29]. Thus, the actual voltage range above and below the stated levels is defined by industry standards such as the North American International Electrotechnical Commission (IEC) 60950 and the European Telecommunications Standards Institute (ETSI) 300-132-2 [29], which may be found in Fig. 2.6. In the presence of these variable

voltage limits it is crucial to take them into consideration in order to validate equipment performance under worst case conditions when testing them during design and manufacturing.

DC bus (VDC)	Abnormal low (VDC)	Normal low (VDC)	Nominal (VDC)	Normal high (VDC)	Abnormal high
-48	0 to -40.0	-40.0	-53.0	-57.0	-57.0 to -60.0

Fig. 2.6 - Voltage ranges for conventional DC mains supplying telecommunications equipment [29, 45]

The -48 V bus is generally the most used in existing and new installations because it meets the -60 V DC maximum criteria for Safety Extra Low Voltage (SELV) operation [29]. However, nowadays there are already a few cases with higher voltage level values such as 380 V DC used to feed data centres[3] [33, 36, 41, 46] along with others. Nevertheless, these voltage values are beyond the scope of this work, so they will not be further discussed.

Regarding most of LED lamps, one of the subtle obstacles they have to face, despite of their otherwise compelling benefits, is that driver circuits for these devices must include power conversion capability to transform AC voltage (typically single phase: 230 V AC in Europe and 115 V AC in USA) into low DC voltage. While this process is fairly simple, it adds cost and can dramatically reduce the power conversion efficiency of the whole LEDs driver device. Not only LEDs, but also other digital devices (almost all electronic ballasts, computers, printers, mobile devices, basic building controls, sensors, HVAC systems, security systems, audio-visual systems, etc.) and local energy generation systems (such as photovoltaic, wind power, etc.), face this issue because they are basically "*native DC power users trying to co-exist in an AC environment*". For instance, due to the accumulated conversion losses, only half of the measured (in the energy meter) and paid electric energy is used by a typical device in a building data center [47]. Besides, concerning LED drivers, the major benefits of its direct connection to -48 V DC power would be the increase of safety, flexibility, efficiency and the decrease of the monetary cost. More specifically, by the use of low-voltage system, wiring and device protection could be simplified and much cheaper in order to reduce spark, fire hazards and eliminate shock/startle hazards [47]. It could also make it easier and less expensive to install lighting systems and structures to avoid device re-wiring in possible future renovations [47] etc. Other major benefits would be, not only, the dramatic reduction of design complexity and manufacture cost due to the use of simpler devices with fewer materials and components and without AC-DC conversion systems, but also a facilitation in a possible direct connection to alternative energy sources such as solar or wind local power energy generation systems [47]. This possibility of using DC power from photovoltaic

[3] *"A **data centre** is a facility to house computer systems and associated components such as telecommunications and storage systems"*

systems to feed electricity loads in building, rather than converting it first to AC power and once again to DC power, has recently aroused a high interest in the scientific community, not only because of the sustained and rapid growth in the adoption of rooftop photovoltaic systems happening in the last few years due to the world's concernment about climate changes, but also because of more three important factors, namely the use of batteries as energy storage, the coincidence of higher day-time loads working in commercial buildings when the PV power generation is around its nominal capacity, and inherent internal operation with DC power of most of all electric appliances [48].

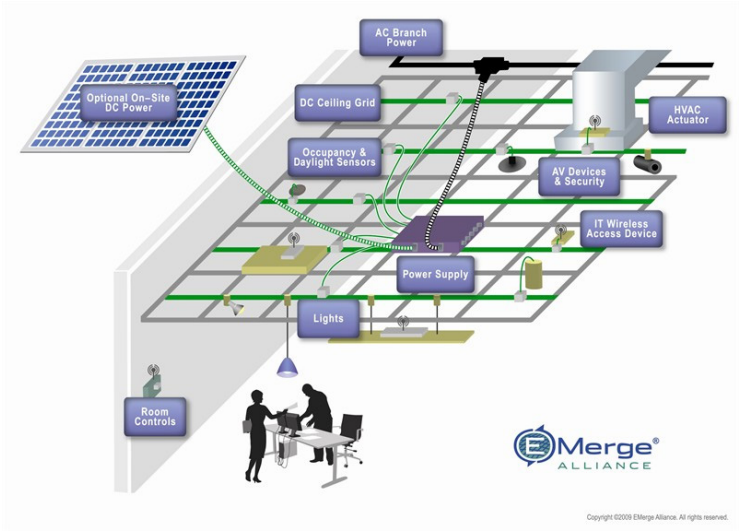

Fig. 2.7 - Example of an industrial application [49]

In order to accelerate the conversion to LED lighting supplied by DC power, an alliance, namely the EMerge Alliance®, was officially launched in November 2008 and currently 24 V DC and 380 V DC standards are being developed [50]. Its main goal is to develop suitable standards leading to the rapid adoption of DC power distribution in commercial buildings, such as the one shown in Fig. 2.7, so that they could have a higher flexibility and sustainability.

To sum up, regarding what has been discussed in this section, the selected input voltage for the driver developed in this work is 48 V DC. In addition, other eventual possibilities than common general lighting, featuring also 48 V DC input power, are to use the proposed driver, for automotive lamps, within the new next generation 48V automotive power systems [51, 52], in light-to-light systems (LtL), which aim is to directly convert the sun irradiation into artificial light [53] or in Permanent Emergency Lamps (PELs) supplied from UPS systems [54-58].

2.3 LED Lighting - Control and Communication Protocols

"Lighting systems control is a key for energy saving in building lighting installations with the additional benefit of increased comfort and safety" [59]. A system, must be properly designed in order to fulfil demands, such as personal control over lighting, that change constantly. However

most of the systems do not possess any lighting control features to go along such changes. To perform such demanded tasks a signal is required, which can be generated manually by an interface such as switches or transmitters, or automatically, through light or movement sensors and/or microprocessors or computer programs, etc [13]. In Fig 2.8 can be observed the general assembly of a lighting control system, together with a few of its features, elements and some of the most common communication protocols used. While in Fig 2.9 is sketched an example of application of DALI and KNX protocols both integrated to complement each other on a lighting system.

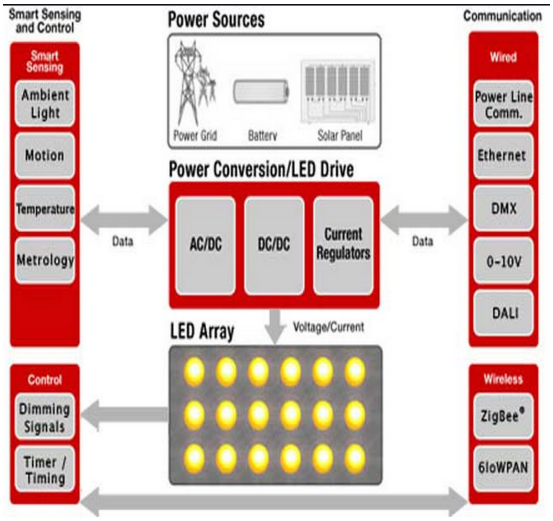

Fig. 2.8 - General LED lighting system - block diagram [60]

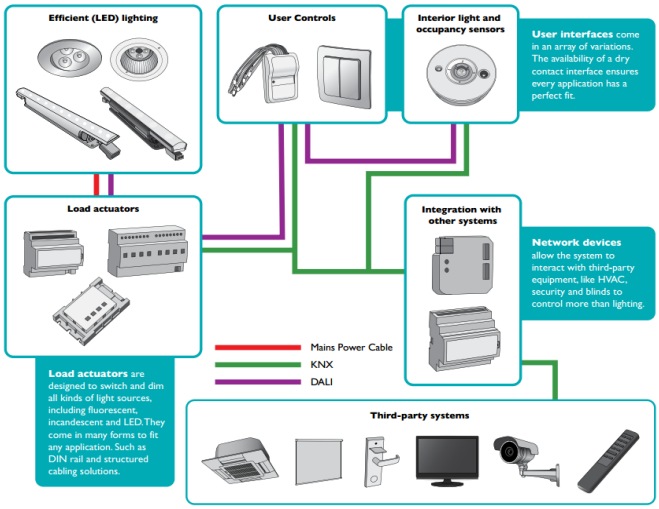

Fig. 2.9 – System with Integration of DALI and KNX protocols [61]

Currently, there are several main lighting control systems, such as the previously referred DALI which allows sixty four ballasts to be controlled/operated simultaneously [61]. In addition to those there are other commonly found communication protocols, wired or wireless such as CAN, ASCII, BACnet, EnOcean, LonWorks, MIDI, Modbus, RDM, SMPTE, TCP/IP, XML, Z-Wave, PLC, LIN, RS232/RS485, USB, etc [62, 63]. Several of these protocols are compatible with 48 V DC mains, like DALI or KNX protocols, i.e. in [64-66]. In addition, numerous commercially available LED drivers are also compatible with the previously referred control protocols as well as with 48 V DC input, i.e. such as those in [67-72].

In brief, lighting control systems should contain all the necessary sensors and intelligence to manage the mains input and LED lamp output functions of the driver, i.e. dimming, lamp start-up and shut down, or other additional features, such as a stop circuit or safety switch-off, output over-voltage or over-current protection, among other protection features.

2.4 LED Lamp Drivers

LEDs are a very peculiar type of light source, very distinct from other light sources, due to their nature. In order to develop a satisfactory LED lamp, several considerations must be taken

into account to overcome the main challenges, namely efficiency and lifetime. One of the main challenges is to surmount the typical difference between LED lifetime and driver lifetime. On the one hand, as previously mentioned, the LED itself can reach more than 100,000 hours [11, 12], while on the other hand, common driver topologies have a limited lifetime due to the use of electrolytic capacitors, which have a high capacitance/(volume*cost) ratio and generally last no longer than 10.000 hours under strict temperature conditions [27, 73]. Hence, a LED driver should be designed in order to obtain a good efficiency while working with low capacitance values, allowing for the use of non-electrolytic capacitors [74]. In addition, through the recent increasing use of smart electronic devices, as well as other state-of-the-art technologies, LED drivers present a high performance with increasing functionalities such as variable input voltage operation range, dimming and emitted colour change capabilities, and auxiliary circuits for protection, along with others. Moreover, a LED driver that comprises such functionalities should be an attractive low-cost solution while accomplishing a high performance.

2.4.1 LEDs – Supplying Issues

The main challenges in the development of LED Lamp drivers are directly related to the photometric, electric and thermal characteristics of LEDs. The most important challenges, which developers have to deal with mandatorily, are briefly described below:

- Concerning *photometric characteristics*, there is a highly linear dependency on the LEDs current and their luminous flux emitted [2].
- Relating to the *electrical characteristics* issue, discussed in section 2.4.5.1, it shows that small variations of the LEDs voltage leads to high LEDs current variations [2].
- Regarding *thermal characteristics*, the major issue is the effects of the variations on the LED's p-n junction temperature. They highly affect the built-in voltage and the effective resistance of the chip. This means that for a given forward voltage, an increase on the junction temperature will lead to an undesired increase of current, which in turn will lead to a temperature increase on the p-n junction. Therefore, it is mandatory to use a current control circuit to avoid this issue, which is identified, for instance, in Fig. 2.10. In this figure are sketched the *I-V* curves of a single LED for three different junction temperatures, and it is, indeed, confirmed the undesired shift on the LED forward current. Because it is a crucial issue, that may result in LEDs or LED driver failure if not taken into account, generally manufacturers of LEDs provide this kind of chart or information in the respective datasheets.

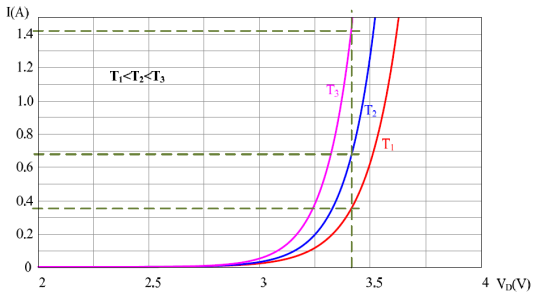

Fig. 2.10 - Effect of the junction temperature on the I-V curve of a LED

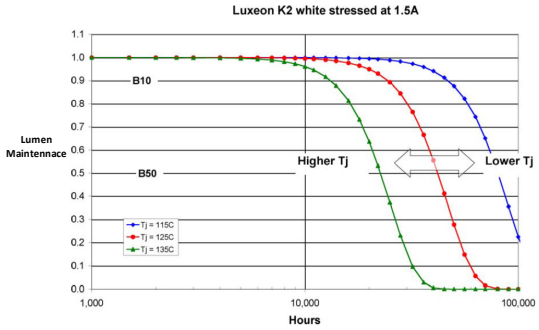

Fig. 2.11 - Lumen maintenance vs junction temperature of a LED [75]

Hence, in order to overcome the three mentioned issues, LED lamps shall be supplied by current sources, or at least they should have a current-limiting feature [2]. In addition, regarding thermal characteristics, a crucial aspect to take into account while designing a LED lamp or LED lighting system, is the development of a proper heat sinking system. Such system is obviously mandatory in order to remove excessive heat and to ensure a longer lifetime of the LED lamp. For instance, Fig. 2.11 presents, briefly, how the LED's junction temperature affects the useful lifetime, which, indeed, confirms that it is desired to operate LEDs at junction temperatures as lower as possible to guarantee a longer useful lifetime.

2.4.2 Commonly Used Topologies

There are numerous possible topologies, depending on the type of power converters used. However they all have something in common: to deal with three major issues which were briefly described in the previous section (2.4.1). Typically, the topology required is determined mostly by the input supply voltage and the LED forward voltage characteristics [27, 76]. Consequently each topology has its advantages and disadvantages and obviously its proper selection is strongly dependent upon the specific application requirements. Generally, if fed by AC power supplies, i.e. the grid, LED driver topologies must feature an EMI filter followed by a rectifier and a PFC stage, in order to comply with related international standards such as (IEC)-61000-3-2, and Energy Star [27], EN 55015, EN 61547, etc. Regarding not only those standards, but also the field of application (AC fed), LEDs can be supplied with three different types of driver architecture, single stage, two-stages or integrated:

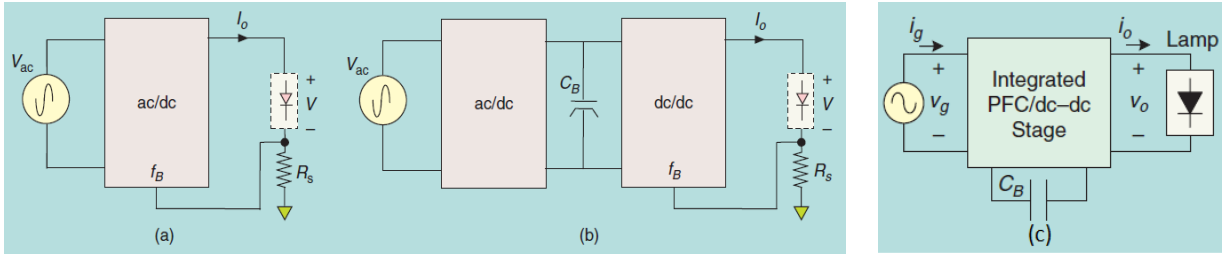

Fig. 2.12 - (a) Single-Stage (b) Two-Stages (c) Integrated Stages, architectures of AC LED drivers [27]

The most commonly employed one is the architecture (b) from the previous figure where the PFC stage (AC/DC) is generally followed by a second stage responsible not only, for supplying the LEDs and controlling their current, but also for fulfilling the role of a current source, ever since, as previously referred, LEDs must be supplied by a current source [77]. Regarding the second stage (DC/DC), the most common topologies commercially available are SMPS [2, 78], which can be found in the following table:

Topology	Vin vs. Vout Relationship	Power Range (max)	Peak Efficiency
Buck	Vin > Vout	1000W	>90%
Boost	Vin < Vout	150W	>90%
Buck/Boost	Vout < Vin < Vout	150W	>80%
SEPIC, Cuk, Zeta	Vout < Vin < Vout	150W	>90%
Flyback	Vout < Vin < Vout	150W	>80%
Resonant	Vout < Vin < Vout	500W	>90%
Push-Pull	Vout < Vin < Vout	1KW	>90%

Table A - Common LED driver topologies [76]

There are also, in the literature, complex and more advanced integrated topologies that feature all the previous requirements in a single, integrated architecture as shown in Fig. 2.12 (c); "*The integration of the power factor correction and LED driver stages results in a robust and cost-effective solution*" [27].

Regarding the topology adopted in this thesis, the resonant switched capacitor converter, during the research for this work, any case where this type of converter is used to supply LED lamps was not found in literature. Although it is possible to find non-resonant switched capacitor converters to supply, only, very low power LEDs in commercial products such as cellular phones, PDAs, indicators, laptop, etc [79]. Thus, the investigation of resonant switched capacitors for LED driving purposes gains an extra motivation.

Operation Frequency

A crucial step in the design of power converters for lighting applications is the proper selection of a suitable operation frequency. On the one hand, a high frequency will guarantee higher levels of luminous output and resonant elements with lower size and weight, while on the other hand it will induce higher switching losses. An initial lower boundary, in order to avoid audible frequencies, could be 20 kHz, however video, audio apparatus, computers, and lighting installations are commonly operated with IR remote controls that use frequencies in the range of 30-40 kHz or even a little lower [13]. That is why, most of commercially available LED drivers are typically operated between 50 kHz - 1 MHz [77]. Higher frequencies, generally are not selected because they would, as previously mentioned, lead to higher switching losses and therefore decrease the overall efficiency of the LED driver [77]. For resonant converters, the most employed

type of control is frequency modulation, for which the switching frequency f_s is varied in order to change the ratio f_s/f_r. In this work, as previously mentioned, the control variable is resonant frequency f_r and therefore f_s is selected to be constant. A constant frequency operation, which overcomes the drawbacks of variable frequency, makes the switching control and the EMI filter design easier, and the resonant circuit can be optimized for a given type of LED lamp. In order to minimize the passive components size and to overcome some of the previously described issues, a 100 kHz switching frequency was selected for this work.

2.4.3 Dimming in LED Lighting Systems

As previously mentioned, the *luminous flux* emitted by a LED (or light output) is directly proportional to its driving current. In many instances, real-time changes in light output and consequently LED drive current are required. This function is commonly referred to as *dimming* or *luminous flux* control and it is a very interesting functionality which allows for energy efficiency and rational use of energy leading not only to energy savings but also to the fulfilment of specific needs in terms of illuminance levels and ambiance intelligence, along with others. Naturally, it is one the most important features in modern lighting systems, then it is obvious that for an intelligent and cost-effective light-management system, a reduction of the power consumption is not synonym of turning off the lights completely. Thus, developing an efficient dimming technology, while guaranteeing an adequate operation and ensuring a visual comfort has been a determinant goal over the last decade for the lighting industry, especially in LED lighting systems. Nowadays, state-of-the-art control systems allow for commissioning and control of LED luminaires (as well as other lighting types) simply with a smartphone or tablet along with autonomous adaptive controls based on occupancy and ambient light sensors.

2.4.3.1 Step Dimming and Continuous Dimming

Typically dimming can be employed in two different manners: *continuous dimming* and *step dimming*:

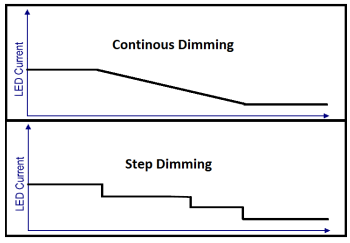

Fig. 2.13 - Continuous vs Step Dimming

Continuous dimming is generally understood as a technology capable of dimming a lamp from 100% of light output down to approximately 1%, without interruptions while step dimming (as the name suggests - by steps) provides a discrete variation of the light output level according to some predetermined levels [80].

Step dimming, in spite of providing specific light control and some energy savings, does not offer the same freedom that continuous dimming offers.

2.4.3.2 Analogic and PWM Dimming

Generally dimming can be accomplished/employed by two main techniques:

- *Analogic* or *Amplitude Modulation* (*AM*) dimming
- *Digital* or *Pulse-Width Modulation* (*PWM*) dimming

Both methods control the time-averaged (DC) current supplied to LED lamp, but in different manners as shown in the following illustration:

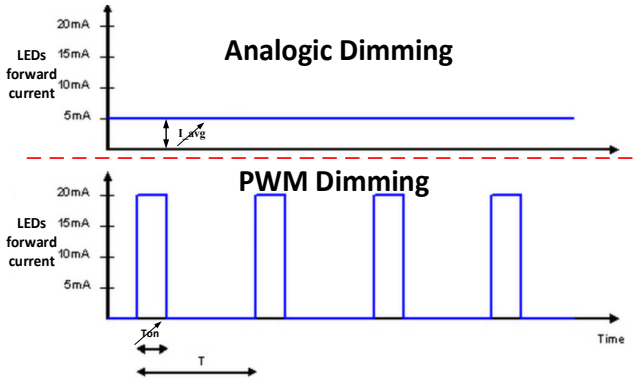

Fig. 2.14 – LED forward current - Analogic vs PWM dimming

Analogic Dimming

This method of luminous flux control is the simplest one since it is based on a simple premise, the fair linearity existing between LED forward current and luminous flux emitted. Thereby the luminous flux is simply varied by adjusting the DC current level supplied to the LED.

PWM Dimming

Regarding PWM dimming, this is by far the most complex method. It relies on a different principle: the LED is turned ON and OFF, as the previous figure shows, by means of supplied current square wave with a constant peak value. In this manner, by adjusting the duty-cycle, the average current value is controlled. Basically, with this type of dimming the LED is rapidly switched on and off so that the light flickers. The minimum recommended frequency is 1 kHz [81], because at such high frequency, under no circumstances the human eye can perceive the

individual light pulses, thus avoiding any possibility of the flicker effect. The main advantages and disadvantages of both previous dimming techniques are summarized as follows:

PARAMETER	ANALOG DIMMING	PWM DIMMING
Ease of Design	Easier if controller fitted with analog dim pin.	Requires processer or timers to create PWM input signal.
Relative Cost	Usually cheaper to derive analog input signal.	More expensive to implement PWM input signal.
Shift in Color Temperature	Dimming produces visible color shift.	Relatively constant color over all dim levels.
Dimming range	Fairly limited in most designs.	Can achieve very high contrast ratios.
Flexibility	Changes to dim range hardware adjustable	Changes to dim range possibly software adjustable
Efficacy	Better than PWM at lower dim levels	Lower efficacy at high peak currents
Interaction Issues	No low frequency envelopes of current pulses	PWM presents a low-frequency current draw to the system. This may couple into other circuitry.
EMC	Usual issues with switching supplies	LED shunt FET could exhibit hard edges that can be radiated or conducted.

Table B - Advantages and disadvantages of Analogic and PWM Dimming

Analogic dimming, compared to PWM dimming, requires least control overhead, it is generally more efficient particularly for low dimming levels due to the droop effect [2] and, most importantly, it is deprived of EMI emissions [2]. This technique however, applied to LEDs faces a major disadvantage, namely the shift in the chromatic coordinates and in the CRI due to these parameters dependence in the drive current [2, 81]. Therefore, this technique shall not be applied to drivers of LED lamps under circumstances where the chromatic coordinates and CRI have extremely strict requirements. Nevertheless, for most of cases it is a cost effective and top performance solution, and for that it was selected to use in this work.

2.4.3.3 Dimming Techniques and Schemes

Regarding LED lamps, except for very-low-power dimming levels, its voltage does not change significantly. Thereby, the lamp power, and consequently the luminous flux level, can simply be varied by controlling the lamp current due to their highly linear relation. Up to now, the proposed dimming techniques use different control parameters which have an immediate effect on the lamp current. These techniques are widespread and typically the most common are:

- *Simple variable resistors, semiconductors or integrated circuits in series with the LEDs*, also known and series or shunt regulator, which are the most simple and cost-effective solutions, but also the most inefficient [2, 82].
- *Regulation of the DC bus voltage*, which is capable of providing a smooth and broad range of dimming control, however it requires an additional power stage which is capable of supplying the DC stage with a variable DC voltage [13].

- *The employment of switching converters: PWM - control via switching frequency (f_s), duty-cycle* [82] or *phase-shift control* [83-85]. This type of control, in spite of being quite complex and sometimes even very intricate to analyse, is probably the mostly employed technique due to its robustness and reliability. Usually the switching frequency is the control variable, which generally leads to higher levels of current harmonics that result in high EMI. This inherent drawback requires the inclusion of an extra stage, namely a PFC stage in order to comply with related standards, to ensure safety and reliability, etc.

To overcome most of the previous issues, in the present work, as previously mentioned, it is proposed a different dimming technique from those explained above, namely the employment of the *variable inductor*, a non-dissipative component [82]. This technique, whether specifically used for dimming purposes or for other ends, is based on a simple premise, already stated before: controlling the circuit through the variation of the resonant frequency, instead of varying the converter operating frequency and it is described in section 3. It is very important to state, once again, that there are not yet any commercially available lighting products using this type of control which motivates the work developed on this thesis. As stated earlier, the variable inductor concept is not new, but until the last few years the concept has drawn little attention. Thus, applying this concept to perform dimming of LED lamps is considered to be a new, innovative and promising technique. Furthermore, during the whole period of research for this work, only in one literature article ([82]), a LED driver using a variable inductor for the purpose of dimming, was found. In that publication, the variable inductor is applied to a converter which resembles a forward converter, not only for the purpose of LED lamp dimming but also for current equalization in parallel LED strings. Other prototypes using similar magnetic regulators, namely magnetic amplifiers, in LED drivers, were also found in literature, namely in [86] and [87], however the main purpose of the regulator in these papers is to overcome some issues found in traditional multi-output converters [88], namely to achieve power factor correction without requiring an additional stage, and not to specifically perform dimming.

2.4.4 LED strings/branches - Current Sharing Methods

Most of times, the luminous flux output emitted by a single LED is not enough to meet design criteria or certain standards, and therefore they are usually used in a large number [82, 89]. Ideally, the best option would be to connect them all in series (a string) so that the current flowing through them would be the same and only a single current control circuit would be required. However, the total voltage of the LED string would be the sum of each LED voltage, which would result in a high voltage that may be difficult to supply from low voltage sources and may

compromise electrical safety [82, 90]. Thereby, generally the parallel connection of several LED strings is employed. This approach allows the strings to be operated at lower voltages while the number of LEDs is increased [82, 89]. Conversely, an issue associated with paralleled LED strings is the difficulty to achieve current equalization for every string [12, 82]. This is due to the fact that LEDs characteristics can be different even for LEDs from the same type and lot/batch resulting in slightly different forward voltage drops which can cause considerably different currents in each branch/string which in turn will directly affect the luminous flux emitted by LEDs [2, 82, 89]. Even provided that LED manufactures apply the concept of *binning*[4], the former is not enough to guarantee that LEDs have exactly the same characteristics. Hence, lighting engineers have to overcome these issues, especially in the development of high performance LED lamps, and typically the most common methods to perform LED strings current sharing may divided into two categories, *passive methods* and *active methods* [5, 89]:

Passive Methods

Passive current sharing methods use passive components, such as capacitors and inductors, which are inserted in the AC side of the LED driver and then the AC signal is rectified to power the LED load [5, 72, 89] or in the DC side within more advanced driver topologies limited to two LED branches as in [92]. There are also many applications using resistors in series with LEDs and despite of being the simplest solution it is considered the least efficient due to the high losses [12, 82]. These methods may be simple and cost effective, but regarding applications where high performance and efficiency are required one should look for active methods.

Active Methods

Regarding active methods, generally active devices are employed to arrange a current regulator connected in series with the LED strings [89]. Most of these circuits are simple semiconductors or integrated circuits, such as linear current regulators or switched-mode regulators which can feature higher performance and flexibility, however if the voltage drop in this devices is high it will lead to high losses that will contribute to reduce the overall efficiency of the lighting system [5, 82]. Therefore, the most commonly found active method is the employment of a switching converter (usually DC-DC Converter) with output current control

[4] ***Binning****: due to the manufacturing process LEDs may vary in colour, luminous flux and forward voltage, even for LEDs from the same batch, and since these differences can be very significant, LEDs are generally divided and placed in the market, in groups called bins* [91] Philips. *LEDs - Internet Courses*. Available: http://www.lighting.philips.com/pwc_li/main/connect/Lighting_University/internet-courses/LEDs/led-lamps6.html.

through switching frequency or duty-cycle control [5, 82]. Nevertheless this method faces major drawbacks, such as high-cost, complexity and large component count [5], and more importantly, a single converter is required for each LED string [82]. To overcome these issues, while guaranteeing simplicity and robustness, in the present work is also proposed, in addition to the single output topology, the application of a low-cost multiple-output topology on the current sharing control of multiple sets of series LED strings, using non-dissipative components, namely the variable inductor [82]. The proposed topology is able to perform current sharing in multiple LED strings, as well as in multiple LED lamps, provided that each lamp is composed of a single string of LEDs in series, and it is thoroughly described in section 4.3.3.

2.4.5 LED Modelling

Owing to the non-linear electrical behaviour of LEDs as power load, it is mandatory to use an adequate model to the extent of accurately predict large or small signal variations in their operation point. In order to determine the operation point of LED drivers using a dynamic model generally two approaches may be employed: *large-signal* or *small-signal* modelling. The former is characterized by its high reliability, accuracy and robustness, nonetheless, it is also very complex, and difficult to develop, and therefore its discussion will not be further addressed because an 'extremely high modelling precision' is not required in the present work. Hence, it was decided to employ a large-signal model, namely the piecewise linear model, using the support of the built-in linear model available in the software used.

2.4.5.1 Large-signal Modelling

Large-signal modelling is characterized for being the easiest and simplest approach, therefore several large-signal might be found in literature. The simplest one is based on the static equivalent resistance of the LED R_{eq} at a single operation point using given values of forward current (I_f) and voltage (V_f) of the LED as shown in Fig. 2.15 and (2.1):

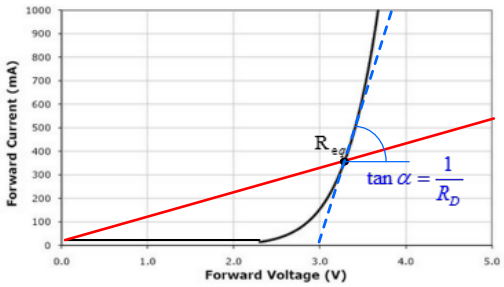

$$R_{eq} = \frac{V_f}{I_f} \qquad (2.1)$$

Fig. 2.15 – Static equivalent resistance of a single LED, at a given operation point, and its I-V curve

The major drawback of this approach however, is the introduction of huge errors if used to determine small-signal dynamics of the LED driver, because the static equivalent resistance differs from the dynamic resistance R_D at a given operation point [2] as shown in Fig. 2.15. Generally R_D has small values while V_f has large values, which means that small changes on the voltage applied to LEDs can cause large and undesirable changes on their current [2]. Hence, LEDs shall not be modelled only by an equivalent resistance [73]. So, the most commonly employed model is the so-called *piecewise linear model* which is briefly described in the next section.

Piecewise Linear Model

This model, selected to be employed in this work, is based on the approximation of the exponential *I-V* curve of a single LED and its electric scheme is illustrated in Fig. 2.16.

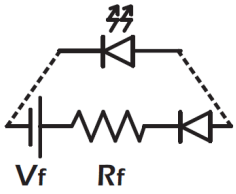

Fig. 2.16 - LED linear equivalent model

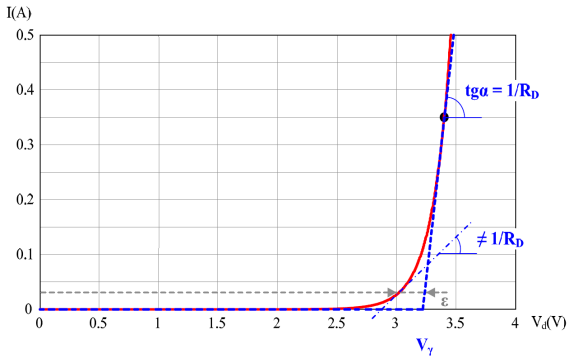

Fig. 2.17 - LED single piecewise linear approximation at a desired operation point [93]

It consists on voltage source V_γ (represented as V_f in Fig. 2.16) which accounts for the threshold voltage of the LED, in series with an ideal diode and a resistance R_D (represented as R_f in Fig. 2.16), which represents the dynamic resistance of the LED [2, 73]. This resistance equals the inverse of the *I-V* curve slope for a selected operation point tangent. Hence, the LED total output voltage V_{LED} may be expressed in function of the forward current I_f as follows:

$$V_{LED} = V_\gamma + I_f \cdot R_D \tag{2.2}$$

the dynamic resistance can, then, be calculated as follows:

$$R_D = \frac{\Delta V_{LED}}{\Delta I_f} = \frac{1}{\tan\alpha} \tag{2.3}$$

Where $\tan\alpha$ is the tangent at the operation point as illustrated in Fig. 2.17. In this figure, there is the exponential *I-V* curve in red while in blue is the single piecewise linear approximation to a selected operation point of the red curve. As depicted, it is possible to identify a problem with this

approach, namely the fact that R_D is usually calculated at high injection currents, and hence its value tends to converge to the LED series resistance which will introduce substantial errors for low current values [2]. This error, represented by ε in the previous figure, is associated to a different slope of the *I-V* curve. Nevertheless, it is still an extremely good approximation at the operation point and good approximation for a few other points around it. Although, if more accuracy is desired, namely to reduce the mismatch mentioned before, the model can be enhanced, for instance, by doubling-up the standard single piecewise linear model or even of higher order – superposition concept [94], which consists on paralleling multiple piecewise-linear LED models/ branches to obtain a model for a single LED. In the following figure is illustrated the case of a two-piecewise linear model, which is, as it will be discussed later, the approach selected to this work:

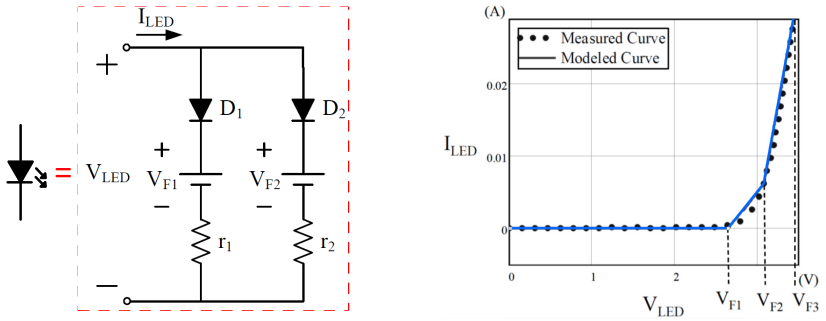

(a) (b)

Fig. 2.18 Two-piecewise linear model. (a) Electric Model. (b) I-V curve (dash) and modelled curve (blue)

In the previous figure, the dynamic resistances r_1 and r_2 of the electric model, corresponding to the two blue line segments V_{F1}-V_{F2} and V_{F2}-V_{F3}, may be calculated as follows:

$$r_1 = \frac{V_{F2} - V_{F1}}{I_{F2}} \tag{2.4}$$

$$r_2 = \frac{V_{F3} - V_{F2}}{I_{F3} - \frac{V_{F3} - V_{F1}}{r_1}} \tag{2.5}$$

where I_{F1}, I_{F2} and I_{F3} are the current values corresponding to the values V_{F1}, V_{F2} and V_{F3}, respectively. It is important to highlight that this model is very simple and it does not take into consideration parameters such as parasitic effects, i.e. temperature variation effects.

3 Variable Inductors (VI)

The concept of VI is quite old and dates from the 1930's however in the first types, the inductance was varied mechanically, either by changing the number of turns of a winding or by changing the core's air gap length [95]. Later in the 1960's with the spreading of electronics, more sophisticated versions were built using electronic switches (firstly thyristors) to replace the mechanical interfaces [96, 97]. Only in 1987 would be proposed, the quasi-linear controllable inductor [98], the first remarkable VI made, with a bias winding acting as control that would later be improved and lead to another invention: the LVI – Linear Variable Inductor. Later, in 1994, it was proposed a current-controlled VI for high frequency resonant power circuits, for which the main goal was to fulfil the role of the typical resonant inductor in high frequency power inverters, which could extend the ZVS operation range, thus reducing duty cycle and switching losses, and voltage ringing [99]. That device, essentially the magnetic regulator analysed and developed in this thesis (VI), is a particular type of device which resembles a saturable reactor or magnetic amplifier or even a transformer. A VI consists in the assembly on magnetic cores, of two windings, a main winding where AC power flows, and an additional DC powered winding, responsible for power flow control in the AC winding.

3.1 Inductance - Fundamentals

In order to proceed into the VI concept one shall recall some of the most remarkable and classic fundamentals of electromagnetism, which are briefly described in the Appendix D. The resulting equations that translate theory through mathematics are presented below:

Table C - Classic Electromagnetism Equations

$B = \mu H$	$\phi = BA$	$\Psi = N\phi$	$\oint_l \vec{H} \cdot d\vec{l} = Ni$	$L = \frac{N^2}{\mathcal{R}}$
$\oint_l \vec{B} \cdot d\vec{l} = \mu i$	$\phi = \int_s \vec{B} \cdot d\vec{S}$	$v_i(t) = \frac{d\phi(t)}{dt}$	$v_i(t) = N\frac{d\phi(t)}{dt} = \frac{d\Psi(t)}{dt}$	$\mathcal{R} = \frac{\mathcal{F}}{\phi} = \frac{Hl}{BA} = \frac{l}{\mu A}$

For a better comprehension of the VI operation principle we shall start by recalling theory about the basic and common definition of inductor/inductance and a few general fundamentals on electromagnetism. Basically an inductor is a device/component, such as a loop or a coil of conductor wire, with properties that allow it to store energy in the form of magnetic field. Inductance in the other way, is a property of the inductor and typically it can be divided into *self-inductance* or simply inductance and *mutual-inductance*, and generally it is expressed in Henry

[H] (SI unit). By another words, inductance may be roughly defined as the property of a coil in which a changing (time-varying) current 'induces' a voltage, also known as electromotive force (emf), in both the conductor itself (in this case it is simply called *inductance*) and in any adjacent coils (in this case it is called *mutual-inductance*) [100]. Inductance however, typically can be defined as *secant inductance* or *differential inductance* with respect to the *B(H)*[5] curve of a specific material/medium. Considering a winding, the general definition of inductance, the secant inductance L, is stated as follows in (3.1):

$L = N\frac{\phi(t)}{i(t)} = \frac{\Psi(t)}{i(t)}$ (3.1)	$L_{dif} = \frac{d\Psi(t)}{di(t)}$ (3.2)

where N is the winding's number or turns, $\phi(t)$ is the magnetic flux, Ψ is the total *flux linkage* and i is the current flowing (all the previous parameters are time-variable) through the winding. The previous definition is only valid for a material with a constant permeability (linear $B(H)$ curve) i.e. air, which means that in the case of materials with a non-linear $B(H)$ curve i.e. ferromagnetic materials, a different and valid definition is required, which is where the concept of *differential inductance* surges [13, 101]. Roughly, *differential inductance* is defined as the ratio of the magnetic flux change over the current change in the winding times the number of turns of the winding as stated in (3.2). Across the present work, it will be implicitly referred to the concept of *differential inductance* whenever the term 'inductance' will come up.

To have a better idea of the difference between the two previously referred definitions, in the following figure they are both graphically represented:

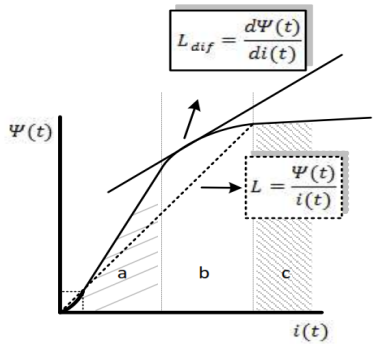

Fig. 3.1 - Flux linkage vs current and inductance sketched definitions [13]

[5] $B(H)$ *is the* ***magnetization curve*** *of the magnetic material – where magnetic flux density* ***B*** *is a function of the magnetic field intensity* ***H*** *applied*

3.2 VI – Principle of Operation

Roughly, the principle of operation of a VI may be explained by recalling the fundamental theory of transformers, which says that a small amount of DC current flowing into the winding of a transformer, mounted on an ungapped core, causes the core to quickly saturate [13]. Thereby, a VI is able to control the power flow in the AC winding simply by means of control circuitry in the DC winding through the changes in the inductance of the AC winding. Some literature articles as well as some patents show several possible applications and structures of VIs, depending on the core structures and winding arrangements selected. Regarding the core material, generally a VI is operated in the knee or in the transition area[6] (saturation to unsaturation area) of the magnetization curve. In the Fig. 3.2 is illustrated the hysteresis loop of ferromagnetic materials typically used in VIs and in the Fig. 3.3 is sketched the typical magnetization curve (first quadrant of the hysteresis loop) typically divided into three main regions.

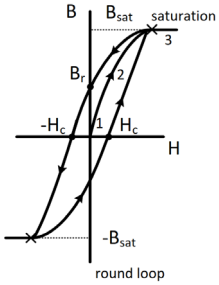

Fig. 3.2 - Hysteresis loop shape of a soft material used in VI's [13]

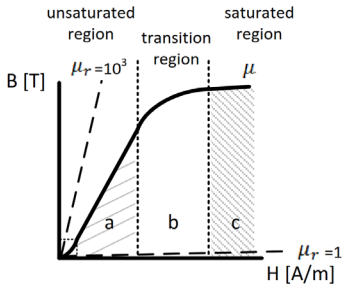

Fig. 3.3 - Typical magnetization curve of a soft magnetic material [13]

The VI structure selected for this work, a double EFD core structure (see Fig. 3.4 (a)) includes an air gap at the centre leg and three windings. The main inductor/winding (L_{ac}) is wound around the centre leg whereas the symmetrical bias windings (L_{dc}), serially connected in opposite polarity so as to cancel out the AC voltages induced by the main inductor [13, 103, 104], are wound around the two side arms of the core (see Fig. 3.4 (b)). This gapped core structure helps maintaining a low effective permeability, thereby avoiding quick saturation of the core by maintaining the magnetic flux density swing ΔB small [13, 104].

The DC current is supplied to the bias winding so that the permeability of the outer arms, as well as the permeability of the upper and lower parts of the core, can be modified by approaching

[6] ***Transition area of the magnetization curve*** *is defined as the threshold point between the unsaturated area and the saturated area. Technically, above this threshold point the magnetic flux density B is continuously increasing, but at the paramagnetic rate/slope, which is 3 orders of magnitude smaller than the ferromagnetic rate/slope seen below the threshold point [102] R. M. Bozorth, Ferromagnetism: Wiley-IEEE Press, 1993.*

the magnetic flux to the knee zone of the magnetization curve [13, 104-106], as the Fig. 3.4 (a) shows. This magnetization, originated even by a relatively small bias current, characterized by an increase of the magnetic flux density, will decrease the effective permeability (which in turn will increase the effective global reluctance) seen by the main winding in the centre leg and hence change the value of the main winding's inductance L_{ac} [13, 104].

In order to accurately predict the behaviour of the VI, namely to estimate how the inductance of the main winding L_{ac} varies, a deep magnetic-circuit analysis has to be addressed, however it is a non-trivial task, thus, the typical approach is to use an equivalent circuit model, namely a quite intricate reluctance model, based in the VI's physical structure and an assignment of magnetic paths. In this approach, each magnetic path is related to a specific reluctance. The identified reluctances, together and superposed on the core geometry will be the base of the model used to predict the device's behaviour.

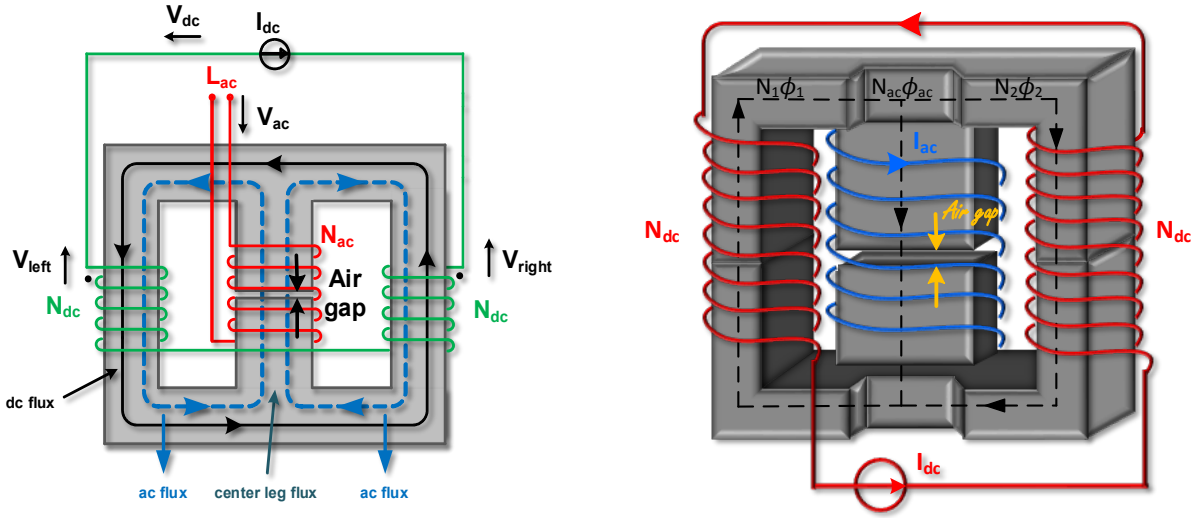

(a) Schematic (b) Physical illustration

Fig. 3.4 - Current-controlled VI – double gapped EFD25 core

In this work, for the sake of simplicity, in order to predict the evolution of the inductance of the main winding L_{ac}, it was decided to obtain the small-signal characteristic since it is a very good representation of the normal behaviour of the VI, as it will be seen posteriorly in the section 6.1. The small-signal characteristic may be easily obtained by means of an impedance analyser or an LCR meter, by simply measuring the inductance of the main winding L_{ac} and varying the control current I_{dc} in the bias winding. With this approach, an accurate and complex model will no longer be required.

3.3 VI Structure and Modelling

Magnetic regulators can be built in several shapes and topologies depending on the available cores. For this work were selected gapped EFD25 cores.

Modelling is essential for a correct understanding of variable inductors and represents an extremely useful and helpful tool for anyone who pretends to design and develop them. Typically in literature three different approaches are used for modelling complex magnetic devices such as multi-winding devices or integrated magnetics [13]:

- *Software finite element-analysis*, provides the best possible accuracy, but it requires an enormous effort and time dedicated to computation analysis [107]. This type of model is also difficult to be applied in transient system simulation and from the practical point of view this would increase the complexity of the approach.

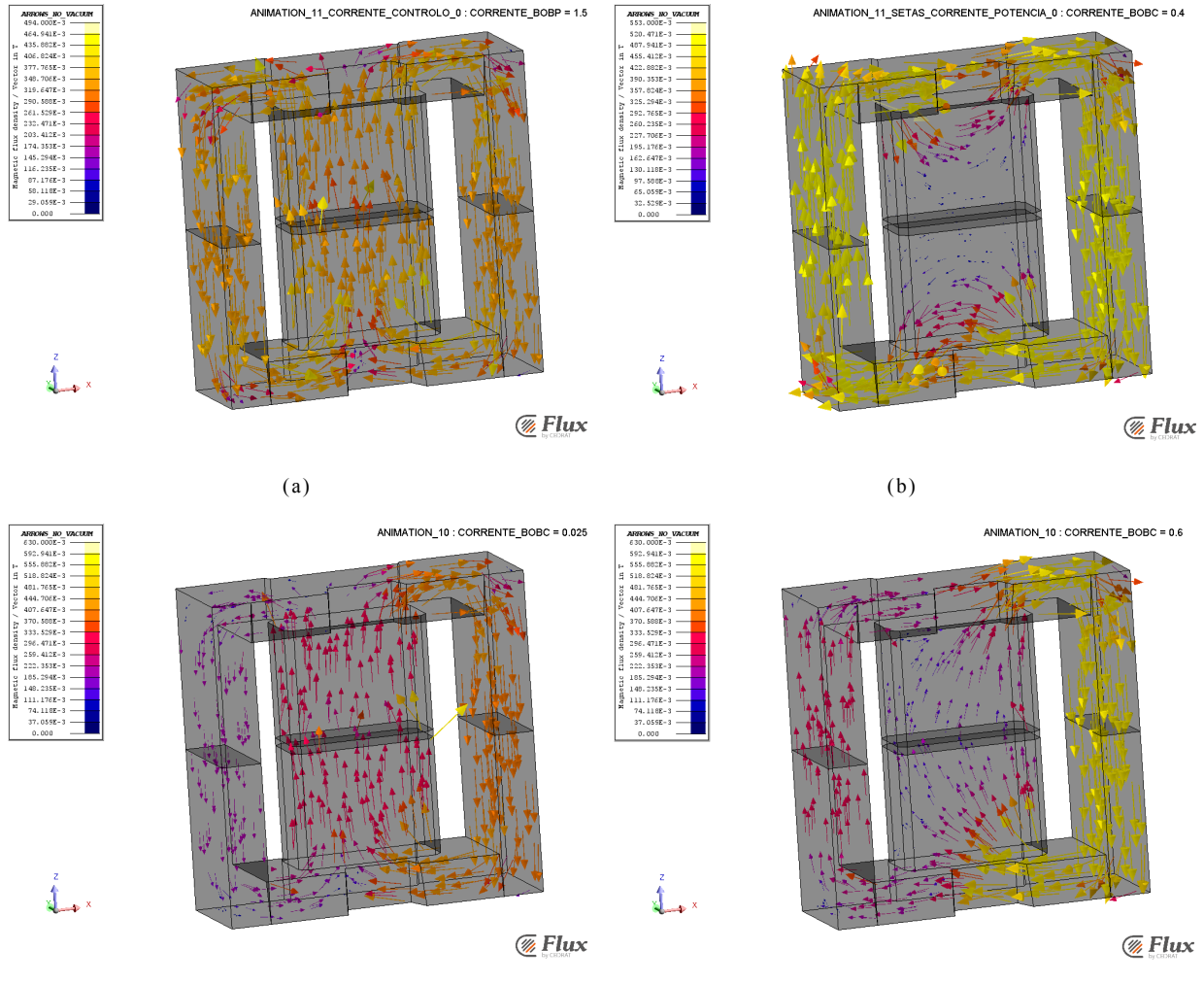

Fig. 3.5 – VI flux density and directions. (a) No bias current supplied and 1.5 A DC current in the AC winding. (b) No current in the AC winding and with 0.4 A DC current in the bias winding. (c) Bias winding supplied with DC current of 25 mA and AC winding supplied with DC current of 1.3 A. (d) DC bias current of 0.6A and AC winding supplied with DC current of 1.3 A. [108]

Nevertheless, to have an idea about the flux density and direction on the VI, some illustrations obtained from a finite element analysis and simulation, developed in Flux[7], may be seen in Fig. 3.5. The VI was simulated using the same data of the VI prototype constructed. It consists of a double EFD 25 core with an air gap of 0.6 mm in the centre leg. The AC winding (copper wire with 35 turns and cross section of 0.63 mm) is wound around the centre leg. The bias windings, are serially connected and wound around each outer leg, and consist, each, of copper wire with 71 turns and cross section 0.315 mm.

In Fig. 3.5 (a) is illustrated the flux density distribution in the VI particularly for the case when only the AC winding is supplied, with a 1.5 DC current. In this case there is a quasi-uniform distribution of flux across all parts of the cores. In Fig. 3.5 (b) is illustrated the flux density distribution due to the DC current flowing through the bias windings, and specifically it is noticeable that the flux density across the centre leg is much lower compared to the outer legs together with upper and lower parts and that a relatively low DC bias current is enough to saturate the cores (yellow arrows in the Fig. 3.5 indicate that the cores are saturated in the respective areas). In Fig. 3.5 (c) and Fig. 3.5 (d) is noticeable the impact of supplying both windings at the same time with DC current (unidirectional), which basically shows the saturation of the right outer arm of the VI. In the case concerning the present work, the AC winding wound around the centre leg is supplied with AC current, which leads to the saturation of both outer legs alternately, i.e. negative current in the AC winding provokes the saturation of the right outer leg while positive current saturates the left outer leg.

- The second approach to model complex magnetic devices is based on the *gyrator-capacitor model* [110]. This technique is based on the employment of a capacitor to simulate the magnetic device. In the gyrator-capacitor approach, the *mmf*[8] is analogous to voltage and the rate-of-change of magnetic flux is analogous to current which resembles the duality principle of the classic reluctance model. The gyrator-capacitor approach is considered as one of the most effective but it is rarely used.
- Thereby, the third and typical approach is the *magnetic reluctance model* [93].

Regarding the present work, none of the three previous approaches was employed. Instead, a simple modelling approach, based in the *small-signal characteristic* of the built VI was developed. This model is addressed and explained in the section 5.2.

---

[7] ***Flux**: Electromagnetic and thermal finite elements analysis software by Cedrat [109] Cedrat. Flux Software. Available: http://www.cedrat.com/en/software/flux.html*

[8] ***mmf**: magnetomotive force*

4 Switched-Capacitor Converters (SCC)

Certainly, the first time when the operating principle of SCC was (unintentionally) referred in literature, probably dates from 1873, when Maxwell demonstrated a method to measure the capacity value of a capacitor, using the process of a SCC, for which the average current flow would be equivalent to that of a resistor of value $1/(2fC)$ where f is the switching frequency and C the capacity value of the capacitor [111]. Nonetheless, the first time that SCC were definitely developed dates from 1940, when they would be used in large banks in distribution systems to generate reactive power needed by the grid [112] and later in the 1970s as filters in discrete time signal processing [113]. Concerning the domain of active power regulation applications (the scope of this work), SCC started to be employed most likely in 1972 [114]. They are still popular nowadays, and used over a wide range of very low power applications, mostly because they are designed exclusively with capacitors and switches which allows them be fully integrated on-chip resulting in a small size and weight, thus making them suitable for mobile applications [115].

4.1 Resonant Switched-Capacitor Converters (RSCC)

Basically, SCC are DC-DC converters that use only switches and capacitors, where the latter are used as energy storage elements, by "moving" charges into and out of them, in order to provide a required output voltage value. Regarding the output-input voltage ratio, three main topologies of SCC, with various combinations of switches and capacitors, are available. They can be divided into *SCC Divider (step-down)*, *Inverter* or *Multiplier (step-up)* [115]. Nevertheless, ever since the scope of this work is aimed to a step-up based RSCC, other types of SCC will not be further discussed. Theoretically, step-up RSCC can provide any fixed voltage ratio depending on the number of switched-Capacitor cells used in its structure, i.e. $\overline{V_{out_{ideal}}} = (n+1).\overline{V_{in}}$, where *n* is the number of SC cells [116, 117]. This interesting and highly useful feature is sketched in the following electric circuit:

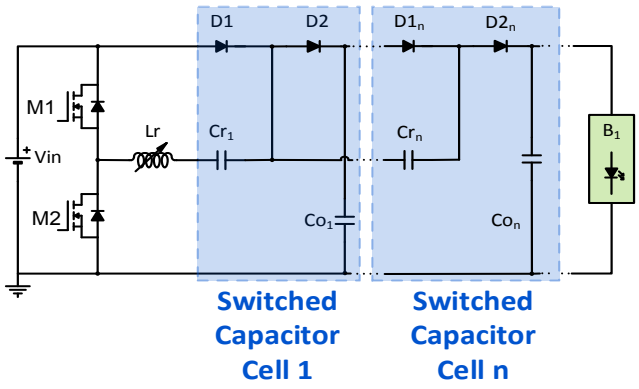

Fig. 4.1 – n-Mode RSCC

In another words, by cascading *n* switched-capacitor cells the output/input voltage ratio can be increased by a factor of *n+1*. dRSCC were developed to overcome major drawbacks of non-resonant SCC which, due to poor load regulation and to their poor efficiency are characterized with hard switching with high current spikes resulting in high EMI and low rated lifetime due to the requirement of large electrolytic capacitors. These issues restricted their use to applications of low power levels [118-120]. In the following two figures are shown the conventional step-up RSCC and the proposed topology of this work, which, as previously mentioned, consists on the conventional topology with the resonant inductor replaced with the variable inductor:

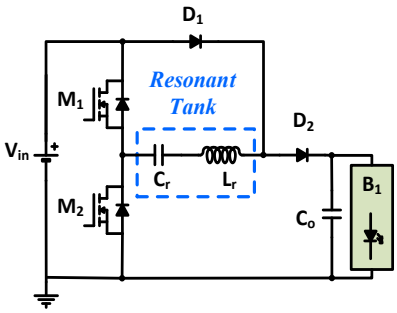

Fig. 4.2 - Conventional RSCC Double Mode [115]

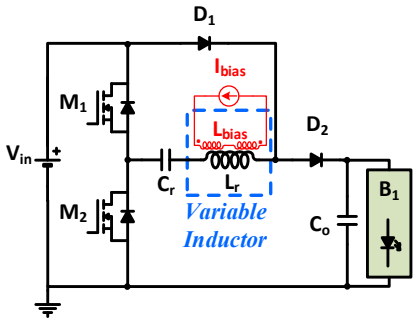

Fig. 4.3 - Proposed RSCC Double Mode

The operation of the proposed topology (Fig. 4.3) is very similar to the conventional. The novelty of the proposed topology is the output regulation via the control of charge flowing through the resonant tank, namely by varying its characteristic impedance Z_c (through L_r).

4.2 Output - Voltage Control Techniques

Concerning load regulation of SCC, where the energy transfer is basically achieved by controlling the charging and discharging process of the switched capacitors, the most commonly employed techniques are:

- *PWM – Duty-cycle control of a single switch or all switches* [121]. This type of technique, however, shows that the output voltage range remains narrow and it is achieved at the expense of decreasing the converter's efficiency [122, 123]. Moreover, methods based on this technique may cause increased switching and on-state losses due to its hard switching operation and large peak current which is a source of EMI, thus leading the decline of the conversion efficiency.
- Simply by *varying switching frequency f_s* [124] – this technique faces the same disadvantages of the previous technique. In addition, it is generally known that varying switching frequency of converters raises difficulties when designing filters.
- *Phase-shift control* [123, 125] – this technique probably offers the best performance, however it is quite complex and complicated, requires a higher component count and most

importantly, the output voltage may have a quite high undesired ripple [123, 126]. The latter issue of this technique is enough to justify the fact that it shall not be applied to converters supplying LED loads, ever since for this type of load, small voltage variations provoke high current variations, as previously mentioned.

To overcome issues of the former techniques, it is introduced a new technique to regulate/control RSCC – the VI, which was already introduced in the section 2.4.3.3. Its application to SCC is new and innovative, however, as previously mentioned, it may be found in prior art regarding the control of Half-bridge resonant and Forward converters [13, 82]. Unlike those techniques available on literature, which are based on output voltage control, the proposed technique is based on current control justified by the type of load (LEDs).

4.3 RSCC Step-Up Mode with Variable Inductor

In this work, the selected input voltage value (V_{in}) of the converter is 48 V, which is a standard value that can be provided by a battery bank, by a power factor correction stage or by a continuous voltage source.

Concerning the switches, regardless of the fact that the switching frequency and duty-cycle are set to be constant, these parameters are still available to be varied if one desires to use them for further control strategies. The generic schematic of the proposed topology and the selected convention of its currents and voltages are shown, respectively, in the Fig. 4.4 and Fig. 4.5:

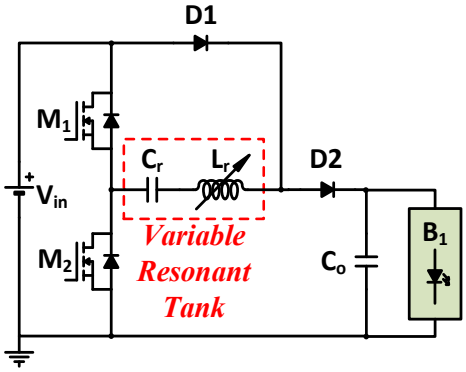

Fig. 4.4 – RSCC Step-Up Mode

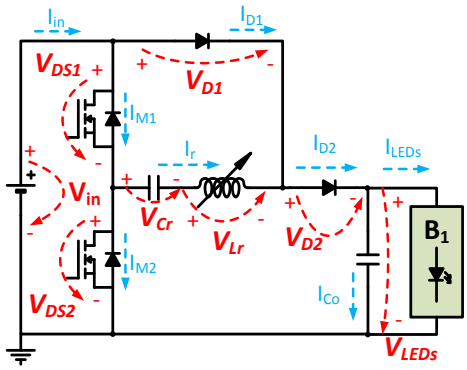

Fig. 4.5 – RSCC Step-Up Mode – convention of currents and voltages

4.3.1 Theoretical Analysis

Considering the operation of the circuit at steady state, it can be described in six states as shown in Fig. 4.6. As stated before, the switching frequency was selected to be 100 kHz, constant, and to be above resonant frequency so that ZVS is naturally achieved in the Mosfets [13], thus reducing switching losses which in turn minimizes the corresponding electromagnetic interferences produced [127] and increases the overall efficiency of the converter. Typically, when

the resonant circuit is designed in order to operate with ZVS under a fixed frequency, a wide dimming range can be easier achieved and the consumption of reactive power minimized [13]. The ZVS operation of the switches during turn-on transitions may be simply confirmed by taking a look into the Fig. 4.8. Concerning the power switches selected, namely Mosfets, they are set in order to switch ON and OFF alternately with a duty cycle of 50%. The use of free-wheeling anti-parallel diodes with Mosfets is mandatory since the resonant period is higher than the switching period, which means that in the end of every half switching cycle there is energy stored in the resonant inductor and therefore its current is non-zero. If no free-wheel diode would be used this non-released energy would damage and destroy (internal sparkling) the power Mosfets during switching stages. Ideally, provided the previously referred conditions, each switch (composed of a Mosfet with an antiparallel diode) is then switched OFF when its current is still positive (and at its maximum value) and switched on when its current is negative (and at its minimum value) which means that the free-wheeling diode will be conducting since the moment when an impulse is applied in its gate and until the current (drain-source) drops to zero. In this condition, due not only, to the free-wheeling diodes but also because $f_s > f_r$it is ensured that the Mosfets begin to conduct at zero voltage and current which means that ideally, during turn-on transitions, the switching losses in the Mosfets can be neglected. This moment corresponds to the instant $t = t_2$ in Fig. 4.7. It is important to notice that in this case, ever since $f_s > f_r$, the phase angle of the resonant current is less than 0º which means that the current lags the voltage, thus the resonant circuit behaves as an inductive load [13].

According to the main principle of operation, and observing Fig. 4.8, the impact of the VI within the whole dimming range, is mostly noticed in the resonant current I_r amplitude and consequently in the LEDs average current $I_{LEDs_{avg}}$. More precisely, by varying the resonant inductance, the *rms*/amplitude value of the resonant current will also vary, which in turn will result in the variation of the average value of the current supplied to the LED lamp - the impedance of the resonant circuit is changed in order to control the desired operation point of the LED lamp.

To start a deeper analysis of the operation of the circuit, without loss of generality, and considering a single point of operation, the following assumptions shall be stated:

- all the switching devices (power Mosfets and diodes) are ideal, i.e. no on-state voltage drop or resistance;
- the output capacitor C_0 is so large, that the ripple in the output voltage $V_{LEDs_{avg}}$ is neglected and it is initially charged to the desired average output voltage value;
- the ripple in the output current is also neglected, then it is considered to be a constant current source $I_{LEDs_{avg}}$;

- the input voltage of the converter V_{in} is ideal, i.e. constant and with null series impedance;
- parasitics of components such as ESR, ESL, along with others, are also neglected.

Stages of Operation (consult Fig. 4.6 and Fig. 4.7 for complementary support)

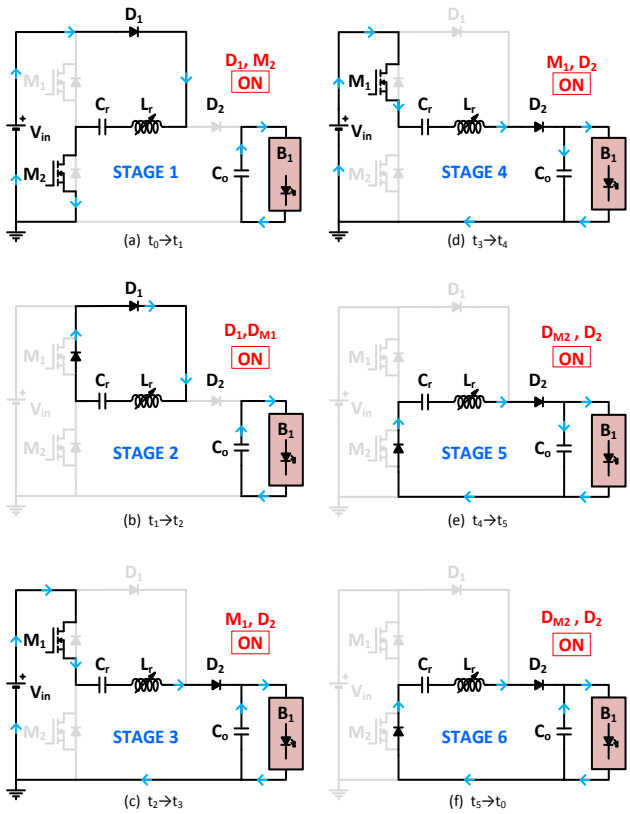

Fig. 4.6 - Steady-state equivalent circuit of the RSCT (a) Stage 1 (b) Stage 2 (c) Stage 3 (d) Stage 4 (e) Stage 5 (f) Stage 6.

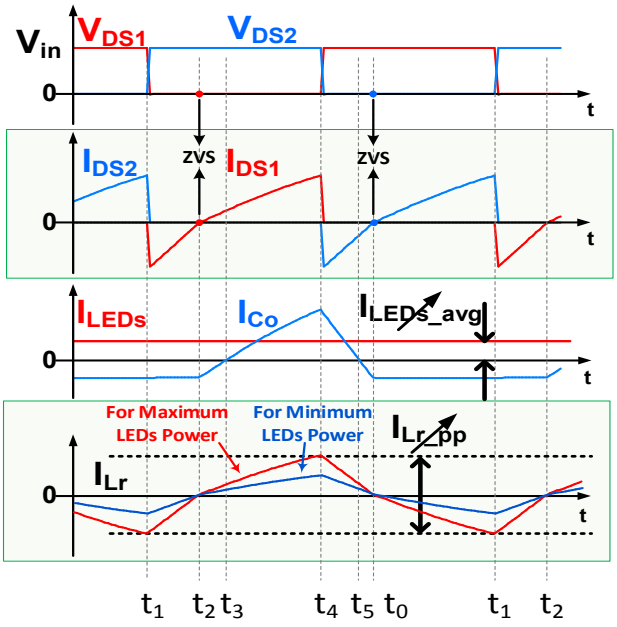

Fig. 4.8 - ZVS and Impact of the VI in the RSCC

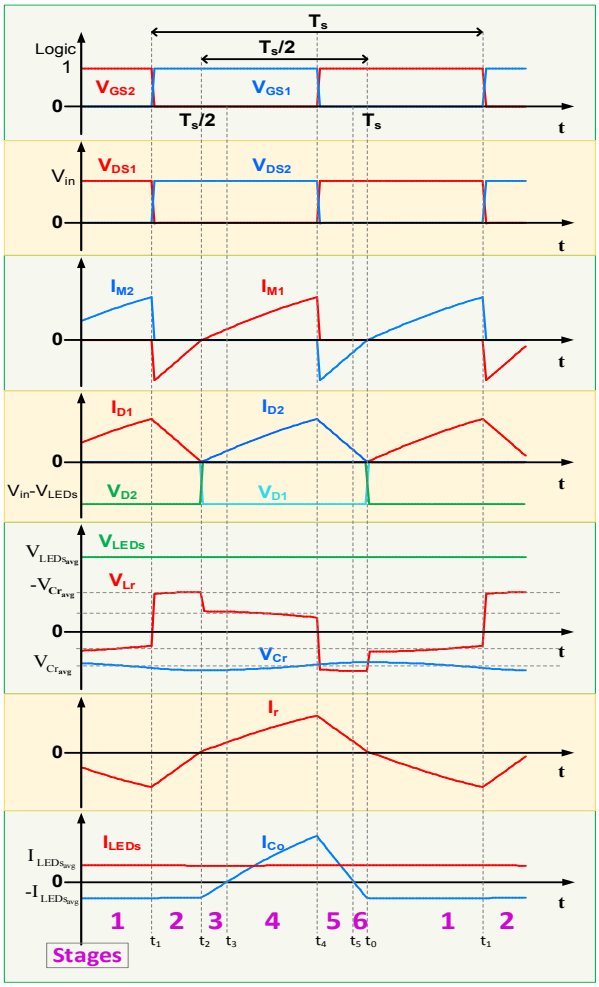

Fig. 4.7 - Step-up RSCC theoretical waveforms (not drawn up to scale)

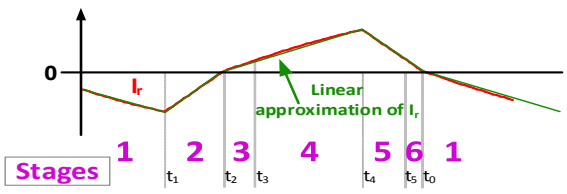

Fig. 4.9 – Waveforms with linear approximations

Stage 1 (Fig. 4.6 (a): $t = t_0 \sim t_1$)

The switch M2 is in the on-state during this stage. The resonant capacitor is charged by the input voltage V_{in} in a nearly resonant (sinusoidal) manner until $t = t_1$. In this stage there is no energy transferred to the load through the resonant circuit, and therefore the output capacitor C_0 is responsible for supplying energy to load during this time. As $i_r(t_0) = 0$ and $i_r(t_0) = 0$ and at t_0 the resonant capacitor's voltage reaches its minimum. Similarly to [128], the stage equations and solutions are:

$$V_{in} + v_{L_r} + v_{C_r} = 0 \Leftrightarrow v_{C_r} = -V_{in} - v_{L_r} \tag{4.1}$$

$$i_{C_o} + I_{LEDs_{avg}} = 0 \tag{4.2}$$

$$i_r(t) = \frac{-v_{C_r}(t_0) - V_{in}}{\omega_o \cdot L_r} \cdot \sin \omega_o (t - t_0) \tag{4.3}$$

$$v_{C_r}(t) = V_{Cr_{avg}} - \frac{\Delta V_{C_r}}{2} \cdot \cos \omega_o (t - t_0) \tag{4.4}$$

where $\omega_o = 1/\sqrt{L_r C_r}$ (angular resonant frequency), ΔV_{C_r} is the resonant capacitor's voltage ripple, $V_{C_{r_{avg}}}$ its average voltage, and $I_{LEDs_{avg}} = V_{LEDs_{avg}}/R_{LEDs}$ where R_{LEDs} is the equivalent static resistance of the LED string at a given operating point.

Stage 2 (Fig. 4.6 (b): $t = t_1 \sim t_2$)

The switch M1 is turned on at $t = t_1$. Due to the operation of the stage 1, and because the resonant period is higher than the switching period, there is not enough time for the resonant current to reach the zero value, thus $i_r(t_1) \neq 0$. Consequently, the anti-parallel diode of M1 (Mosfet 1) conducts from $t = t_1$ until the resonant current drops to zero at $t = t_2$. Analogously to the stage 1, in this stage, the resonant current keeps charging C_r, particularly until it drops to zero, and the output capacitor still supplies the load. The stage equations and solutions are:

$$v_{L_r} + v_{C_r} = 0 \Leftrightarrow v_{C_r} = -v_{L_r} \tag{4.5}$$

$$i_{C_o} + I_{LEDs_{avg}} = 0 \tag{4.6}$$

$$i_r(t) = i_r(t_1) + \frac{v_{C_r}(t_1)}{\omega_o \cdot L_r} \cdot \sin \omega_o (t - t_1) \tag{4.7}$$

where $i_r(t_1)$ is the resonant current minimum value, ever since on the instant t_1 the input voltage source is no longer charging the resonant tank. Together, stage 1 and 2 last half switching cycle $T_s/2$ which corresponds to the time period during which the resonant capacitor is charged.

Stage 3 (Fig. 4.6 (b): $t = t_2 \sim t_3$)

At $t = t_2$ the resonant capacitor stops being charged, thus it reaches its maximum charge value and therefore:

$$v_{C_r}(t_2) = V_{C_r\_\min} = V_{Cr_{avg}} - \Delta V_{C_r}/2 \tag{4.8}$$

in this equation the voltage on the resonant capacitor is referred to minimum instead of maximum due to the selected convention for the voltage of this capacitor, and $i_r(t_2) = 0$. During this stage the energy stored in the resonant capacitor $C_o$is released to the load through the diode D_2, as well as energy stored in the output capacitor, thus the resonant current will increase. The stage equations are as follows:

$$-V_{in} + v_{C_r} + v_{L_r} + V_{LEDs_{avg}} = 0 \Leftrightarrow v_{C_r} = V_{in} - v_{L_r} - V_{LEDs_{avg}} \tag{4.9}$$

$$i_r + i_{C_o} = I_{LEDs_{avg}} \tag{4.10}$$

$$i_r(t) = \frac{V_{in} - v_{C_r}(t_2) - V_{LEDs_{avg}}}{\omega_o \cdot L_r} \cdot \sin \omega_o (t - t_2) \tag{4.11}$$

Stage 4 (Fig. 4.6 (b): $t = t_3 \sim t_4$)

In this stage the circuit operation is basically the same of stage 3 thus the resonant current keeps increasing its amplitude. The only difference is the output capacitor C_o, which is fully discharged at $t = t_3$, and therefore during this stage it will charge:

$$i_r = i_{C_o} + I_{LEDs_{avg}} \tag{4.12}$$

Stage 5 (Fig. 4.6 (b): $t = t_4 \sim t_5$)

During this stage the resonant capacitor is responsible for supplying the load as well as for partially charging the output capacitor. The input voltage is no longer connected to the rest of circuit, thus the resonant current will start decreasing due to the reduction of charge in the resonant capacitor. Therefore, during the whole switching cycle, the resonant current reaches its maximum value for $t = t_4$. The stage equations are as follows:

$$v_{C_r} + v_{L_r} + V_{LEDs_{avg}} = 0 \Leftrightarrow v_{C_r} = -v_{L_r} - V_{LEDs_{avg}} \tag{4.13}$$

$$i_r = i_{C_o} + I_{LEDs_{avg}} \tag{4.14}$$

$$i_r(t) = i_r(t_4) + \frac{-v_{C_r}(t_4) - V_{LEDs_{avg}}}{\omega_o \cdot L_r} \cdot \sin \omega_o (t - t_4) \tag{4.15}$$

where $i_r(t_4)$ is the resonant current maximum value, ever since on the instant t_4 the input voltage source is no longer connected to the load through the resonant tank.

Stage 6 (Fig. 4.6 (b): $t = t_5 \sim t_0$)

Within this stage the circuit operation is basically the same of stage 5 thus the resonant current keeps decreasing its amplitude. The only difference is in the output capacitor C_o, which is fully charged at $t = t_5$, and therefore during this stage its energy will be released to the load:

$$i_r + i_{C_o} = I_{LEDs_{avg}} \tag{4.16}$$

4.3.2 RSCC Design Procedure

The design of the converter is realized in function of the desired LED current level.

The initial selected parameters for the converter are as follows:

- Average input voltage: V_{in}= 48 V;
- Average LED string current: $I_{LEDs\_avg} = 0.1$ A~0.35 A;
- Average LED string voltage: $V_{LEDs\_avg} = 60$ V~64 V;
- Switching frequency: $f_s = 100$ kHz (lower than resonant frequency to ensure natural zero voltage switching - ZVS), and duty-cycle of 50% for both switches.

The design of the converter components is quite empirical, which means that it is approached based on assumptions selected by empirical criteria.

The main components, which require a deep design procedure, are the capacitors and the resonant inductor (variable inductor). The first capacitor, also known as the switched capacitor, is the one present in the resonant tank and it is used to transfer energy. The second capacitor is the output filter capacitor. The voltage ripple across them affects the efficiency of power conversion as well as the stability of the output voltage for the former capacitor. The design begins by taking into account the principle of operation described in section 4.3.1.

4.3.2.1 Resonant capacitor calculation

The amount of charge flowing to C_r during the charging process (stage 1 and 2) should be equal to the amount of charge flowing out of it during the discharging process (stages 3, 4, 5 and

6). Assuming that the output capacitor is ideal, the integration of its current (equals the amount of charge flowing into and out of it) should be equal to zero during one switching cycle and the converter's currents, during the discharging process, can be related as follows:

$$i_r(t) = i_{C_o}(t) + i_{LEDs}(t) \tag{4.17}$$

Therefore, the amount of charge flowing out of the resonant capacitor C_r during the discharging process ($\Delta Q_{r_{discharge}}$), from $t_2 = T_s/2$ to $t_0 = T_s$, should be equal to the amount of charging flowing to the load during one switching cycle (ΔQ_{C_o}).

$$\Delta Q_{r_{discharge}} = \Delta V_{C_r} \cdot C_r = \int_{T_s/2}^{T_s} i_r(t)dt = \frac{\frac{T_s}{2} \cdot I_{r\_\max}}{2} = \frac{T_s}{4} \cdot I_{r\_\max} \tag{4.18}$$

$$\Delta Q_{C_o} = \int_0^{T_s} i_{LEDs}(t)dt = I_{LEDs\_avg} \cdot T_s \tag{4.19}$$

where ΔV_{C_r} is the voltage ripple on the resonant capacitor and T_s the switching cycle period. From the two previous equations results the following relations:

$$\Delta Q_{r_{discharge}} = \Delta Q_{C_o} \leftrightarrow \frac{T_s}{4} \cdot I_{r\_\max} = I_{LEDs_{avg}} \cdot T_s \Leftrightarrow \Delta V_{C_r} \cdot C_r = I_{LEDs_{avg}} \cdot T_s \tag{4.20}$$

$$I_{r\_\max} = 4 \cdot I_{LEDs_{avg}} \tag{4.21}$$

Selecting the capacitor's voltage ripple to be 20% of the input voltage ($48\,V * 0.2$), which equals 9,6 V, the switching frequency of 100 kHz and the maximum required LEDs current 0,35 A, then the value of C_r can be calculated as follows:

$$C_r = \frac{I_{LEDs_{avg}} \cdot T_s}{\Delta V_{C_r}} = \frac{0.35 \cdot 10^{-5}}{48 \cdot 0.2} \approx 0.365 \mu F \tag{4.22}$$

The value of C_r obtained is then 0,365 µF. Therefore the commercial value of 0,47 µF was selected and the voltage ripple for this capacitor value can be recalculated using:

$$\Delta V_{C_r} = \frac{I_{LEDs_{avg}} \cdot T_s}{C_r} = \frac{0.35 \cdot 10^{-5}}{0.47 \cdot 10^{-6}} \approx 7.45V \tag{4.23}$$

As this capacitance is maintained constant during the whole dimming range, the voltage ripple may be calculated also for the minimum dimming level, which corresponds to LEDs current of 0,1 A. The results for this sub-section are then shown in the following table:

I_o	C_r	ΔV_{Cr}
0.35 A	0.47 µF	7.45 V
0.10 A	0.47 µF	2.13 V

Table D – Resonant capacitor's voltage ripple and capacitance

4.3.2.2 Output Capacitor Calculation

The output filter capacitor can be determined also from the following relation:

$$\Delta Q_{C_o} = \Delta V_{C_o} \cdot C_o = \int_{T_s}^{3.T_s/2} i_{C_o}(t)dt \tag{4.24}$$

During the charging process, from $t_0 = T_s$ to $t_2 + T_s/2$, the current flowing through the output capacitor is the same flowing through the LEDs load:

$$i_{C_o}(t) = i_{LEDs}(t) \tag{4.25}$$

Whereas during the discharging process the current through the output capacitor can be given by (4.17) as follows:

$$i_{C_o}(t) = i_r(t) - i_{LEDs}(t) \tag{4.26}$$

Assuming the current in LEDs as constant, i.e. with a neglected ripple, and substituting (4.26) into (4.24) during the discharging period of time, it is obtained:

$$C_o = \frac{1}{\Delta V_{C_o}} \cdot \int_{T_s}^{3T_s/2} (i_r(t) - i_{LEDs}(t))dt \leftrightarrow C_o = \frac{\frac{T_s}{2} \cdot (I_{r\_\max} - I_{LEDs_{avg}})}{2} = \frac{\frac{T_s}{2} \cdot (3I_{LEDs_{avg}})}{2} \tag{4.27}$$

Substituting (4.26) into (4.27), and after a few steps it is obtained:

$$C_o = \frac{3 \cdot T_s \cdot I_{LEDs_{avg}}}{\Delta V_{C_o} \cdot 4} \tag{4.28}$$

From the previous equation it is already possible to determine the value of the output capacitor. Generally, in this type of converter the percentage of output voltage ripple is usually specified to be less than 1% [129]. Therefore, the percentage selected for this work is 0.5% of the maximum theoretical mean output voltage (64 V = 20 LEDs *3.2 V - from the manufacturer's datasheet the nominal voltage of a single LED is approximately 3.2 V). Thus using the selected ripple, the switching frequency of 100 kHz and the maximum mean value of the LEDs current (0.35 A) it is obtained:

$$C_o = \frac{3 \cdot 10^{-5} \cdot 0.35}{64 \cdot (0.5\%) \cdot 4} \approx 8.2 \mu F \tag{4.29}$$

thus the commercial value of 10 µF was selected.

4.3.2.3 VI - AC Inductance Range Calculation

The design of the VI range is based on the determination of two static values of inductance, namely the minimum and maximum required values. In prior literature, the converter selected for this thesis, was found to be operated only in ZCS ($f_s < f_r$), for which the principle of operation is rather different than for ZVS operation, consequently all stages of operations and mathematical relations are different for both types of operation. Shortly, it was not possible to find any relations that could easily give or lead to the calculation of the resonant inductor's inductance and therefore a mathematical relation, that can be used to determine the necessary value of the resonant inductor, had to be deduced for the ZVS operation. This deduction is described below, and having also an empirical character, it is based on few indispensable assumptions, from which some were already and previously referred. In addition to those assumptions i.e. ideal components, a few more have to be set:

- the capacitor are large enough so that their voltage ripple can be neglected. Therefore the output voltage v_{LEDs} can be assumed as a constant voltage source $V_{LEDs_{avg}}$ and the resonant capacitor's voltage v_{Cr} might be, analogously, assumed as a constant voltage source $V_{Cr_{avg}}$
- f_s is high enough to satisfy (at least partially) the condition $f_s \gg f_r$ so that the changes on the resonant current (i_r) can be approximated as linear with time.

Firstly let's recall the resonant inductor current equation (4.11) during stages 3 and 4 ($t_2 \sim t_4$):

$$i_r(t) = \frac{V_{in} - V_{Cr_{avg}} - V_{LEDs_{avg}}}{\omega_o \cdot L_r} \cdot \sin \omega_o (t - t_2) \tag{4.30}$$

Analogously to the classic procedure taken in buck and boost converters analysis, complemented by the assumptions mentioned above, the previous current equation can be approximated as linear. In addition, provided that it is null at t_2, it can be related as follows:

$$i_r(t) = \frac{V_{in} - V_{Cr_{avg}} - V_{LEDs_{avg}}}{L_r} \cdot (t - t_2) \tag{4.31}$$

At t_4, the input voltage source V_{in} is no longer connected to the output voltage source $V_{LEDs_{avg}}$ by the resonant tank, hence, this is the time instant when the resonant current reaches its maximum value and for this instant the equation (4.31) can be rewritten as follows:

$$I_{r_{\max}} = i_r(t_4) = \frac{V_{in} - V_{Cr_{avg}} - V_{LEDs_{avg}}}{L_r} \cdot (t_4 - t_2) \tag{4.32}$$

In order to proceed with the calculation of L_r the time interval $(t_4 - t_2)$ has to be determined.

Calculation of $(t_4 - t_2)$

This period of time which is the period that stages 3 and 4 last together may be obtained as follows:

$$t_4 - t_2 = \Delta t_3 + \Delta t_4 \tag{4.33}$$

where Δt_3 and Δt_4 are the period of time that the stages 3 and 4 last, respectively. The sum of these 2 periods of time may be calculated using the following relation:

$$\Delta t_2 + \Delta t_3 + \Delta t_4 = \frac{T_s}{2} \Leftrightarrow \Delta t_3 + \Delta t_4 = \frac{T_s}{2} - \Delta t_2 \tag{4.34}$$

where Δt_2 is the time that the stage 2 lasts. This period can be determined by recalling the equation (4.5) for the stage 2 $(t_1 \sim t_2)$ provided that at t_1 the resonant current reaches its minimum value $i_r(t_1)$, which equals $-I_{r_{max}}$. Recalling (4.5) :

$$-v_{C_r}(t) = v_{L_r}(t) \tag{4.35}$$

Using a linear approximation it may be rewritten for the instant t_2 as follows:

$$-V_{Cr_{avg}} = \left(L_r \cdot \frac{-i_r(t_1)}{\Delta t_2} \right) = L_r \cdot \frac{-(-I_{r_{\max}})}{\Delta t_2} \Leftrightarrow -V_{Cr_{avg}} = L_r \cdot \frac{4 \cdot I_{LEDs_{avg}}}{\Delta t_2} \tag{4.36}$$

Hence, Δt_2 can be obtained by re-organizing the previous equation:

$$\Delta t_2 = \frac{4 \cdot L_r \cdot I_{LEDs_{avg}}}{-V_{Cr_{avg}}} = \frac{4 \cdot L_r \cdot I_{LEDs_{avg}}}{-\left(-\frac{V_{LEDs_{avg}}}{2} \right)} = \frac{8 \cdot L_r \cdot I_{LEDs_{avg}}}{V_{LEDs_{avg}}} \tag{4.37}$$

Hereafter, the relations to determine the three required parameters were deduced and are shown in the following table:

$I_{r_{\max}} = 4 \cdot I_{LEDs_{avg}}$	$V_{Cr_{avg}} = -\frac{V_{LEDs_{avg}}}{2}$	$\Delta t_2 = \frac{8 \cdot L_r \cdot I_{LEDs_{avg}}}{V_{LEDs_{avg}}}$	$t_4 - t_2 = \Delta t_3 + \Delta t_4 = \frac{T_s}{2} - \Delta t_2$

Table E – Deduced parameters

Henceforth, the equation (4.32) can be rewritten as follows:

$$I_{r_{\max}} = 4 \cdot I_{LEDs_{avg}} = \frac{V_{in} - V_{Cr_{avg}} - V_{LEDs_{avg}}}{L_r} \cdot \left(\frac{T_s}{2} - \frac{8 \cdot L_r \cdot I_{LEDs_{avg}}}{V_{LEDs_{avg}}} \right) \tag{4.38}$$

Solving it in order to L_r and after a few simplifications, it is obtained the following relation:

$$L_r = \frac{(2 \cdot V_{in} - V_{LEDs_{avg}}) \cdot V_{LEDs_{avg}}}{32 \cdot f_s \cdot I_{LEDs_{avg}} \cdot V_{in}} \tag{4.39}$$

The required inductance values for both maximum and minimum dimming levels may be simply obtained from the previous equation by introducing the desired LED current value $I_{LEDs_{avg}}$ (and its corresponding voltage $V_{LEDs_{avg}}$). Thus, for maximum and minimum dimming levels, the variable inductance L_r should be in the range from **38.1 µH ~140.6 µH** (these values were obtained from a Mathcad program which was used to solve the previous equation and that may be found in Appendix A.1). With these values, and with the value of the resonant capacitor determined previously it is possible to determine the range of resonant frequency variation for the whole dimming range as shown below:

$$f_r = \frac{1}{2\pi\sqrt{L_r \cdot C_r}} \tag{4.40}$$

Thus, the resonant frequency ranges from ≈ 19.58 kHz to 37.61 kHz, which corresponds to the minimum and maximum dimming levels, respectively. Thereby, it is clear that the converter will not operate near resonance, as desired, ever since the switching frequency is set to 100 kHz.

4.3.3 Multi-Watt and Multi-output Operation

The term multi-Watt refers to a specific type of electronic device which is able to supply different loads of the same type without requiring any physical change in the hardware [80]. Under the circumstances of this work, the multi-watt property is a major advantage because it guarantees

that different LED modules, from different manufacturers, etc, may be connected to the driver without requiring any hardware change.

In terms of multi-output properties, a substantial advantage is the degree of freedom on the regulation of the outputs. Without requiring additional control circuits or components, all the outputs can be designed to provide, equal or different input/output voltage ratios, which, allied with the current control performed by the VI L_{r_n} results in independency on the regulation of each output; i.e., output 1 can be designed to be a *n*-step-up RSCC and output 2 a *n*-step-down RSCC, where *n* is the desired output/input voltage of each RSCC (as seen in the section 4.1). Thus, as previously mentioned, since we can design each output to provide a different voltage level, supplying a different amount of LEDs, LEDs with different electrical characteristics, different models, manufacturers and lots or also RGB-LEDs, will no longer be a problem [82]. An additional problematic which can be solved with this topology is the achievement of the branch currents equalization in multi-array LED lamps. To do so each LED branch should be connected to a different output and the current reference value shall be the same for each output. This strategy can also be applied to different LED lamps, for which a single lamp is connected to a different output.

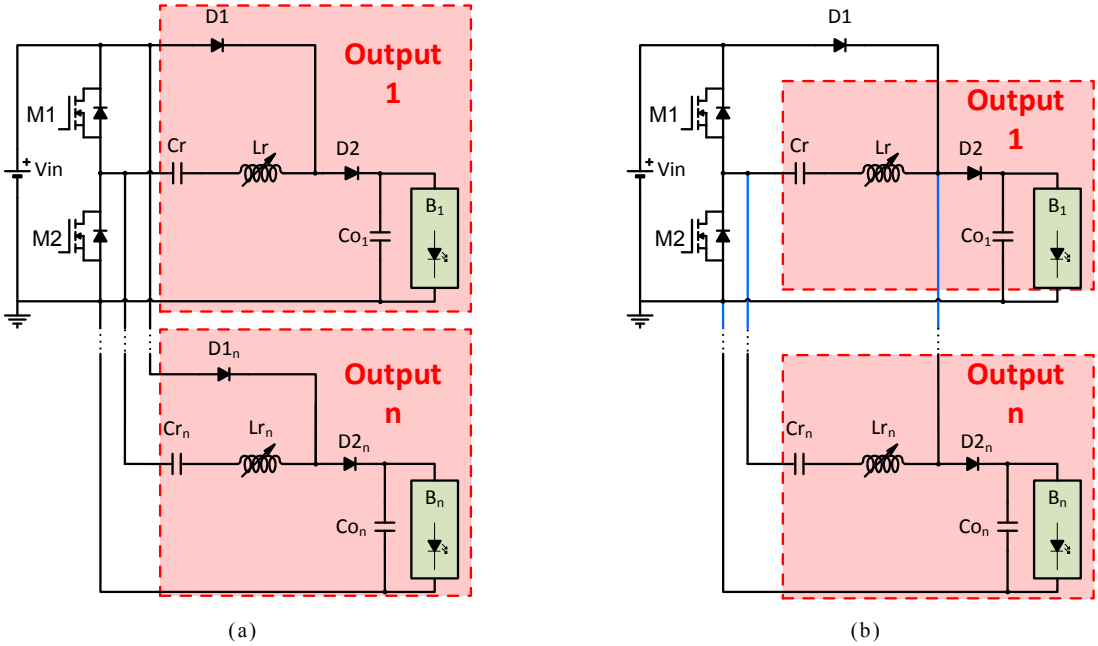

Fig. 4.10 - Multi-output Step-up RSCC. (a) Topology 1 (b) Topology 2

The Fig. 4.10 shows the Step-up RSCC in two possible multiple outputs version that can be simply achieved by cascading multiple cells, each represented within a red rectangle. It is important to note that each output cell can be exchanged, if desired, by another topology to achieve other output/input voltage ratios, i.e. step-down, 1:1 or fractional voltage ratios. The main difference between the two multi-output versions is the number of diodes *D1* used. Regarding

topology 1 a single diode $D1_n$ is used in each output cell while in topology 2 a single diode $D1$ is used whatever the number of output cells, and therefore, in the topology 2 the diode $D1$ has to support n times the current value which a diode $D1_n$ supports in the topology 1, where n is the number of output cells. Concerning the present work, the topology 1 was adopted.

4.3.4 VI - Bias Winding Control

Several solutions to control the bias winding (DC winding) of the VI could be employed. The most appropriate solution to control the bias winding is a *separated and regulated DC-DC converter using a microcontroller* (generally with a microcontroller it is ensured a lower component count). When operated under closed-loop control, the DC-DC converter ensures that the DC current at its output is maintained constant by compensating eventual changes in other parameters such as input voltage, load impedance, clock frequency, resonant elements, etc. Despite of the higher cost and component count, it is the most reliable, robust and flexible, not only because nowadays it is almost mandatory to use digital control, but also because it is possible to find DC-DC converters in literature, as well in the market, with more than 99% of power conversion efficiency. It is, in fact, the most efficient solution, especially when a proper design of the VI requires a low bias winding current to control a converter. The drawbacks of this solution are, once again, the increase on the cost and complexity, and a possible obstacle for some applications in which the space/volume available may be a restriction. The most advantageous types of DC-DC converters that might be used control the bias winding of the VI are the forward converter and the buck converter, as those employed in [13], if one desires to have galvanic isolation or not, respectively.

A simpler and alternative solution is the employment of commercially available simple *voltage regulators* (i.e. LM7805 and LM7815, 5 V and 15 V voltage regulators, respectively) as current regulators. Taking into account the very low level of power typically handled by the bias winding, even if the voltage regulator has a poor efficiency it will not have a significant impact on the efficiency of the whole system, thus making it a simple and cost effective solution. The major drawbacks of this solution are the restrictions/limits of these voltage regulators, for instance, their maximum input voltage limit is typically 40 V which means that under circumstances in which it is not possible to have a DC voltage lower or equal than 40 V this solution cannot be applied unless an extra converter is used to provide the necessary voltage value. This is the case of this work, since the only DC power source available provides 48 V DC, and for this reason this solution will not be further discussed.

From the point of view of the prototype testing, investigation and simplicity, in this work the separated DC-DC converter was not employed, and its role was fulfilled with a simple, *analogic voltage controlled current source*, previously employed in [82], which was developed using a few classic components and an external 5 V DC power source. The schematic of this solution is shown below:

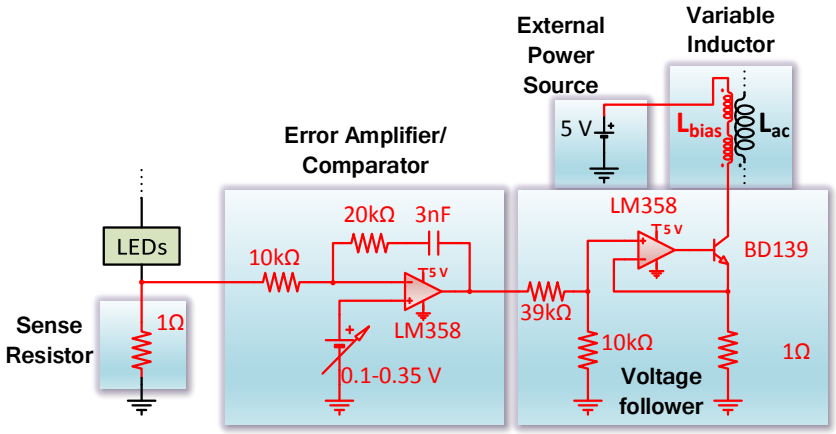

Fig. 4.11 – Voltage-controlled current source

The previous controller may be simply described: a sense resistor is used in series with the LEDs load and the compared to a reference which is imposed manually. The resultant error is then used in a voltage follower to ensure that the transistor, which is in series with the bias winding of the VI, will be working in the active region or by another words, as a voltage controlled source and not as a switch. The current needed (≈ 0 A - 0.4 A) by the bias winding is provided by means of a Yokogawa GS610 power source. As the LEDs current varies, the compensator actuates and the control current (in the VI's bias winding) is changed accordingly to maintain the LEDs current at the reference value. For instance, the higher control current, the lower the inductance of the AC winding and the higher the output voltage, current and power of the RSCC. As it will be seen ahead of this section, from the results obtained during practical experiments, the maximum power handled by the bias winding was of 0.21 W.

5 LED Driver and Simulation

PSIM software was selected to simulate the RSCC together with the VI and the LEDs lamp, because it is easy to use, fast and it has a flexible control representation. Even without prior experience with CAD software, one can build a circuit and obtain results in minutes while retaining excellent simulation accuracy. This makes it particularly desirable for simulation of power electronics converters systems when performing multiple-cycle simulation. The simulation tests conducted during this work where realized under closed loop conditions.

5.1 LED Modelling

In order to design the power converter properly, the LEDs load had to be modelled so that its characteristics can be described for different load conditions within the whole dimming range.

In the present work, is employed a simple LED model, developed by means of a multiple piecewise linear method as mentioned previously. The model is based on the superposition of the multi-branch equivalent circuit, in which branch is formed by a DC voltage source V_f, a series resistance R_f and an ideal diode, as described in the section 2.4.5.1, Fig. 2.18 (double piecewise linear approximation). The first step to develop a suitable model consisted on experimental tests, namely collecting several values of forward voltage for several current values on a single LED, with reference DRAGON Plus LCW W5AM.PC from OSRAM. According to the manufacturer this LED shall not be driven at lower current values than 0.1 A and the rated current value is 0.35 A [130], therefore the dimming range for the present work is selected to be comprised between these two values (0.1 A → 0.35 A), which will be used to assemble the piecewise linear model. The *I-V* curve of a single LED given by the manufacturer is shown in Fig. 5.1 (a) while the measured and simulated *I-V* curves are in Fig. 5.1 (b). The blue curve represents the experimental *I-V* values obtained with the tested LED and the *I-V* curve, composed by the green and violet line segments, represents the simulated, modelled and plotted curve for a single LED in PSIM. The relevant points from the measured curve are highlighted in red. They are used to determine the two-piecewise linear segments (simple double linear regression). In fact, for the selected dimming range the piecewise linear approximation would be required only in the interval comprised between the points V_{F1} and V_{F2} in the Fig. 5.1 (b), however, the process is realized considering the interval comprised between V_{F0} and V_{F3}. This approach is adopted because a built-in linear LED model in PSIM is used for simulation and it requires only two input values, namely the LED threshold voltage V_f and the equivalent dynamic resistance R_D.

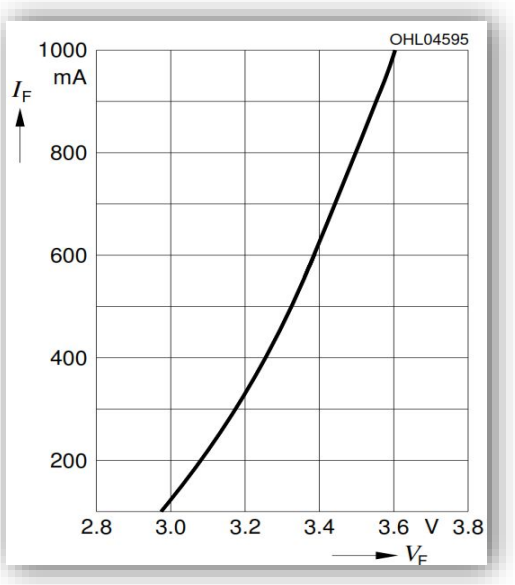

(a) Dragon Plus from the manufacturer's datasheet

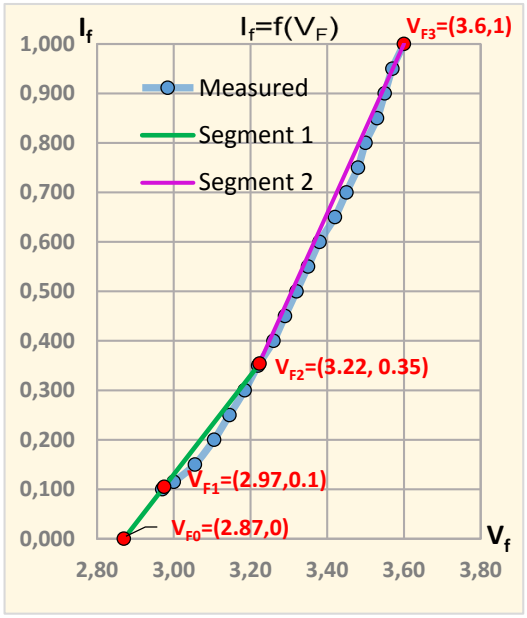

(b) Measured Dragon Plus and Simulated in PSIM

Fig. 5.1 - I-V characteristic of the LEDs

After selecting the points on the measured curve (V_{F1}, V_{F2} and V_{F3}) the model curve is calculated using the process described in the section 2.4.5.1. Firstly the required values of V_f and R_D, correspondent to the green line segment in the previous figure, are calculated. Afterward the same process is applied to obtain the violet line segment. The design and description of this model is fully described in the Appendix B.1, from which the following results were obtained:

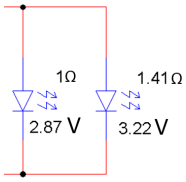

Fig. 5.2- PSIM single LED model

V_{F0}	2.87 V	I_{F0}	0 A		
V_{F1}	2.97 V	I_{F1}	0.10 A	r_1	1 Ω
V_{F2}	3.22 V	I_{F2}	0.35 A	r_2	1.41 Ω
V_{F3}	3.60 V	I_{F3}	1 A		

Table F – Two piecewise linear model parameters

In the Fig. 5.2, is shown the resulting model for a single LED based on the calculated values presented in the previous table. A final comparison of the plotted curve from simulation (green and violet lines in Fig. 5.1 (b)) with the measured curve of a real LED (blue curve in Fig. 5.1 (b)) shows a good agreement between simulation and real world results. A quite acceptable level of accuracy is achieved, thus guaranteeing that simulation will be reasonably approximate to the real behaviour of real LEDs when connected to the converter and neglecting any temperature variation secondary effects.

5.2 Variable Inductance Modelling

Simulation is particularly useful when we are dealing with a non-linear behaviour that cannot be easily handled analytically, which is our case. Being the VI non-linear, it may highly

affect some parameters of the converter such as the inrush current, magnitude of the load current ripple, small signal transfer functions and others.

In this work the simulation software used to model the magnetic regulator was the same used to simulate the converter - PSIM, which has a non-linear magnetic core model. However its adaption to our specific application and available magnetic cores proved to be very frustrating if not practically impossible. For this reason a simple and dynamic model of the VI, very similar to the one employed in [131], was developed in PSIM and its schematic is shown below:

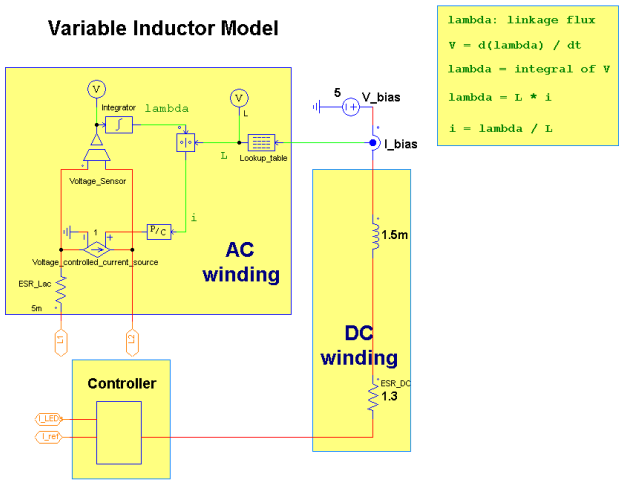

Fig. 5.3 - Model of the VI

The model is based on the small-signal characteristic of the VI built experimentally in this work which was obtained after carrying out some experimental measurements following the measurements setup present in the section 6.1. The resulting model is by no means perfect, namely because it does not include core losses, temperature effects, air gaps effect, frequency dependence of the permeability, the hysteresis effect along with others. Nevertheless, it is indispensable for the simulation analysis of its application on the LED driver designed in this work. More details concerning the model may be found in the Appendix B.2.

5.3 Simulation Results

The main steady-state waveforms of the converter, obtained by the simulation, may be observed from Fig. 5.4 to Fig. 5.9. To avoid being repetitive, the most relevant observations regarding those six figures, are introduced, by comparison with experimental results, in the section 6.2.1 due to the very good agreement verified between simulation and experimental results. In addition, from the results shown in Fig. 5.10 and Fig. 5.11, it is noticeable a very good and fast response regarding stability/performance of the system when the faulty/undesired events were simulated. Furthermore, and most importantly, from the results shown in Fig. 5.12 and Fig. 5.13,

it is proved that current on each LED string current is regulated independently and efficaciously, i.e. regulation of a string current does not have impact on the other string current.

Maximum dimming level ($I_{LEDs} = 0.35$ A)	***Minimum dimming level*** ($I_{LEDs} = 0.1$ A)
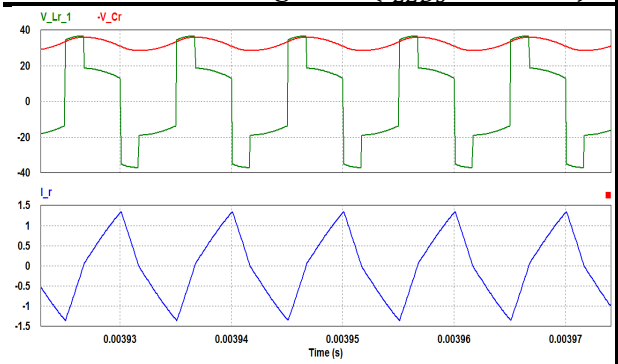	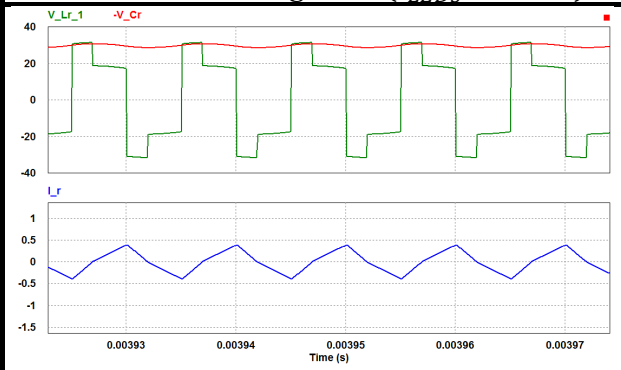
Fig. 5.4 – VI voltage, resonant capacitor voltage (inverted polarity) and resonant tank current (green, red and blue waveforms, respectively)	Fig. 5.5 - VI voltage, resonant capacitor voltage (inverted polarity) and resonant tank current (green, red and blue waveforms, respectively)
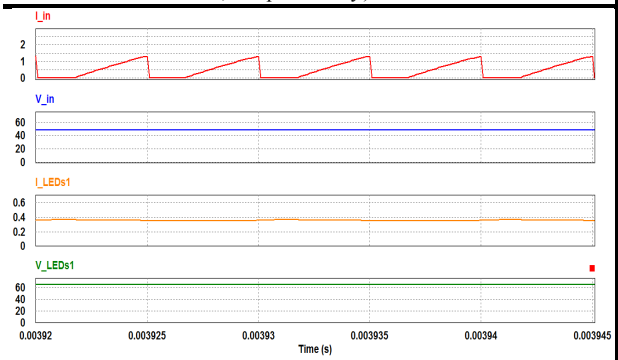	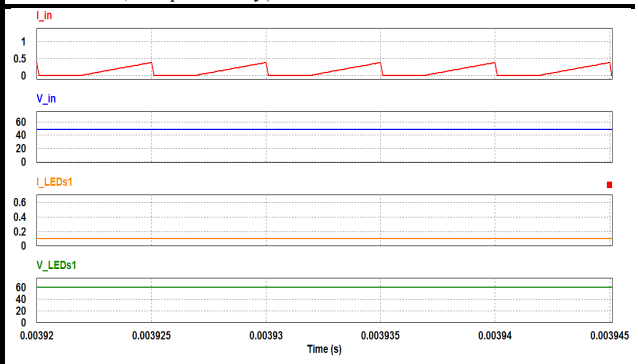
Fig. 5.6 – RSCC input current and voltage, and LED string 1 current and voltage (red, blue, orange and green waveforms, respectively)	Fig. 5.7 - RSCC input current and voltage, and LED string 1 current and voltage (red, blue, orange and green waveforms, respectively)
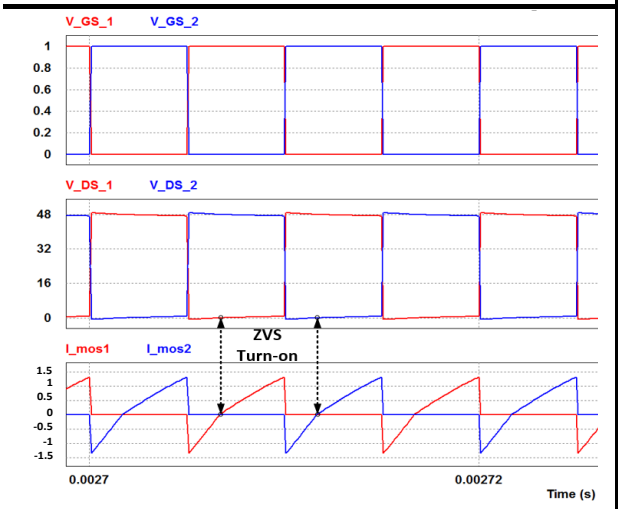	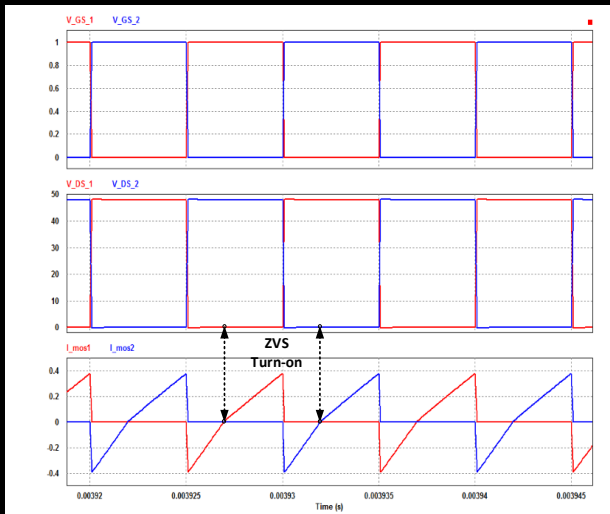
Fig. 5.8 - Mosfets ZVS turn-on: gate-source voltages, drain-source voltages and drain-source currents, respectively	Fig. 5.9 - Mosfets ZVS turn-on: gate-source voltages, drain-source voltages and drain-source currents, respectively

RSCC Dynamic response

Simulation results regarding the dynamic behaviour of the RSCC when it is set to work at nominal conditions, are shown as follows:

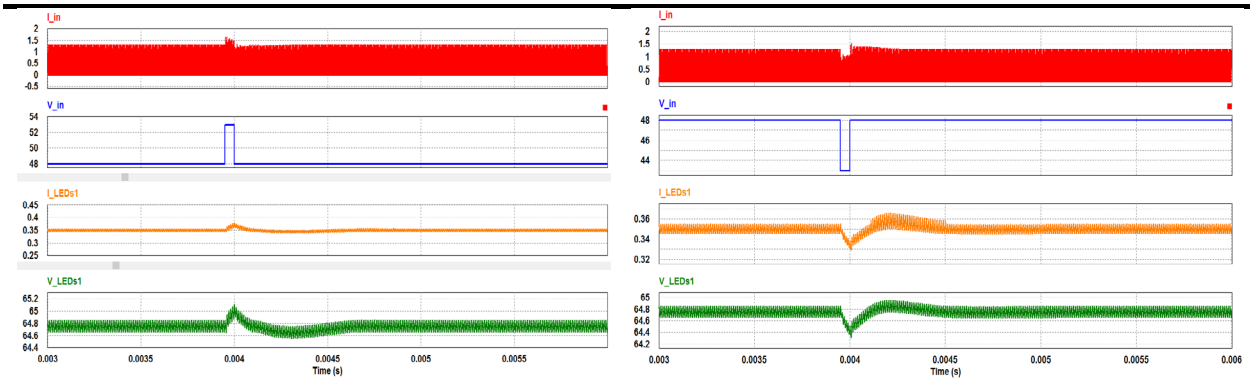

(a) (b)

Fig. 5.10 - Dynamic response of the RSCC: Input current and voltage (red and blue waveforms, respectively), and LED string 1 current and voltage (orange and green waveforms, respectively) (a) during a step in the input voltage of 5 V, 0.05 *ms*, (b) during a step in the input voltage of -5 V, 0.05 *ms*

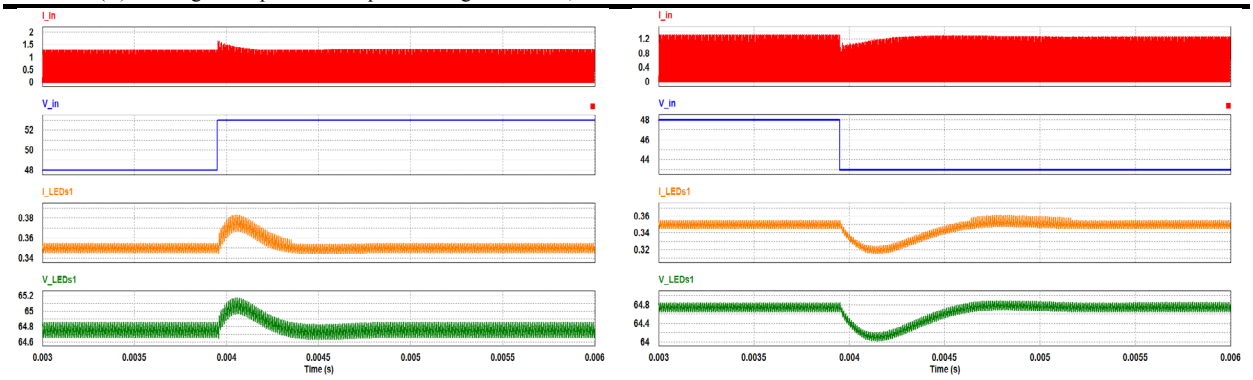

(a) (b)

Fig. 5.11 - Dynamic response of the RSCC: Input current and voltage (red and blue waveforms, respectively), and LED string 1 current and voltage (orange and green waveforms, respectively) (a) during a step-up in the input voltage of from 48 V to 53V (b) during a step-down in the input voltage from 48 V to 43 V

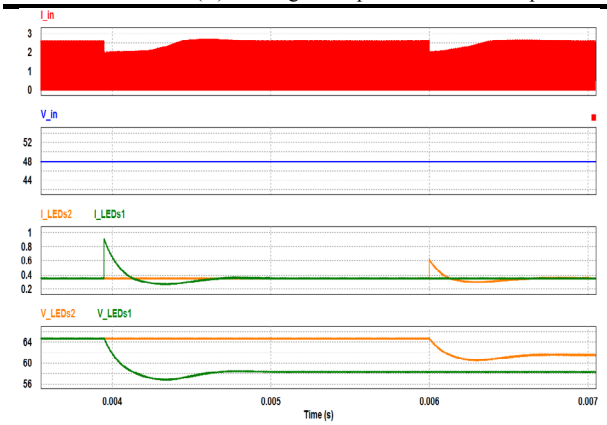

Fig. 5.12 - Dynamic response of the RSCC: Input current and voltage (red and blue waveforms, respectively), LED strings 1 and 2 currents (3rd graph - green and orange waveforms, respectively) and LED strings 1 and 2 voltages (4th graph - green and orange curves, respectively), where the output voltage of string 1 was decreased 6.4 V by short-circuiting two LEDs and output voltage of string 2 was decreased 3.2 V by short-circuiting one LED

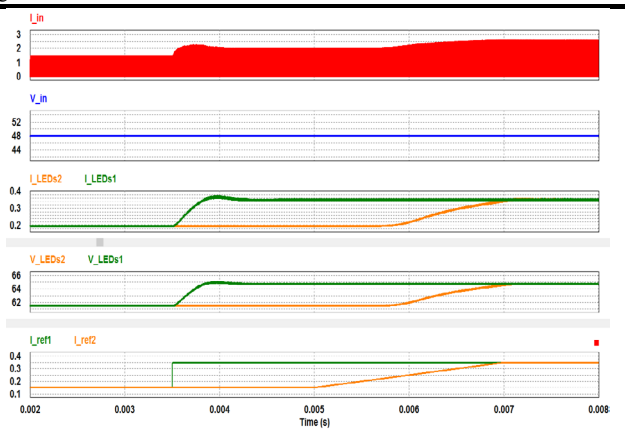

Fig. 5.13 - Dynamic response of the RSCC: Input current and voltage (red and blue waveforms, respectively), LED strings 1 and 2 currents (3rd graph - green and orange waveforms, respectively), LED strings 1 and 2 voltages (4th graph - green and orange waveforms, respectively) and output current references 1 and 2 (5th graph - green and orange curves, respectively) varied from 0.1 A to 0.35 A by means of a step-up and a 2 *ms* ramp, respectively

The dynamic behaviour of the RSCC to a SC[9] in the load, and to a variation in the output current reference (for a step and for a ramp) can be seen in Fig. 5.12 and Fig. 5.13, respectively.

[9] ***SC*** – *Short-Circuit*

6 Practical Prototype Implementation and Results

To verify and validate the both theory and simulation described in the previous sections, a prototype was built. It includes a LED lamp, two VIs and the RSCC together with all control components, which were all designed and built from scratch. The full schematic of the experimental prototype assembled is shown in the following figure

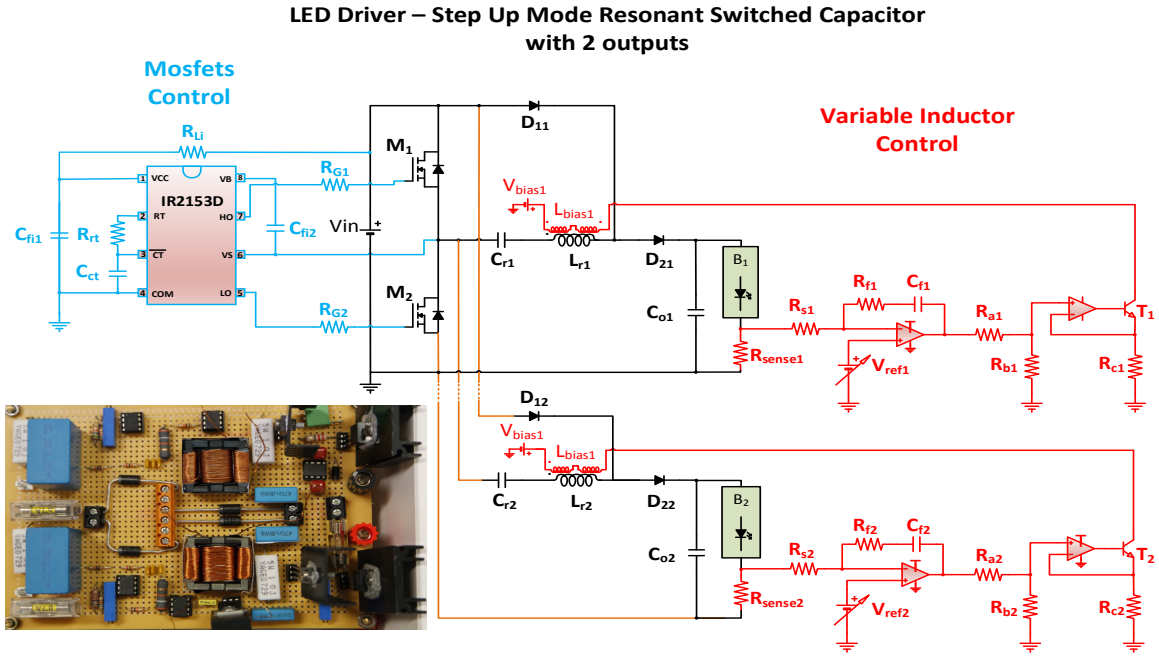

Fig. 6.1 - General schematic, and experimental prototype built

Full details and illustrations regarding practical implementation can be found in Appendix C.

6.1 Variable inductance

For the prototype built were selected EFD25 cores with N87 material by Siemens and an air gap of 0.6 mm (based on laboratory availability). As usual, two DC control windings, with the same number of calculated turns, were mounted in the lateral legs of the core and serially connected in anti-polarity. For the main winding corresponding to the AC resonant inductor, its number of turns was calculated and then mounted in the centre leg in order to have the required variable inductance range. To proceed with the variable inductors construction it was necessary to follow a design procedure, described ahead. The design was done considering that the AC winding should have an inductance variation between 38.1 µH and 140.6 µH (from the RSCC analysis addressed in section 4.3.2.3).

VI: Simplified Design Procedure

The VI design procedure used in this work, the same employed in [13], begins by selecting the core type and dimensions and the desirable variable inductance range. The approach used is, in fact, a simplified approach, based on approximated effective parameters given in datasheets of typically used magnetic cores, by manufacturers. As initial conditions it is established that a maximum AC inductance value should be obtained for a zero DC control current, $L_{ac\_max} \rightarrow I_{dc=0}$ and thereby, the minimum AC inductance value should be obtained for a maximum value of DC control current, $L_{ac\_min} \rightarrow I_{dc\_max}$.

The maximum AC inductance value can be obtained using the classic inductor equation and simplified approach as follows:

$$L_{ac\_\max} = \frac{N_{ac}^2}{\mathcal{R}} = \frac{N_{ac}^2}{\frac{l_e}{\mu_r \cdot \mu_0 \cdot A_e} + \frac{g}{\mu_0 \cdot A_e}} \tag{6.1}$$

Where N_{ac} is the number of turns in the centre leg, $\mathcal{R}$ is the global reluctance of the magnetic circuit as seen from the ac winding, $A_e$is the effective magnetic cross section expressed in $[m^2]$, l_e is the effective magnetic path length expressed in $[m]$, g is the air gap expressed in in $[m]$ and μ_0 is the permeability of the vacuum. In (6.1) μ_r is the relative permeability of the core material, which in this situation is equal to the initial permeability[10]. This parameter can be found in the cores datasheet as well as the parameters A_e, g and l_e.

A constraint, which the design of the VI should obey, is the permissible peak value of the AC current flowing through the main winding I_{ac_max}, for which is desirable to operate the core at the peak value of the AC magnetic flux density B_{max}, which in turn should be agree with the following relation [13]:

$$B_{\max} \approx 0.1B_{\text{sat}} \rightarrow 0.3B_{\text{sat}} \tag{6.2}$$

The main goal of the simplified design procedure is to obtain the number of turns of each winding N_{ac} and N_{dc}, and may be described as follows:

Firstly it is selected the core, particularly the EFD25 core due to laboratory availability, and its parameters A_e, g and l_e are identified. The next step is to set the required maximum inductance value, which shall be slightly higher than the value given by the RSCT design

[10] ***Initial permeability****: permeability of a demagnetized magnetic material (for low values of B)*

procedure (corresponding to $I_{dc} = 0$). For this case, the peak value of the AC magnetic flux density can be easily calculated, using the peak value of the AC current I_{ac_max} as follows:

$$B_{\max} = \frac{N_{ac}^2}{\mathcal{R} \cdot A_e} \cdot I_{\text{ac\_max}} \tag{6.3}$$

Using (6.2) and the selected value of L_{ac_max}, (6.3) may be re-written as follows:

$$N_{ac} = \frac{L_{\text{ac\_max}} \cdot I_{\text{ac\_max}}}{B_{\max} \cdot A_e} \cdot \tag{6.4}$$

which will give the number of turns for the AC winding. Thereby, the air gap value g can be obtained as follows:

$$g = \frac{\mu_0 \cdot N_{ac}{}^2 \cdot A_e}{L_{\text{ac\_max}}} - \frac{l_e}{\mu_r} \tag{6.5}$$

The diameter, d_{ac} of the wire for the main winding may be selected using the following relation, obtained from the density current formula:

$$\delta = \frac{Iac\_\max}{S} = \frac{Iac\_\max}{2\pi \cdot r_{ac}^2} = \frac{Iac\_\max}{2\pi\left(\frac{d_{ac}}{2}\right)^2} \Leftrightarrow d_{ac} = \sqrt{\frac{4 \cdot Iac\_\max}{\pi \cdot \delta}} \tag{6.6}$$

Where δ is the selected current density expressed in $[A/m^2]$, S is the area of the wire's cross section expressed in $[m^2]$ and r_{ac} the respective radius expressed in $[m]$.

Regarding the wire of the DC winding, its diameter d_{dc} can be obtained as follows:

$$d_{dc} = \sqrt{\frac{4 \cdot Idc\_\max}{\pi \cdot \delta}} \tag{6.7}$$

Concerning the total winding occupation area A_w, composed by the AC and DC windings occupation area, it can be calculated as follows:

$$A_w = N_{ac} \cdot \pi \cdot \left(r_{ac}\right)^2 + N_{dc} \cdot \pi \cdot \left(r_{dc}\right)^2 = N_{ac} \cdot \pi \cdot \left(\frac{d_{ac}}{2}\right)^2 + N_{dc} \cdot \pi \cdot \left(\frac{d_{dc}}{2}\right)^2 \tag{6.8}$$

The available area for the windings can be defined as $K_u \cdot W_a$, where W_a is the core window area and K_u is the window utilization factor or fill factor. In the present case (EFD cores) W_a is considered as the area on one of the sides as the following figure illustrates:

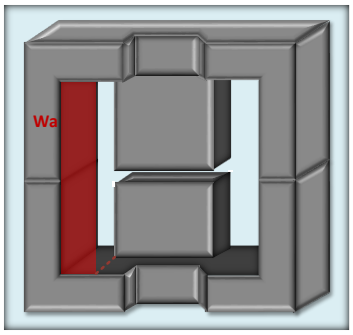

Fig. 6.2 - Double EFD core - window area

To fit the windings into the core window the following constraint must be obeyed:

$$K_u \cdot W_a \geq A_w \tag{6.9}$$

where a typical value of K_u is 0.4 [132-135].

To estimate the number of turns of each control winding N_{dc}, we shall consider that the external path of the EFD25 cores assembly must reach saturation at a stipulated maximum value of the DC control current. Thus the following relation takes place:

$$\phi_{dc} \cdot \mathcal{R}_{ext} = 2 \cdot I_{dc\_mac} \tag{6.10}$$

where $\mathcal{R}_{ext}$ is the reluctance of the external path of the core. Considering I_{dc_max} the maximum value of the DC control current for which the minimum AC inductance value is obtained, the N_{dc} can be obtained by re-writing (6.10) as follows:

$$N_{dc} = \frac{1}{2} \cdot \frac{k \cdot B_{sat} \cdot l_{ext}}{\mu_{kB_{sat}} \cdot \mu_0 \cdot I_{dc\_\max}} \tag{6.11}$$

where l_{ext} is the length of the external path of the core, $k.B_{sat}$ is the flux density in the external path due to I_{dc_max} for a zero AC current, and $\mu_{B_{sat}}$ is the permeability of the core material at the mentioned conditions. Therefore, for I_{dc_max} the core is expected to be near saturation, which means that the permeability value should be in fact the permeability of the core at that point. The value of k may be selected to be 80% [13].

To build-up the variable inductor, the previously described design procedure of the VI was solved using a Mathcad program, shown in Appendix A.2, and the results are as follows:

	N_{dc}	N_{ac}
Turns	**2 * 71.18**	**35.14**
Cross Section	**0.357mm**	**0.618**

Table G – Windings characteristics

According to the design procedure, the calculated parameters were 2x71 turns and 35 turns for the DC windings and AC winding, respectively. More details regarding the construction of the VIs may be found in Appendix C.2. The presented simplified design procedure represents only a brief summary of the VI, since it is, in fact, a simplified and approximated approach. Nevertheless, as the results will show, it is probably the best approach since it is not very complex, does not require a deep analysis on magnetic theory and the practical prototypes show a good agreement with theoretical predictions.

Small-signal characterization

To verify the effectiveness of the VIs a first approach consisted on measuring their small-signal characteristic. Small-signal characteristics are usually used to evaluate the dynamic response and stability of one determined system. As it will be found posteriorly, due to several reasons, small-signal characterization might not be enough to fully characterize the behaviour of the VI. The small-signal characteristic of the VI is nothing else than its AC winding inductance as function of the DC control current applied in the bias/control winding. In order to obtain the values of the AC winding inductance a BK Precision 889A Bench LCR/ESR Meter was used. This meter supplied the AC winding with 1 V rms at 100 kHz, while the DC current of the bias winding was provided and measured using a Yokogawa GS610 power source, as the following measurement setup illustrates:

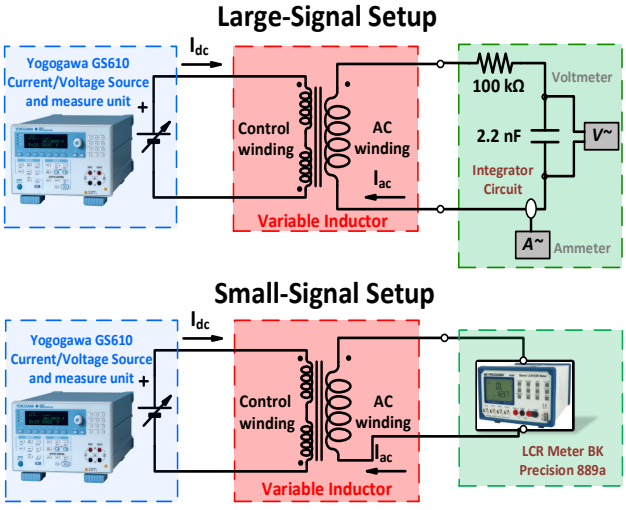

Fig. 6.3 - VI: Small-signal and large signal measurement setup

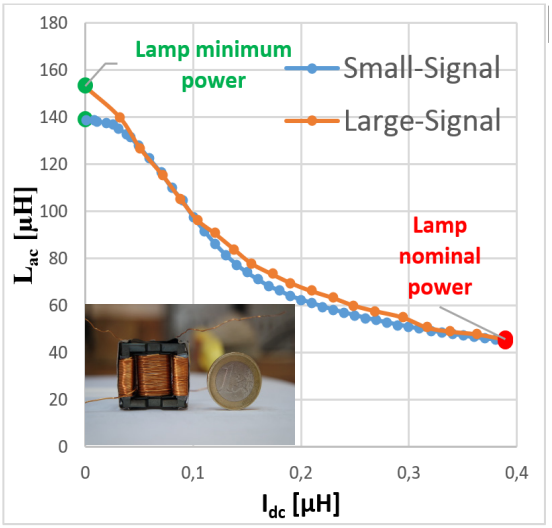

Fig. 6.4 – VI 1 small-signal vs large-signal characteristics

The results obtained in experimental measurement tests are shown on the curve from the Fig. 6.4. It is clearly visible the effect of the cores saturation at DC current values slightly higher than 0.4 A, i.e. a further increase on the DC current will not have a significant impact on the inductance of the AC winding. In addition, as mentioned earlier, the small-signal characterization

might not be enough to validate the effectiveness of the magnetic regulator because it is not made under the operating conditions of the VI. The problem is the nonlinearity of the VI's inductance because it can operate in saturation or near the saturation region while the total AC flux does not vary linearly with the resonant current [13, 110]. Thus, a second approach shall be selected: the large-signal characterization, which is presented and discussed in next section.

Large-signal Characterization

To obtain the large-signal characteristic, the VIs needed to be tested under operating conditions, in this case within the RSCT prototype developed in this work. The first step to obtain the large-signal characteristic is to create a method to determine the average AC inductance for each operating point. Thus, the method selected consisted on a simplified approach using a peak-to-peak based inductance model while the LEDs current was varied. This approach is accomplished by means of an integrator circuit composed by a 100 *k*Ω resistor *R* and a 2.2 *nF* capacitor *C*, a voltmeter, an ammeter and a DC power source as shown in Fig. 6.4. The ammeter is used to measure the current flowing in the AC windings of the VI, and the voltmeter the voltage on the integrator circuit capacitor. The integrator is used to estimate the flux linkage measured through the AC winding using the relations presented in Appendix D as follows:

$$L_{ac} = \frac{\Psi(t)}{i(t)} \rightarrow L_{ac} = \frac{N_{ac} \cdot \phi_{ac,pp}}{i_{ac,pp}} = \frac{\Psi_{ac,pp}}{i_{ac,pp}} \tag{6.12}$$

Setting v_c as the integrator-capacitor voltage and $v_{L_{ac}}$ as the VI voltage we have:

$$v_{L_{ac}} = L_{ac} \frac{di_{ac}}{dt} = \frac{d\Psi_{ac}}{dt} \tag{6.13}$$

if $R >> X_c$:

$$v_c \cong \frac{1}{R \cdot C} \int v_{L_{ac}} \tag{6.14}$$

where X_c is reactance of the integrator-capacitor. Using the previous stated relations we obtain:

$$\Psi_{ac} = N_{ac} \cdot \phi_{ac} = R \cdot C \cdot v_c \tag{6.15}$$

substituting (6.15) into (6.12) we obtain the final relation that gives us the inductance value:

$$L_{ac} = \frac{R \cdot C \cdot v_{c,pp}}{i_{ac,pp}} \tag{6.16}$$

Subsequently, the AC inductance value may be simply obtained by multiplying the constants *RC* with the measured peak-to-peak voltage of the integrator capacitor and then dividing it by the measured peak-to-peak value of the AC resonant current. Below are shown the corresponding waveforms obtained for minimum and maximum dimming levels:

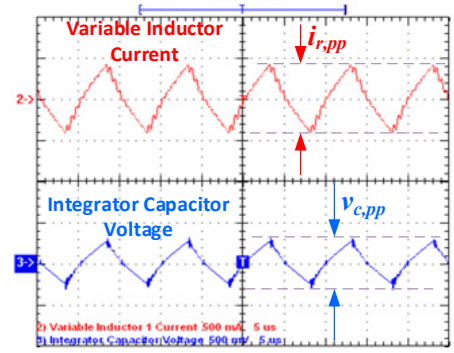

Fig. 6.5 – VI current and integrator capacitor voltage, 0.5 A/div, 500mV/div, /div, Ch. 2, 3, respectively, 5 µs/div, at minimum dimming conditions

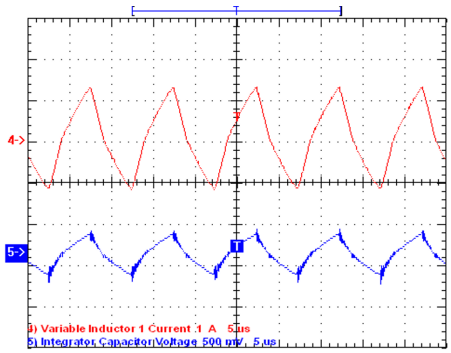

Fig. 6.6 – VI current and integrator capacitor voltage, 1 A/div, 500mV/div, /div, Ch. 4, 5, respectively, 5 µs/div, at minimum dimming conditions

Small-signal vs Large-signal Characterization

Theoretically, by comparison with small-signal characterization, large-signal characterization should result in lower inductance values due to higher saturation level reached in cores, since for this case there is, not only the contribution of the flux produced by the bias winding, but also the contribution of the flux produced by the AC winding. Though, from Fig. 6.4 it is, indeed, clear that there is not a perfectly good agreement with what was stated. Nonetheless, there is only a minimal difference between both signals across the whole range. Thus, it is confirmed and validated that small-signal characteristic shall be a very reasonable approach to start the simulation of the VIs integrated in power electronics converters in this particular situation and similar ones. Naturally, if high precision is required, it should be performed a large-signal characterization of the VI, however it may be a compromising approach because, generally, it is not possible to obtain this type of characterization before the VI is tested within the power electronics converter.

6.2 Full Driver Assembly

The full Driver assembly adopted for the practical experimental was already shown in the schematic present in Fig. 6.1. Photos from the prototype may be found in Appendix C.3. The selected input voltage V_{in} of 48 V DC is provided by means of a batteries bank, namely four 12 V batteries connected in series. The control for the power Mosfets, i.e. duty-cycle and switching frequency, were provided by the integrated circuit IR2153D and its design procedure is briefly presented in Appendix C.3. All tests were conducted under closed loop conditions.

6.2.1 Experimental Results and Comparison with Simulation

Due to the high similarity between results on both LED outputs, only the results concerning a single LED output (string) are presented. Therefore, a few of the resulting waveforms, concerning the LEDs string 1, are shown below:

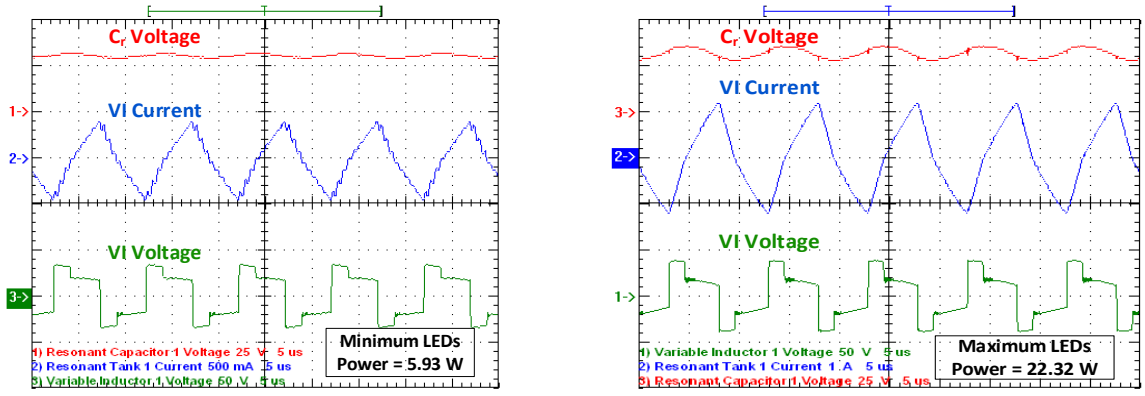

(a) (b)

Fig. 6.7 - Resonant capacitor voltage (inverted polarity), resonant current and VI voltage, respectively, 5 µs/div. (a) At minimum diming level conditions, 25 V/div, 0.5 A/div, 50 V/div, Ch. 1, 2, 3, respectively. (b) At maximum diming level conditions, 25 V/div, 1 A/div, 50 V/div, Ch. 3, 2, 1, respectively.

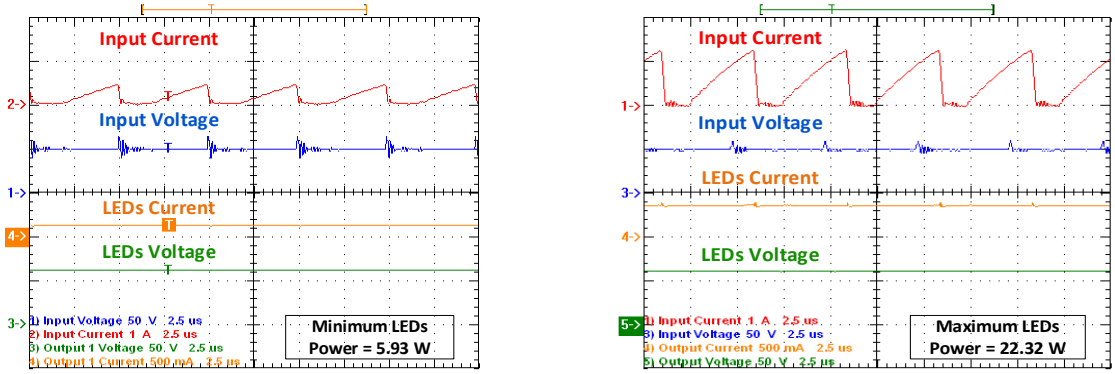

(a) (b)

Fig. 6.8 - Input current and voltage, and LEDs branch current and voltage, 1 A/div, 50 V/div, 0.5 A/div, 50 V/div, respectively, 2.5 µs/div. (a) At minimum diming level conditions, Ch. 2, 1, 4, 3, respectively. (b) At maximum dimming level conditions, Ch. 1, 2, 3, 4, respectively

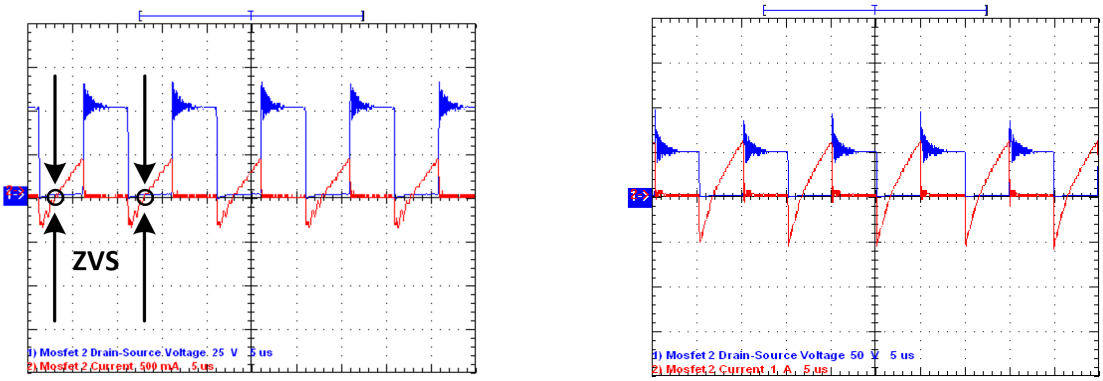

(a) (b)

Fig. 6.9 - Mosfets turn-on ZVS, drain-source voltage and current (blue and red waveforms, respectively) (a) 25 V/div, 5 µs/div, for minimum dimming level (b) 25 V/div, 50 µs/div, for maximum dimming level

The remaining waveforms gathered, are presented in Appendix C.3 due to their lower relevance.

Simulation vs Experimental Results

Comparing the results presented in Fig. 5.4 to Fig. 5.9, corresponding to the practical results shown in Fig. 6.7 to Fig. 6.9, a very good agreement is clearly noticed between simulation and practical results, thus validating the proposed simulation model as a very good approximation of reality. Regarding the first pair of figures for both simulation (Fig. 5.4 and Fig. 5.5) and experimental waveforms (Fig. 6.7), which show the main parameters of the resonant circuit for the two extremes of the dimming range, it is noticeable the change in the amplitude of the resonant current, which confirms the theoretical prediction and validates the main objective of this work. With regard to the voltage on both elements of the resonant tank (capacitor and VI), it might be observed a slight change on their shape but it is not significant/relevant. In terms of resonant current, its shape is not very sinusoidal due to the fact that the resonant frequency is a few times smaller than switching frequency, thus it presents highly linear ramps that build up a triangular waveform. Concerning the second pair of figures (simulation - Fig. 5.6 and Fig. 5.7; experimental - Fig. 6.8), which show input and output voltages and currents, it is clear the change in amplitude on both input (red waveform) and output current (orange waveform), where the former presents a very good DC shape, practically without ripple, which constitutes a major benefit for LEDs to the extent of ensuring their proper operation conditions in order to, not only to preserve their rated life time but also to eliminate any flickering possibility. The output voltage, obviously, also features a very good DC shape, but in terms of amplitude it does not change significantly across the whole dimming range, which agrees with the characteristic behaviour of LED loads. The only simulation result that slightly differs from the experimental result, is the input voltage, which presents some ripple during every switching transition of the Mosfets. This is simply justified by the fact that during practical experiments the input voltage was provided directly by batteries, which have no specific mechanism to regulate voltage, nevertheless this issue is not critical for the present work.

Concerning the last pair of figures (simulation – Fig. 5.8 and Fig. 5.9; experimental - Fig. 6.9, where are shown Mosfets voltage and current (drain-source), it is confirmed the ZVS operation of Mosfets over the whole dimming range (the two extremes cases are presented). Moreover, there is a very good agreement between simulation and experimental results. Nevertheless, it is noticeable some ringing ripple in the voltages, which could be reduced using a snubber[11], however because it is not very problematic, and since it would require a really careful design and study, no snubber was employed. Besides, a snubber also introduces power losses, thus

[11] ***Snubber****: device used to supress some phenomenon, for instance voltage transients.*

it should be applied only when it is strictly required/mandatory, and therefore the application of the snubber in this converter is expected to be addressed only in future work.

In Fig. 6.10 are drawn the large-signal characteristics of both VIs (orange and green curves), where, as desired, it is clear the impact of the bias current on the AC winding inductance, thus validating the performance of the VIs. Based on the VI theory, the serial connection of the two side arm windings (which compose the bias winding) should cancel out the voltage induced, by the AC winding, on each of them because those induced voltages have, under the assumption of symmetry (ideally), opposite polarities which means that the AC winding would not influence the bias winding. However, as verified in fig Fig. 6.10, that is not what effectively happens, since it is slightly clear a non-linear coupling between bias current and AC inductance. This is mostly due to the non-linearity of the magnetic material [110], and in some cases it may also be due to eventual imperfections in the assembling of the VI since, particularly when made by hand. Nonetheless, the performance of the VIs on the RSCC might be validated by simply observing the blue and red curves in Fig. 6.10 (LED string 1 and 2 average power, respectively) which show a highly linear relation between the LED strings average power and the control/bias current.

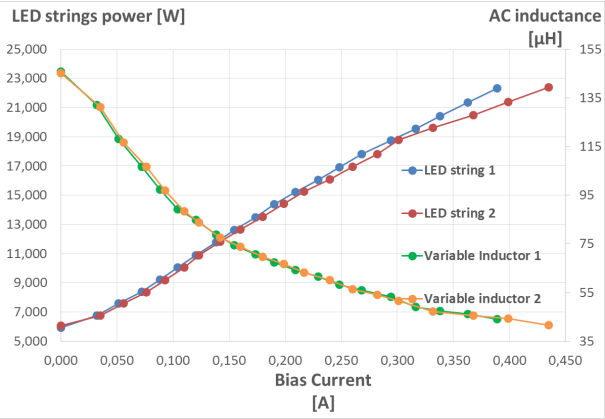

Fig. 6.10 - LED strings power vs VI bias current (blue and red waveforms), and VI's AC inductance vs bias current (yellow and green waveforms)

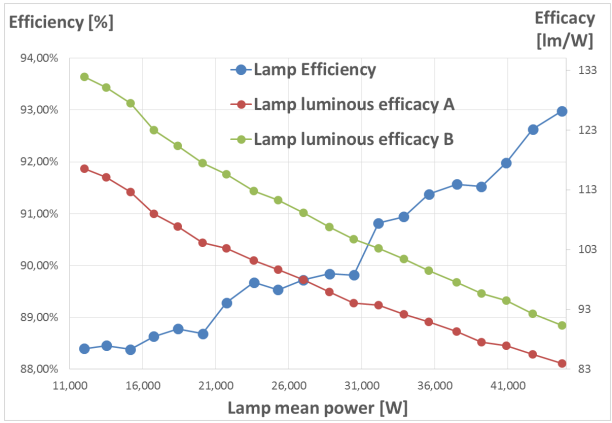

Fig. 6.11 - Lamp Efficiency vs load (LEDs) mean power and Lamp luminous efficacy vs load (LEDs mean power

With concern to the overall prototype, from the Fig. 6.11 it is, indeed, clear that the RSCC controlled by the VI features a very good performance over the whole expected dimming range: the electrical conversion efficiency of the RSCC, calculated from (6.17), ranges from 88.40% to 92.98% for the lamp mean output power ranging from 11.99 W to 44.72 W (blue curve in Fig. 6.11).

$$\eta = \frac{P_{LEDs_{avg}}}{P_{in_{avg}}} = \frac{\left(V_{LEDs1_{avg}} \cdot I_{LEDs1_{avg}}\right) + \left(V_{LEDs2_{avg}} \cdot I_{LEDs2_{avg}}\right)}{V_{in_{avg}} \cdot I_{in_{avg}}} \tag{6.17}$$

Regarding the power losses, introduced to the system by the bias winding, they may me estimated using the following relation:

$$P_{DC\_losses} = R_{DC} \cdot I_{dc}^{\ 2} \tag{6.18}$$

where R_{DC}, equal to 1.29 Ω , is the measured resistance of the bias winding at 100 kHz and I_{dc} the maximum bias current, for maximum dimming level, which equals 0.4 A, thus the maximum bias winding power losses equal ≈ 0.21 W. Based on input and output power, in order to validate the proposed dimming technique, the luminous efficacy (luminous flux per power consumed) of the lamp was estimated. For this purpose it was measured the illuminance of the lamp and then converted to the equivalent luminous flux. The process used to determine the luminous efficacy is described in the Appendix C.4. With the data gathered and determined the luminous efficacy curves were obtained, and are shown in Fig. 6.11, where the red and green curves show the luminous efficacy regarding the lamp average input power and lamp average output power, respectively.

Conclusions and Future Work

Conclusions

Based on the respective merits of the VI control on the RSCC, a new cost-effective dimmable LED driver was proposed. The driver offers, not only the possibility to perform dimming over wide ranges, as shown, but also currents equalization in multiarray based LED lamps.

The main circuit operation was briefly analysed, simulation and practical experiments were conducted in order to validate the theoretical analysis, the effectiveness and feasibility of the converter as well as goals for this work.

The full model developed in PSIM was found to reproduce faithfully the behaviour of the RSCC with the VI in the practical application, thus the model might be easily extended, for instance, to VIs with separate DC bias windings, to characterise the non-linearity of the magnetization Inductance of transformers [13], as well as current equalization for RGB based LED lamps, etc.

The proposed technique has the advantage of using a non-dissipative element to regulate the current through the LEDs, thus providing high efficiency, as the results show: an efficiency of the RSCC prototype in the range of 88.4% to 92.98% was verified over the whole dimming range (≈ 30 % to 100% for average input power ranging from ≈ 14 W to 48 W), with the Mosfets featuring ZVS during turn-on transitions while switching frequency and duty-cycle are maintained constant, thus reducing switching losses and EMI.

The proposed topology (RSCC with VI), in comparison to existing topologies, might be considered less costly, not only because it is simple and with fewer component count, while ensuring robustness, but also due to the relative ease of control and because the switches and measurements (by the control sensors) are implemented at the same reference point [73], thus avoiding the need for further control components and techniques. Moreover, unlike most of topologies available, this topology does not require an inductive output filter, which reduces, beneficially and considerably, the driver size/volume.

In addition to the proposed LED driver, a special care was taken, during this work, to modelling, design, and small-signal and large-signal characterization of the VIs. This analysis has proved, not only, how important it is to model the VI, but also shows its good performance and flexibility, whether applied to LED lamp drivers or potentially new and different applications/technologies.

Future Work

The main focus of this work was, not only to investigate the application of a new dimming technique, namely the VI control, for LED lamps, but also to investigate a new DC LED driver based on a step-up quasi-resonant switched-capacitor topology. Thus, the main objective in terms of future work is to continue this line of research, especially regarding the pursuit of an optimized version of the proposed LED driver prototype with VI. The work developed on this thesis validates the proposed technique and driver topology but also points out some issues, which are expected to be dealt with in the near future.

Thereby, regarding LED driving applications, future work is focused on the following relevant guidelines:

- ✓ Optimization of the prototype built, firstly regarding optimal components in order to achieve the best possible performance and efficiency, and secondly to implement a small DC-DC converter to control the bias winding using a digital controller, i.e. forward or buck converter. In addition, the best advantage of the application of a microcontroller is that it opens a door to many benefits and features that are mandatory in nowadays LED driving applications, such as protection features or dimming. It is also expected to integrate, in the RSCC with VI, a modern and compatible communication protocol, i.e. DALI or KNX. Furthermore it is also planned to integrate VLC (Visible light Communication) in the RSCC with VI.

- ✓ Study the operation of the RSCC in near-resonance conditions, in order to achieve optimum-operation for all dimming levels. This requires a state-plane analysis from the point view of the resonant circuit.

- ✓ Since RSCC are not profoundly studied in the literature, it is also planned to make a deep study of the existing topologies.

- ✓ Make an experimental analysis of the dynamic response/stability of the RSCC.

- ✓ Study the RSCC with VI, not only using small-signal dynamic models of LED lamps in order to determine optimal-operation range and the limits of stable operation, but also using models of the VI based on finite elements.

- ✓ Investigate the inclusion of PFC techniques in LED drivers controlled via the VI, for applications supplied by AC mains, namely two-stages or integrated driver topologies.

- ✓ Investigate and study LED drivers controlled with VI for 380 V DC mains or directly by renewable energy systems such as low power Wind-Power systems and solar PV systems.

- ✓ Study and investigate the control technique based of the variation of the resonant frequency, implemented with variable capacitors instead of variable capacitors.

Regarding further applications with application of the CI, the main interests are to:

- ✓ Investigate the VI technique to control other topologies, namely step-down and inverter RSCC as well as classic buck, boost and buck-boost converters.

- ✓ Study the VI to control actively the saturation level of buck-boost inductors in applications for electric vehicles

- ✓ In applications of wireless charging of mobile devices such as mobile phones, tablets, laptops, electric tooth-brushes

- ✓ Control of induction heating applications

- ✓ Maximum power point tracking (MPPT) in solar PV applications, etc.

Expected publications

One of the goals of this thesis was to publish this new dimming technique and dimmable RSC LED driver. With the cooperation of the supervisor and co-supervisor of this dissertation, a digest was written and sent to the 2015 IEEE ECCE (Energy Conversion Congress & Expo) conference. At the moment the group is still waiting for the final decision which will be publish on May 1st, 2015.

References

[1] INE and DGEG, "Inquérito ao Consumo de Energia no Setor Doméstico," ed, 2011.

[2] D. G. Vaquero, *Off-line Supply of Solid-state Lamps: Lamp Modelling, Application of the Integrated Buck-flyback Converter, and Proposal of a New Optimised Dimming Scheme : PhD Thesis*: Universidad de Oviedo, Vicerrectorado de Extensión Universitaria, Servicio de Publicaciones, 2013.

[3] (2014). *EIA - U.S. Energy Information Administration: How much electricity is used for lighting in the United States?* Available: http://www.eia.gov/tools/faqs/faq.cfm?id=99&t=3

[4] A. d. Almeida, G. Zissis, M. Quicheron, P. Bertoldi, and "ACCELERATING THE DEPLOYMENT OF SOLID STATE LIGHTING (SSL) IN EUROPE " 2012.

[5] Z. Junming, X. Lianghui, W. Xinke, and Q. Zhaoming, "A Precise Passive Current Balancing Method for Multioutput LED Drivers," *Power Electronics, IEEE Transactions on,* vol. 26, pp. 2149-2159, 2011.

[6] Z. Chen, X. Xiaogao, and L. Shirong, "Multioutput LED Drivers With Precise Passive Current Balancing," *Power Electronics, IEEE Transactions on,* vol. 28, pp. 1438-1448, 2013.

[7] IEA. (2014). *Energy efficiency: Lighting*. Available: http://www.iea.org/topics/energyefficiency/lighting/

[8] (2013). *LightMaster KNX*. Available: http://www.lighting.philips.com/pwc_li/main/products/controls/assets/lightMaster-KNX-commercial-presentation-april2013-final.pdf

[9] (2014). *Cree First to Break 300 Lumens-Per-Watt Barrier*. Available: http://www.cree.com/News-and-Events/Cree-News/Press-Releases/2014/March/300LPW-LED-barrier

[10] CREE, "Cree® XLamp® LED Long-Term Lumen Maintenance, Application note," ed, 2014.

[11] G.-S. Seo, B.-H. Cho, and K.-C. Lee, "DC level dimmable LED driver using DC distribution," in *Energy Conversion Congress and Exposition (ECCE), 2013 IEEE*, 2013, pp. 4650-4654.

[12] S. M. Baddela and D. S. Zinger, "Parallel connected LEDs operated at high to improve current sharing," in *Industry Applications Conference, 2004. 39th IAS Annual Meeting. Conference Record of the 2004 IEEE*, 2004, pp. 1677-1681 vol.3.

[13] M. M. S. D. Perdigão, "Research and Development on New Control Techniques for Electronic Ballasts based on Magnetic Regulators " Ph. D Thesis, Universidade de Coimbra, 2011.

[14] IES. *Lighting Histroy*. Available: http://www.ies.org/lighting/history/

[15] T. Klet and H. v. Weltzien, *Geschichte der Lichttechnik/History of Light* vol. Jubiläum 2012.

[16] Biographiq, *Thomas Edison : life of an electrifying man (Biography)*: Filiquarian Publishing, LLC 2008.

[17] *Timeline of lighting technology*. Available: http://en.wikipedia.org/wiki/Timeline_of_lighting_technology

[18] CIE. *Commission Internationale de l´Eclairage, International Lighting Vocabulary*. Available: http://eilv.cie.co.at

[19] *History of the LED*. Available: http://havelights.com/2013/02/hello-world/

[20] *Shuji Nakamura - Blue LED Inventor*. Available: http://en.wikipedia.org/wiki/Shuji_Nakamura

[21] *Diode I-V Curve*. Available: http://en.wikipedia.org/wiki/File:Diode-IV-Curve.svg

[22] *Light*. Available: http://www.ushio.co.jp/en/ir/ar2014/story/light.html

[23] OSRAM, "General Information on the Assembly and Solder Pad Design of the DRAGON Family," December 2013.

[24] *AC LEDs*. Available: http://www.ledsmagazine.com/articles/2006/11/seoul-semiconductor-launches-ac-led-lighting-source-acriche.html

[25] *How LEDs Produce White Light*. Available: http://www.photonstartechnology.com/learn/how_leds_produce_white_light

[26] E. F. Schubert, *Light-Emitting Diodes (First Edition, 2003)*: E. Fred Schubert, 2003.

[27] C. Branas, F. J. Azcondo, and J. M. Alonso, "Solid-State Lighting: A System Review," *Industrial Electronics Magazine, IEEE,* vol. 7, pp. 6-14, 2013.

[28] G. Zissis and P. Bertoldi, "Status Report on Organic Light Emitting Diodes (OLED)," ed: Joint Research Centre, Institute for Energy and Transport, 2014.

[29] A. Technologies, "Selecting DC Sources for Telecommunications Equipment Test Systems ", ed, 2009.

[30] G. K. Wolff, "Multiple grounding of 48 V DC power supply units endangers devices and causes the loss of availability," in *Telecommunications Energy Conference 'Smart Power and Efficiency' (INTELEC), Proceedings of 2013 35th International*, 2013, pp. 1-5.

[31] C. Kraft, "Conducted noise from 48 volt DC-DC converters used in telecommunications systems and its mitigation for EMC," in *Telecommunications Energy Special Conference, 2000. TELESCON 2000. The Third International*, 2000, pp. 327-331.

[32] T. Babasaki, T. Tanaka, T. Tanaka, Y. Nozaki, and F. Kurokawa, "Development of -48-V DC power supply system for high power ICT equipment," in *Telecommunication - Energy Special Conference (TELESCON), 2009 4th International Conference on*, 2009, pp. 1-6.

[33] T. Babasaki, T. Tanaka, K. Murai, and Y. Nozaki, "Development and standardization of higher-voltage direct current power feeding system," in *Renewable Energy Research and Applications (ICRERA), 2012 International Conference on*, 2012, pp. 1-4.

[34] D. Cooper and R. Duvnjak, "A novel self-powered, isolated power management device for 48 V power systems," in *Applied Power Electronics Conference and Exposition, 2005. APEC 2005. Twentieth Annual IEEE*, 2005, pp. 1380-1385 Vol. 3.

[35] W. Allen and S. V. Natale, "Achieving ultra-high system availability in a battery-less -48VDC power plant," in *Telecommunications Energy Conference, 2002. INTELEC. 24th Annual International*, 2002, pp. 287-294.

[36] Y. Hayashi, H. Toyoda, T. Ise, and A. Matsumoto, "Design consideration for contactless DC connector in high power density future 380 V DC distribution system," in *Energy Conversion Congress and Exposition (ECCE), 2014 IEEE*, 2014, pp. 5690-5697.

[37] M. Schweizer-Berberich and H. Willmes, "Concept for a 48 V DC Power Supply System with Lithium Ion Batteries for Telecom Applications," in *Telecommunications Conference, 2005. INTELEC '05. Twenty-Seventh International*, 2005, pp. 31-36.

[38] S. M. Lisy, B. J. Sonnenberg, and J. Dolan, "Case study of deployment of 400V DC power with 400V/-48VDC conversion," in *Telecommunications Energy Conference (INTELEC), 2014 IEEE 36th International*, 2014, pp. 1-6.

[39] R. Yuancheng, X. Ming, D. Sterk, and F. C. Lee, "1 MHz self-driven ZVS full-bridge converter for 48 V power pods," in *Power Electronics Specialist Conference, 2003. PESC '03. 2003 IEEE 34th Annual*, 2003, pp. 1801-1806 vol.4.

[40] X. Ming, R. Yuancheng, J. Zhou, and F. C. Lee, "1-MHz self-driven ZVS full-bridge converter for 48-V power pod and DC/DC brick," *Power Electronics, IEEE Transactions on,* vol. 20, pp. 997-1006, 2005.

[41] W. Cong and P. Jain, "A quantitative comparison and evaluation of 48V DC and 380V DC distribution systems for datacenters," in *Telecommunications Energy Conference (INTELEC), 2014 IEEE 36th International*, 2014, pp. 1-7.

[42] R. Yuancheng, X. Ming, K. Yao, and F. C. Lee, "Two-stage 48 V power pod exploration for 64-bit microprocessor," in *Applied Power Electronics Conference and Exposition, 2003. APEC '03. Eighteenth Annual IEEE*, 2003, pp. 426-431 vol.1.

[43] J. Akerlund, "-48 V DC computer equipment topology-an emerging technology," in *Telecommunications Energy Conference, 1998. INTELEC. Twentieth International*, 1998, pp. 15-21.

[44] S. Pan, M. Pahlevaninezhad, and P. K. Jain, "Adaptive Hybrid Primary/secondary-side Digital Control for Series Resonant DC-DC Converters in 48V VR applications," *Emerging and Selected Topics in Power Electronics, IEEE Journal of,* vol. PP, pp. 1-1, 2014.

[45] ETSI, "Standard ETSI EN 300 132-2 V2.4.6 : Environmental Engineering (EE);Power supply interface at the input to telecommunications and datacom (ICT) equipment; Part 2: Operated by -48 V direct current (dc)", ed, October 2011.

[46] Y. Hayashi, "Power density design of SiC and GaN DC-DC converters for 380 V DC distribution system based on series-parallel circuit topology," in *Applied Power Electronics Conference and Exposition (APEC), 2013 Twenty-Eighth Annual IEEE*, 2013, pp. 1601-1606.

[47] (January/February 2009) Technology and Applications of Light Emitting Diodes. *LEDs MAGAZINE*.

[48] V. Vossos, K. Garbesi, and H. Shen, "Energy savings from direct-DC in US residential buildings," *Energy and Buildings,* vol. 68, pp. 223-231, 2014.

[49] E. Alliance®. (2009). Available: http://blog.circuitprotection.com/wp-content/uploads/2011/08/Industrial_Application_eMerge.png

[50] E. Alliance®. Available: http://blog.circuitprotection.com/blognews/low-voltage-direct-current-lvdc-microgrids-%E2%80%93-becoming-a-reality/

[51] P. M. Roschatt, R. A. McMahon, and S. Pickering, "A gallium nitride FET based DC-DC converter for the new 48 V automotive system," in *Power Electronics, Machines and Drives (PEMD 2014), 7th IET International Conference on*, 2014, pp. 1-6.

[52] K. Changsung Sean, P. Kyeounghun, K. Hantae, L. Geunhong, L. Kwanghyun, Y. Hyun Jik*, et al.*, "48V Power Assist Recuperation System (PARS) with a permanent magnet motor, inverter and DC-DC converter," in *Future Energy Electronics Conference (IFEEC), 2013 1st International*, 2013, pp. 137-142.

[53] N. Femia, M. Fortunato, and M. Vitelli, "Light-to-Light: PV-Fed LED Lighting Systems," *Power Electronics, IEEE Transactions on,* vol. 28, pp. 4063-4073, 2013.

[54] "Emergency Lighting," ed: Daisalux, 2014.

[55] "EMERGENCY POWER AND SOLAR KITS," ed: Obsta, 2014.

[56] Speaker. (2014). *Emergency Lamps*. Available: http://www.invisionsales.com/lighting/pdfs/Speaker-Emergency.pdf

[57] GIMAX. *Emergency lights*. Available: http://www.gimaxsrl.it/articolo_ing.php?idarticolo=A0000102

[58] Cosine. *Emergency Luminaires*. Available: http://www.cosine.co.za/central-battery-system.html

[59] *Discover DALI*. Available: http://www.dali-ag.org/discover-dali.html

[60] Available: http://www.digikey.com/product-highlights/us/en/texas-instruments-lighting-solutions/2201

[61] Philips, "DALI lighting control systems," ed, 2013.

[62] *Lighting Control Protocols*: IES Controls Protocol Committee, 2011.

[63] (2014). *Communication & Networking*. Available: http://www.microchip.com/pagehandler/en-us/technology/intelligentLighting/products/communications.html

[64] *NXP OM13042 KNX* Available: http://pl.mouser.com/new/NXP-Semiconductors/nxp-lighting-boards/#tabs-2

[65] *Shutter/blind actuator 4/2gang 230V AC/24-48V DC*. Available: http://descargas.futurasmus-knxgroup.org/DOC/GB/BERKER/4925/75314018.pdf

[66] ActiveLED. *Specifications for ActiveLED AC and DC Powered LED Drivers*. Available: http://www.activeled.com/products/power_supplies/specification_ac_apfc/

[67] Amperor. *Ways to Raise LED Lighting System Efficiency*. Available: http://www.amperor.com/products/led/Increase_LED_Driver_Efficiency.html

[68] N. Semiconductor. (2011). *LED Drivers for High-Brightness Lighting*. Available: http://www.ti.com/lit/sl/snvy001/snvy001.pdf

[69] *LM3402HV - LED driver board for Street Lamp/stage lamp, up to 500mA*. Available: http://www.em.avnetasia.com/Products/DesignSolutionShow.aspx?pagesId=27&MasterPageId=17&ID=76

[70] "LT3590-48V Buck Mode LED Driver in SC70," ed: LINEAR Technology.

[71] "LT-401-CC," in *DALI LED Dimming Driver Manual*, ed: LTECH, 2013.

[72] Z. Shaobin, C. Qiaoliang, S. Julu, X. Ming, and Q. Yang, "High-accuracy passive current balancing schemes for large-scale LED backlight system," in *Applied Power Electronics Conference and Exposition (APEC), 2011 Twenty-Sixth Annual IEEE*, 2011, pp. 723-727.

[73] D. Camponogara, D. Ribeiro Vargas, M. A. Dalla Costa, J. M. Alonso, J. Garcia, and T. Marchesan, "Capacitance Reduction With An Optimized Converter Connection Applied to LED Drivers," *Industrial Electronics, IEEE Transactions on,* vol. 62, pp. 184-192, 2015.

[74] R. A. Pinto, M. R. Cosetin, A. Campos, M. A. Dalla Costa, and R. N. do Prado, "Compact Emergency Lamp Using Power LEDs," *Industrial Electronics, IEEE Transactions on,* vol. 59, pp. 1728-1738, 2012.

[75] P. Lumileds, "Understanding power LED lifetime analysis," ed, 2012.

[76] *LED Lighting Technology*. Available: http://www.microchip.com/pagehandler/en-us/technology/intelligentLighting/technology/led.html

[77] T. Instruments, "LED-driver considerations," *Analog Application Journal* 2004.

[78] H. Van der Broeck, G. Sauerlander, and M. Wendt, "Power driver topologies and control schemes for LEDs," in *Applied Power Electronics Conference, APEC 2007 - Twenty Second Annual IEEE*, 2007, pp. 1319-1325.

[79] T. I. Incorporated, "Switched Capacitor Circuits Provide Efficient and Functional White-LED Drive," ed, 2011.

[80] M. S. Perdigao, H. V. Marques, J. M. Alonso, and E. S. Saraiva, "Step-dimming for multi-Watt electronic ballast with magnetic control: SoS limits analysis," in *Universities Power Engineering Conference (UPEC), 2012 47th International*, 2012, pp. 1-6.

[81] "Dimming LEDs with respect to grouping current, Application Note," ed: OSRAM Opto Semiconductors, December, 2013.

[82] R. Pinto, M. Alonso, M. Perdigão, M. da Silva, and R. N. do Prado, "A New Technique to Equalize Branch Currents in Multiarray LED Lamps Based on Variable Inductor," presented at the ILDC 2014, Tucson, Arizona, USA, 2014.

[83] M. Doshi and R. Zane, "Reconfigurable and fault tolerant digital phase shifted modulator for luminance control of LED light sources," in *Power Electronics Specialists Conference, 2008. PESC 2008. IEEE*, 2008, pp. 4185-4191.

[84] M. Doshi and R. Zane, "Digital Architecture for Driving Large LED Arrays with Dynamic Bus Voltage Regulation and Phase Shifted PWM," in *Applied Power Electronics Conference, APEC 2007 - Twenty Second Annual IEEE*, 2007, pp. 287-293.

[85] Intersil. *6-Channel LED Driver with Phase Shift Control*. Available: http://www.intersil.com/content/dam/Intersil/documents/isl9/isl97676.pdf

[86] W. Chen and S. Y. R. Hui, "A dimmable light-emitting diode (LED) driver with cascaded mag-amp postregulators for multistring applications," in *IECON 2010 - 36th Annual Conference on IEEE Industrial Electronics Society*, 2010, pp. 2523-2528.

[87] W. Chen and S. Y. R. Hui, "A Dimmable Light-Emitting Diode (LED) Driver With Mag-Amp Postregulators for Multistring Applications," *Power Electronics, IEEE Transactions on,* vol. 26, pp. 1714-1722, 2011.

[88] B. Mammano, "Magnetic Amplifier Control for Simple, Low-cost, Secondary Regulation," ed: Unitrode Corporation Seminar, 1986.

[89] L. Quanming, Z. Shubo, Z. Can, L. Weiguo, and Z. Luowei, "An LED Driver With Dynamic High-Frequency Sinusoidal Bus Voltage Regulation for Multistring Applications," *Power Electronics, IEEE Transactions on,* vol. 29, pp. 491-500, 2014.

[90] K. I. Hwu and Y. T. Yau, "Applying One-Comparator Counter-Based Sampling to Current Sharing Control of Multichannel LED Strings," *Industry Applications, IEEE Transactions on,* vol. 47, pp. 2413-2421, 2011.

[91] Philips. *LEDs - Internet Courses*. Available: http://www.lighting.philips.com/pwc_li/main/connect/Lighting_University/internet-courses/LEDs/led-lamps6.html

[92] W. Jianfeng, Z. Junming, H. Xiucheng, and X. Lianghui, "A family of capacitive current balancing methods for multi-output LED drivers," in *Applied Power Electronics Conference and Exposition (APEC), 2011 Twenty-Sixth Annual IEEE*, 2011, pp. 2040-2046.

[93] J. Vollin, F. D. Tan, and S. M. Cuk, "Magnetic regulator modeling," in *Applied Power Electronics Conference and Exposition, 1993. APEC '93. Conference Proceedings 1993., Eighth Annual*, 1993, pp. 604-611.

[94] L. Ray-Lee and C. Yi-Fan, "Equivalent Circuit Model of Light-Emitting-Diode for System Analyses of Lighting Drivers," in *Industry Applications Society Annual Meeting, 2009. IAS 2009. IEEE*, 2009, pp. 1-5.

[95] D. J. B, "Variable inductance system," ed: Google Patents, 1933.

[96] P. Sen, P. P. Biringer, and R. Segsworth, "Thyristor-controlled single phase variable inductor," *Magnetics, IEEE Transactions on,* vol. 3, pp. 240-245, 1967.

[97] B. D. Anderson, W. New, and R. Newcomb, "A tapped electronically variable delay line suitable for integrated circuits," *Proceedings of the IEEE,* vol. 54, pp. 1118-1119, 1966.

[98] A. S. Kislovski, "Quasi-linear controllable inductor," *Proceedings of the IEEE,* vol. 75, pp. 267-269, 1987.

[99] A. F. Bakan, "A new LVI assisted PSPWM DC-DC converter," in *Electrical and Electronics Engineering, 2009. ELECO 2009. International Conference on*, 2009, pp. I-230-I-233.

[100] H. D. Young, R. A. Freedman, A. L. Ford, and F. W. Sears, *Sears and Zemansky's university physics: with modern physics*, 13th ed.: Pearson Addison Wesley, 2012.

[101] *Inductance, Flux and Energy Computation by LMATRIX and SENERGY Macros*. Available: https://www.sharcnet.ca/Software/Ansys/fluent/14.0/help/ans_thry/thy_emg6.html#elecdiffinductdef

[102] R. M. Bozorth, *Ferromagnetism*: Wiley-IEEE Press, 1993.

[103] B. R. O. Baptista, "Balastros Electrónicos: Uma nova Tecnologia de Regulação de Fluxo Luminoso," MSc Thesis, Universidade de Coimbra, Coimbra, 2009.

[104] D. Medini and S. Ben-Yaakov, "A current-controlled variable-inductor for high frequency resonant power circuits," in *Applied Power Electronics Conference and Exposition, 1994. APEC '94. Conference Proceedings 1994., Ninth Annual*, 1994, pp. 219-225 vol.1.

[105] J. M. Alonso, M. S. Perdigao, J. Ribas, D. Gacio, and E. S. Saraiva, "A digitally-controlled universal ballast based on magnetic regulator and PSoC device," in *Industrial Electronics, 2009. ISIE 2009. IEEE International Symposium on*, 2009, pp. 2010-2015.

[106] M. S. Perdigao, J. M. Alonso, M. A. Dalla Costa, and E. S. Saraiva, "A variable inductor MATLAB/Simulink behavioral model for application in magnetically-controlled electronic ballasts," in *Power Electronics, Electrical Drives, Automation and Motion, 2008. SPEEDAM 2008. International Symposium on*, 2008, pp. 349-354.

[107] Y. Bi and D. C. Jiles, "Finite element modeling of an electrically variable inductor," *Magnetics, IEEE Transactions on,* vol. 35, pp. 3517-3519, 1999.

[108] F. S. F. Samuel, "Estudo do comportamento eletromagnético de uma bobina variável, controlada através de uma corrente DC," MS.c Thesis, Universidade de Coimbra, September 2015 (expected).

[109] Cedrat. *Flux Software*. Available: http://www.cedrat.com/en/software/flux.html

[110] E. Rozanov and S. Ben-yaakov, "Analysis of current-controlled inductors by new SPICE behavioral model," *HAIT Journal of Science and Engineering B,* vol. 2, pp. 558-570, 2005.

[111] J. C. Maxwell, *A Treatise on Electricity and Magnetism, pp. 384-385* vol. 2: Oxford, Clarendon Press, 1881.

[112] J. W. Butler, "Analysis of factors which influence the application, operation, and design of shunt-capacitor equipments switched in large banks," *Electrical Engineering,* vol. 59, pp. 795-800, 1940.

[113] D. L. Fried, "Analog sample-data filters," *Solid-State Circuits, IEEE Journal of,* vol. 7, pp. 302-304, 1972.

[114] Z. Singer, A. Emanuel, and M. S. Erlicki, "Power regulation by means of a switched capacitor," *Electrical Engineers, Proceedings of the Institution of,* vol. 119, pp. 149-152, 1972.

[115] K. W. E. Cheng, "Zero-current-switching switched-capacitor converters," *Electric Power Applications, IEE Proceedings -,* vol. 148, pp. 403-409, 2001.

[116] O. Abutbul, A. Gherlitz, Y. Berkovich, and A. Ioinovici, "Step-up switching-mode converter with high voltage gain using a switched-capacitor circuit," *Circuits and Systems I: Fundamental Theory and Applications, IEEE Transactions on,* vol. 50, pp. 1098-1102, 2003.

[117] L. Yuang-Shung, K. Yi-Pin, and C. Chien-An, "A Novel QR ZCS Switched-Capacitor Bidirectional Converter," in *Power Electronics and Drive Systems, 2007. PEDS '07. 7th International Conference on*, 2007, pp. 151-156.

[118] K. K. Law, K. W. E. Cheng, and Y. P. B. Yeung, "Design and analysis of switched-capacitor-based step-up resonant converters," *Circuits and Systems I: Regular Papers, IEEE Transactions on,* vol. 52, pp. 943-948, 2005.

[119] Y. P. B. Yeung, K. W. E. Cheng, S. L. Ho, K. K. Law, and D. Sutanto, "Unified analysis of switched-capacitor resonant converters," *Industrial Electronics, IEEE Transactions on,* vol. 51, pp. 864-873, 2004.

[120] M. Shoyama, T. Naka, and T. Ninomiya, "Resonant switched capacitor converter with high efficiency," in *Power Electronics Specialists Conference, 2004. PESC 04. 2004 IEEE 35th Annual*, 2004, pp. 3780-3786 Vol.5.

[121] Q. Dongyuan, Z. Bo, and Z. Chunfang, "Duty ratio control of resonant switched capacitor DC-DC converter," in *Electrical Machines and Systems, 2005. ICEMS 2005. Proceedings of the Eighth International Conference on*, 2005, pp. 1138-1141 Vol. 2.

[122] M. S. Makowski, "Voltage Regulation in Switched-Capacitor Converters - A Problem Revised," in *Proc. 5th Eur. Space Power Conf.*, Tarragona, Spain, 1998.

[123] S. Kiratipongvoot, T. Siew-Chong, and A. Ioinovici, "Phase-Shift Interleaving Control of Variable-Phase Switched-Capacitor Converters," *Industrial Electronics, IEEE Transactions on,* vol. 60, pp. 5575-5584, 2013.

[124] M. Shoyama and T. Ninomiya, "Output Voltage Control of Resonant Boost Switched Capacitor Converter," in *Power Conversion Conference - Nagoya, 2007. PCC '07*, 2007, pp. 899-903.

[125] K. Sano and H. Fujita, "Improving dynamic performance and efficiency of a resonant switched-capacitor converter based on phase-shift control," in *Energy Conversion Congress and Exposition, 2009. ECCE 2009. IEEE*, 2009, pp. 3509-3515.

[126] Taufik and J. J. Mullins, "Parallel Operation of Hybrid Loaded Resonant Converter Using Phase-Shift Control," in *Industrial Electronics, 2006 IEEE International Symposium on*, 2006, pp. 988-992.

[127] L. Rui, X. Dehong, C. Min, F. Bo, K. Mino, and H. Umida, "Improving the Power Density of the ZVS-SVM Controlled Three-Phase Boost PFC Converter," in *Power Conversion Conference - Nagoya, 2007. PCC '07*, 2007, pp. 1274-1279.

[128] T. Wenjuan, Q. Dongyuan, Z. Bo, and L. Jianyuan, "General Laws of Sneak Circuit in Resonant Switched Capacitor Converters," in *Power Electronics Specialists Conference, 2007. PESC 2007. IEEE*, 2007, pp. 708-712.

[129] H. Jifeng, A. von Jouanne, and G. C. Temes, "A New Approach to Reducing Output Ripple in Switched-Capacitor-Based Step-Down DC–DC Converters," *Power Electronics, IEEE Transactions on,* vol. 21, pp. 1548-1555, 2006.

[130] "Golden Dragon Plus: Datasheet," ed: Osram.

[131] M. S. Perdigao, B. Baptista, E. S. Saraiva, and J. M. Alonso, "A dynamic-inductance model for magnetically controlled Electronic Ballasts," in *Universities Power Engineering Conference (UPEC), 2009 Proceedings of the 44th International*, 2009, pp. 1-5.

[132] *Computer-Aided Analysis and Design of Switch-Mode Power Supplies*: Taylor & Francis, 1993.

[133] C. W. T. McLyman, *High Reliability Magnetic Devices: Design & Fabrication*: Taylor & Francis, 2002.

[134] C. W. T. McLyman, *Transformer and Inductor Design Handbook, Third Edition*: Taylor & Francis, 2004.

[135] J. Lloyd H. Dixon, *Design of Flyback Transformers and Filter Inductors*, 2001.

[136] "IR2153(D)(S) &(PbF) SELF-OSCILLATING HALF-BRIDGE DRIVER, Datasheet No. PD60062 revO," ed: International Rectifier.

[137] "IRS2153D(S) SELF-OSCILLATING HALF-BRIDGE DRIVER IC, Data Sheet PD No.60238," ed: International Rectifier.

[138] "HV Floating MOS-Gate Driver ICs , Application Note AN-978," ed: International Rectifier.

Appendix

Appendix A – Converter Theoretical Design

A.1 – RSCC Design

VI – Calculation of the AC Inductance range

Using the selected input and desired output parameters, the procedure to determine the VI AC inductance range described in section 4.3.2.3 was solved in a Mathcad program which is shown below. The results obtained with it, indicate that the required variable inductance range is:

38.1 µH ~140.6 µH

Mathcad program:

Main Input parameters:

$Vin := 48$ Input voltage [V]

$fs := 100 \cdot 10^{3}$ Switching frequency [Hz]

$Cr := 0.47 \cdot 10^{-6}$ Resonant Capacitor [F]

Calculation of Lr minimum:

$Io\_max := 0.35$ Maximum LEDs current [A]

$Vo\_max := 64$ Maximum LEDs voltage [V]

$$Lr\_min := \left[\frac{(2Vin - Vo\_max) \cdot (Vo\_max)}{(32 \cdot fs \cdot Io\_max \cdot Vin)} \right]$$ $Lr\_min = 3.81 \times 10^{-5}$

$$fr\_max := \frac{1}{2 \cdot \pi \cdot \sqrt{Lr\_min \cdot Cr}}$$ $fr\_max = 3.761 \times 10^{4}$

Calculation of Lr maximum:

$Io\_min := 0.1$ Minimum LEDs current [A]

$Vo\_min := 60$ Minimum LEDs voltage [V]

$$Lr\_max := \left[\frac{(2Vin - Vo\_min) \cdot (Vo\_min)}{(32 \cdot fs \cdot Io\_min \cdot Vin)} \right]$$ $Lr\_max = 1.406 \times 10^{-4}$

$$fr\_min := \frac{1}{2 \cdot \pi \cdot \sqrt{Lr\_max \cdot Cr}}$$ $fr\_min = 1.958 \times 10^{4}$

A.2 – Variable Inductor – Physical Design Procedure

The simplified design procedure of the variable inductor was solved by the following Mathcad program:

core parameters:

$Ae := 58 \cdot 10^{-6}$ effective magnetic cross section (m^2)

$Wa := 69.86$ area of window (m^2)

$g := 0.6 \cdot 10^{-3}$ air gap (m)

$le := 57 \cdot 10^{-3}$ effective magnetic path length (m)

$lext := 100.4 \cdot 10^{-3}$ external path (m)

$\mu 0 := 4 \cdot \pi \cdot 10^{-7}$ air permeability

$Bs := 0.49$ saturation magnetization (T)

$\mu r := 2200$ relative permeability (initial)

$Idc := 0.5$ maximum control current (A)

magnetic field density and maximum ac current

$Iacmax := 1.5$ Maximum acceptable value in terms of resonant current

$Bmax := \frac{Bs}{5}$

magnetic parameters:

$\delta := 5$ Current density (A/m^2) for a wire isolated from free air (maximum 6, and 4 to non free air isolated)

$Lmax := 150 \cdot 10^{-6}$ Required maximum inductance value

number of turns of the main winding:

$Nac := \frac{Lmax \cdot Iacmax}{Bmax \cdot Ae}$ Number of turns of the main winding $Nac = 39.585$

$d := \sqrt{\frac{4 \cdot Iacmax}{\pi \cdot \delta}}$ Diameter of wire of the main winding $d = 0.618$

number of turns of the control winding:

$k := 0.8$ decreasing permeability factor

$\mu kBsat := \mu r \cdot k$ $\mu kBsat = 1.76 \times 10^{3}$

$Ndc := \frac{k \cdot Bs \cdot lext}{0.5 \cdot \mu kBsat \cdot \mu 0 \cdot Idc}$ Number of turns of the control winding $Ndc = 71.18$

$dc := \sqrt{\frac{4 \cdot Idc}{\pi \cdot \delta}}$ Diameter of the wire of the control winding $dc = 0.357$

ac and dc winding area ocupation:

$Aw := Nac \cdot \frac{\pi \cdot d^2}{4} + Ndc \cdot \frac{\pi \cdot dc^2}{4}$ Ocupied area by the main winding $Aw = 18.993$

$Ku := \frac{Aw}{Wa}$ $Ku = 0.272$ it is within the limit value (0.4), no needs for a second iteration

gap

$$gap := \frac{\left(Nac^2 \cdot \mu r \cdot Ae - le \cdot Lmax\right) \cdot \mu 0}{Lmax \cdot \mu r}$$

$gap = 7.614 \times 10^{-4}$ gap larger than the one available!

$gap2 := 6 \cdot 10^{-4}$ available air gap value for the EF25 core

$$Nac2 := \sqrt{\frac{\left(gap2 \cdot Lmax \cdot \frac{\mu r}{\mu 0} + le \cdot Lmax\right)}{(\mu r \cdot Ae)}}$$

$Nac2 = 35.14$ new value of ac turns

new ac and dc winding area ocupation:

$$Aw := Nac2 \cdot \frac{\pi \cdot d^2}{4} + Ndc \cdot \frac{\pi \cdot dc^2}{4}$$

Ocupied area by the main winding $Aw = 17.66$

$$Ku := \frac{Aw}{Wa}$$

$Ku = 0.253$

Calculation of Inductance:

$$L := \frac{Nac2^2}{\frac{le}{\mu r \cdot \mu 0 \cdot Ae} + \frac{gap2}{\mu 0 \cdot Ae}}$$

Inductance of the main winding $L = 1.438 \times 10^{-4}$

Experimental prototype:

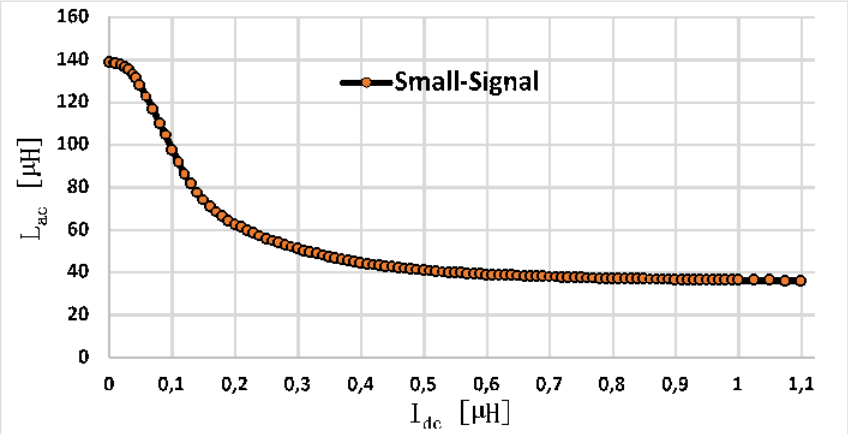

Magnetic flux density in the core:

$$B(I) := \frac{Nac \cdot Iacmax}{\frac{le}{\mu r \cdot \mu 0} + \frac{gap}{\mu 0}}$$

$$\frac{B(Iacmax)}{Bs} = 0.193 \qquad B(Iacmax) = 0.095$$

Appendix B – Converter Simulation

B.1 – LEDs Model

The LED lamp was simulated in PSIM with the model which is shown below:

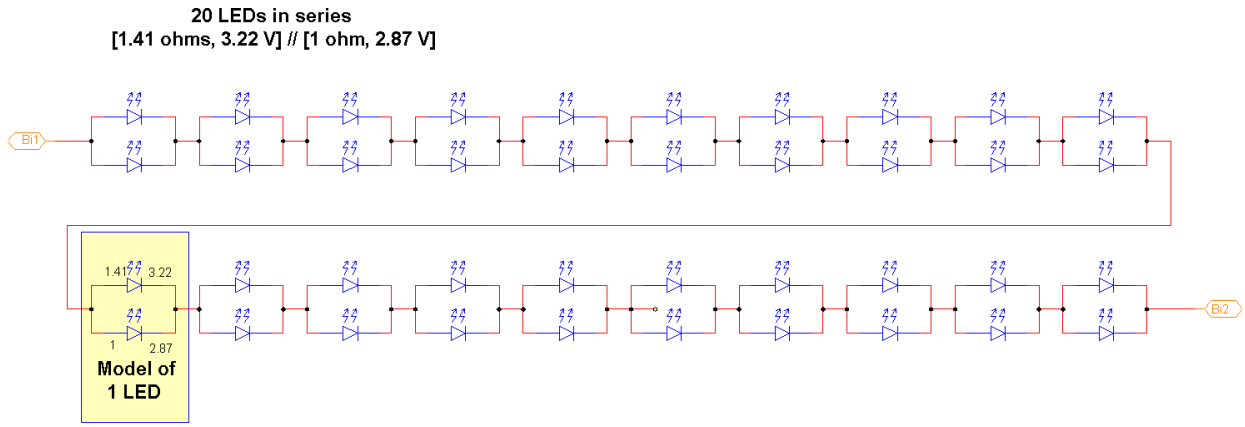

Fig. B. 1 - PSIM LED lamp model

The circuit within a yellow rectangle in previous figure is the model for one single LED. The two LEDs in parallel represent the double piecewise linear model referred in sections 2.4.5.1 and 5.1. The lamp model is composed by a string of 20 LEDs connected in series. Note that each LED is based in the built-in model provided by PSIM's database. The parameters for the LED model are obtained using the design procedure described in section 2.4.5.1, for which are obtained curves that fulfil the y = mx + b type:

$$I_{fn} = r_n \cdot V_{fn} + b_n \tag{6.19}$$

Where I_{fn} r is the equivalent dynamic resistance, expressed in [Ω], for the point *n,* and *b* is simply (specifically in this case) a "virtual" ordinate in the origin of the equation. This is due to the fact that for voltage values under the threshold voltage of a LED the current is null. The coordinates for the key points are given in Fig. 5.1 (b). For the present case first it is obtained the slope (r_1) of the green line segment comprised between V_{F1} and V_{F2} as follows:

$$r_1 = \frac{\Delta V_F}{\Delta I_F} = \frac{V_{F2} - V_{F1}}{I_{F2} - I_{F1}} = \frac{3.22 - 2.97}{0.35 - 0.1} = 1\Omega \tag{6.20}$$

Substituting the obtained value of r_1 and the coordinates of V_{F1} into (6.19) the value of b_1 is calculated and equals -2.87. Hence the value for V_{F0} may be determined using (6.19) by substituting the already known correspondent current value $I_{f0} = 0$, and the value of b_1. The resulting value for V_{F0} is then 2.87 V. Analogously, for the second segment (violet) V_{F2} is already known from the data collected and it equals 3.22 (see Fig. 5.1 (b)), and the unknown value of r_2 can be determined as follows:

$$r_2 = \frac{\Delta V_F}{\Delta I_F} = \frac{V_{F3} - V_{F2}}{I_{F3} - \frac{V_{F3} - V_{F0}}{r_1}} = \frac{3.6 - 3.22}{1 - \frac{3.6 - 2.87}{1}} = 1.41\Omega \tag{6.21}$$

The model parameters, including measured parameters and calculated ones, are listed in the following table:

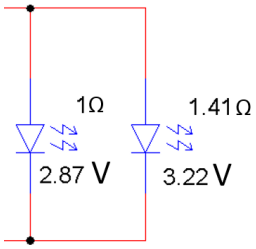

Fig. B. 2 - PSIM single LED model

Table H – Two piecewise linear model parameters

V_{F0}	2.87 V	I_{F0}	0 A		
V_{F1}	2.97 V	I_{F1}	0.10 A	r_1	1 Ω
V_{F2}	3.22 V	I_{F2}	0.35 A	r_2	1.41 Ω
V_{F3}	3.60 V	I_{F3}	1 A		

The single LED model used in PSIM is shown in the previous figure.

B.2 – Variable Inductance Model

As a first approach, with the measurements setup presented in section 6.1 (small-signal characterization) the obtained experimental values (those shown in Fig. 6.4) of the main winding inductance as a function of the DC control current ($L_{ac} = f(I_{dc})$) were introduced in the model by means of a Lookup Table (using a .txt text file) in order to simulate the dynamic-inductance behaviour of the VI. This lookup table approximates a one-dimensional function using the specified lookup method which was chosen to be the *Interpolation-Extrapolation* method. This method performs a linear interpolation and extrapolation of the inputs where the inputs are the values of the DC control current. As a simple approach, the DC control current is the input of the lookup table and it is obtained using a current sensor in the DC (bias) winding. Using the specified method, the Lookup Table block automatically determines the inductance value.

DC Winding

The DC winding is simply simulated by means of an equivalent in series resistance (ESR_DC) of 1.3 Ω, which in turn is in series with an inductor of 1.5 mH. These values were obtained during experimental tests of the VI. The winding is supplied with a voltage source of 5V and controlled by means of a simple voltage-controlled current source which actuates a NPN transistor, such as the one proposed in [82], built with a few logic and passive components as follows:

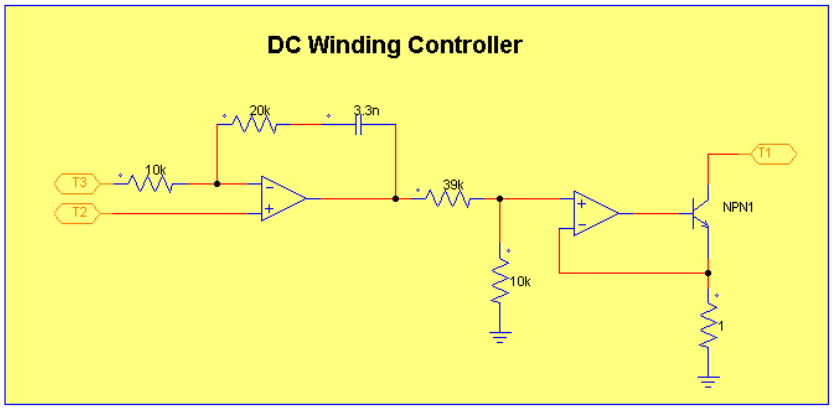

Basically it is a classic analogic PI controller followed by a voltage follower. In the present case, the current sensor measures the LED current and an error amplifier compares this value to a reference value, and then its generated the required output to control the VI. The inputs of the PI controller T3 and T2 are the sensed LEDs current and the current reference value, respectively. The reference is adjusted manually in function of the LEDs lamp current desired value. The voltage follower is used to ensure that the transistor is operated in its active region during the whole desired control range.

AC Winding

The AC winding is simply simulated by means of a voltage-controlled current source (VCCS) in series with an equivalent in series resistance (*ESR_Lac* in the schematic). In this winding, the resonant current is defined to flow from the negative terminal to the positive terminal of the VCCS (the same direction of the arrow in the schematic).

Note that when "inductor Current" is mentioned it is related to the current flowing through the AC winding of the VI. In order to obtain and control the inductor current, firstly its voltage is measured with a voltage sensor (*Voltage _sensor* in the schematic) and then it is integrated. After

that, the resultant parameter is divided by the inductance value given by the lookup table and the inductor current is thus obtained. This process may be mathematically described as follows:

$$i_{L_{ac}} = \frac{1}{L_{ac}(I_{dc})} \cdot \frac{v_{L_{ac}}}{s} \tag{6.22}$$

where $\frac{1}{s}$ is the Laplace integrator.

In order to achieve a higher precision in the simulation results, i.e. as close as possible to practical results, after the prototype was built and tested the VI's large signal characterization, was introduced into the lookup table to replace the previously introduced small signal characteristic. (Firstly simulation was done using data which resulted from the small-signal characterization of the VI).

B.3 – Converter and Simulation Parameters

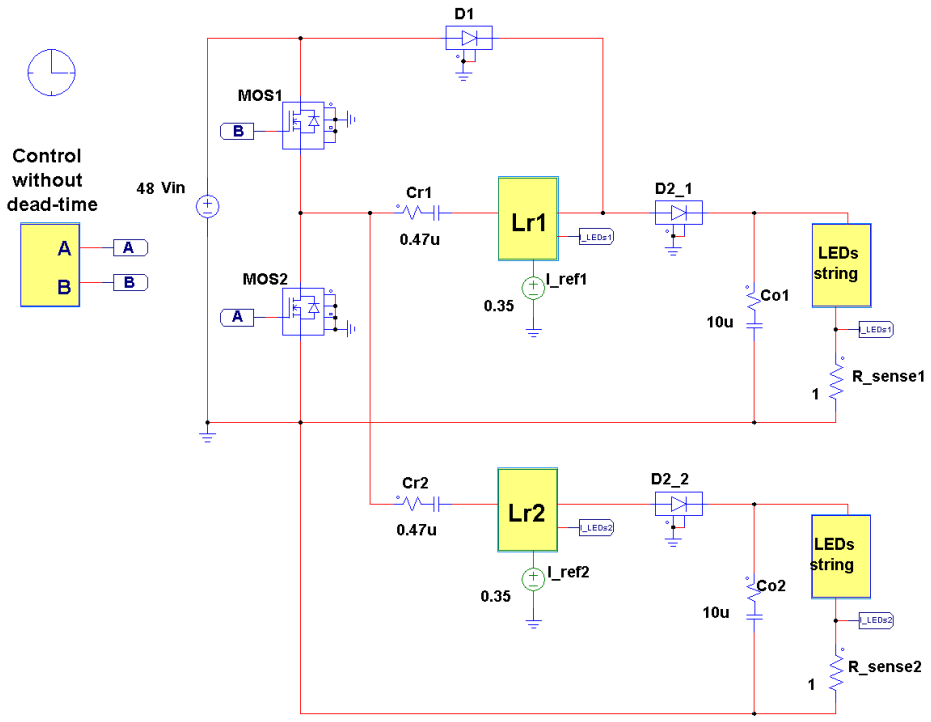

Fig. B. 3 - LED driver Simulation Model for 2 outputs

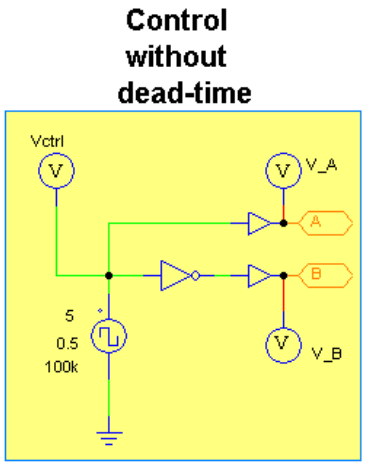

Fig. B. 4 – Mosfets control without dead-time, 100 kHz and 50% duty-cycle

In the following table are presented the main parameters used in the simulation:

Table I - Simulation main parameters

Description	Specification
Simulation Time Step	$10^{-7}s$
Input Voltage	$V_{in} = 48\,V$
Switching frequency	$100\,kHz$
Duty cycle	0.5
Switches	N-channel MOSFETS
Variable Inductor	$L_r = 42\ \mu\text{H} \sim 145\ \mu\text{H}$
Resonant Capacitor	$C_r = 0.47\ \mu F$
Output Capacitor	$C_o = 10\ \mu F$
LED Branch (B_n)	String of 20 LEDs in series, 3.2V, 350 mA

Appendix C – Converter Prototype: Practical Implementation

C.1 – LED Lamp Construction

A LED lamp comprised of two strings, each one with 20 LEDs connected in series, was built. The LEDs used were Golden DRAGON PLUS LCW W5AM from OSRAM as follows:

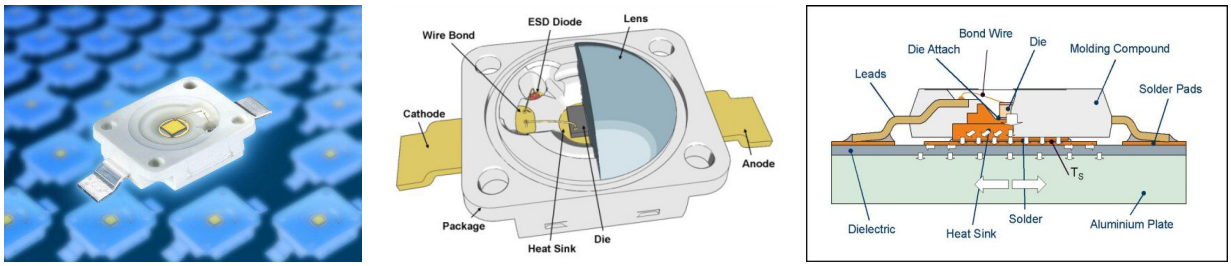

Fig. C. 1 - Golden DRAGON PLUS LCW W5AM [23]

The LEDs were soldered and connected to each other by means of copper wire and assembled on an aluminium heat sink. Due to the high junction temperature of LEDs a dissipation system is mandatory for every LED lamp.

Between the LEDs built-in heat sink (may be seen on the previous figure – orange colour) and the external heat sink, thermal paste was used with a double function, first to serve as a heat spreader by conducting heat out of the LEDs, and second to serve as dielectric layer to provide electrical isolation between the LEDs and the external heat sink because the LEDs built-in heat sink is electrically connected to the cathode. The LEDs lamp prototype built is shown below:

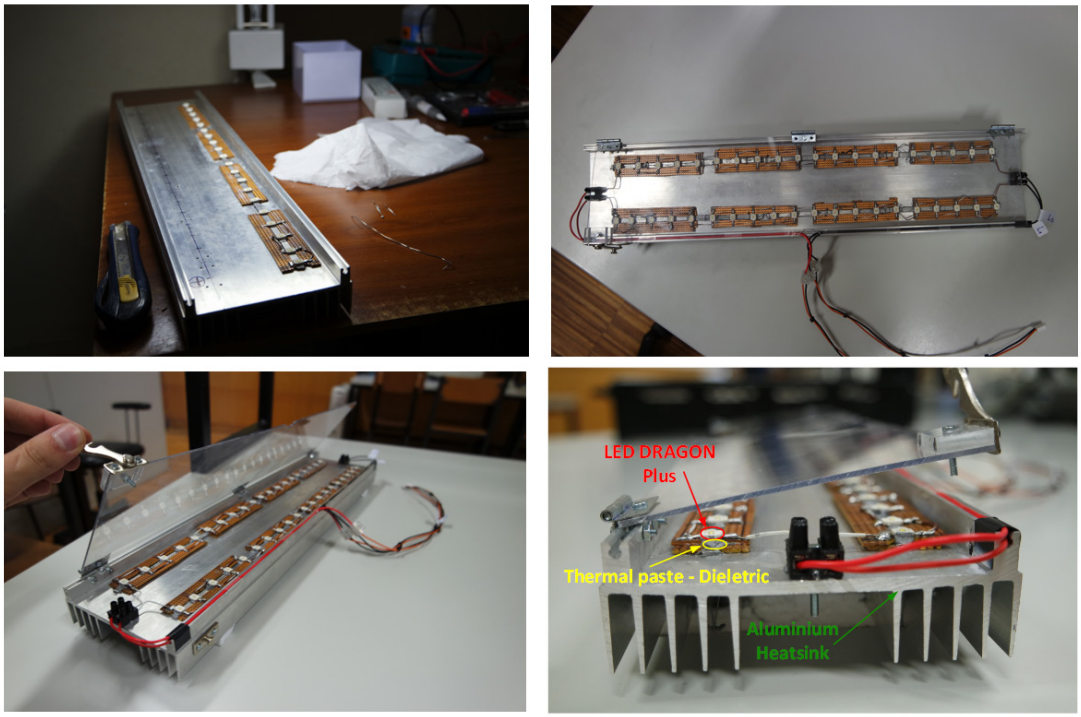

Table J - LEDs lamp prototype

To have a brief idea about the thermal operation of the LEDs and the heatsink, some tests using a thermal imaging camera were taken and can be seen below:

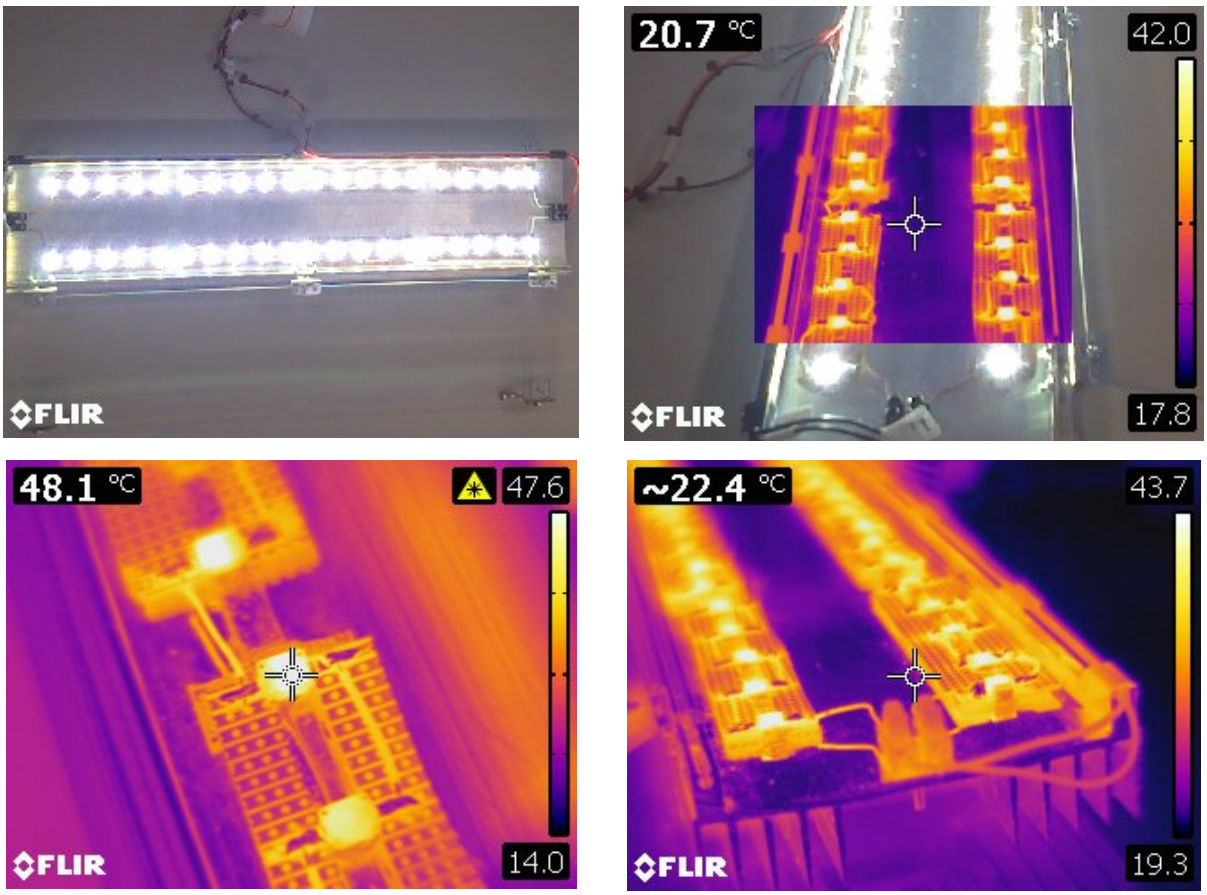

Fig. C. 2 - LED lamp thermal analysis

Nevertheless, it is not clearly visible the real temperature of the polished aluminium heatsink used. This is due to the difficulty in adjusting the emissivity coefficient with the camera in order to overcome a common issue related to measuring temperature of polished aluminium surfaces (such surface behaves like a temperature mirror). Therefore, for future work the same test will be done but with the support of an additional thermo couple to measure directly the temperature of the heatsink.

C.2 – Variable Inductors Construction

Two VIs were built using EFD 25 cores with N87 material from Siemens. In order to get a properly assembly of the windings in the cores a device was built, to serve as a coil winder, using a few plastic sheaves, a small DC motor and a few extra materials. The coil winder built is shown below:

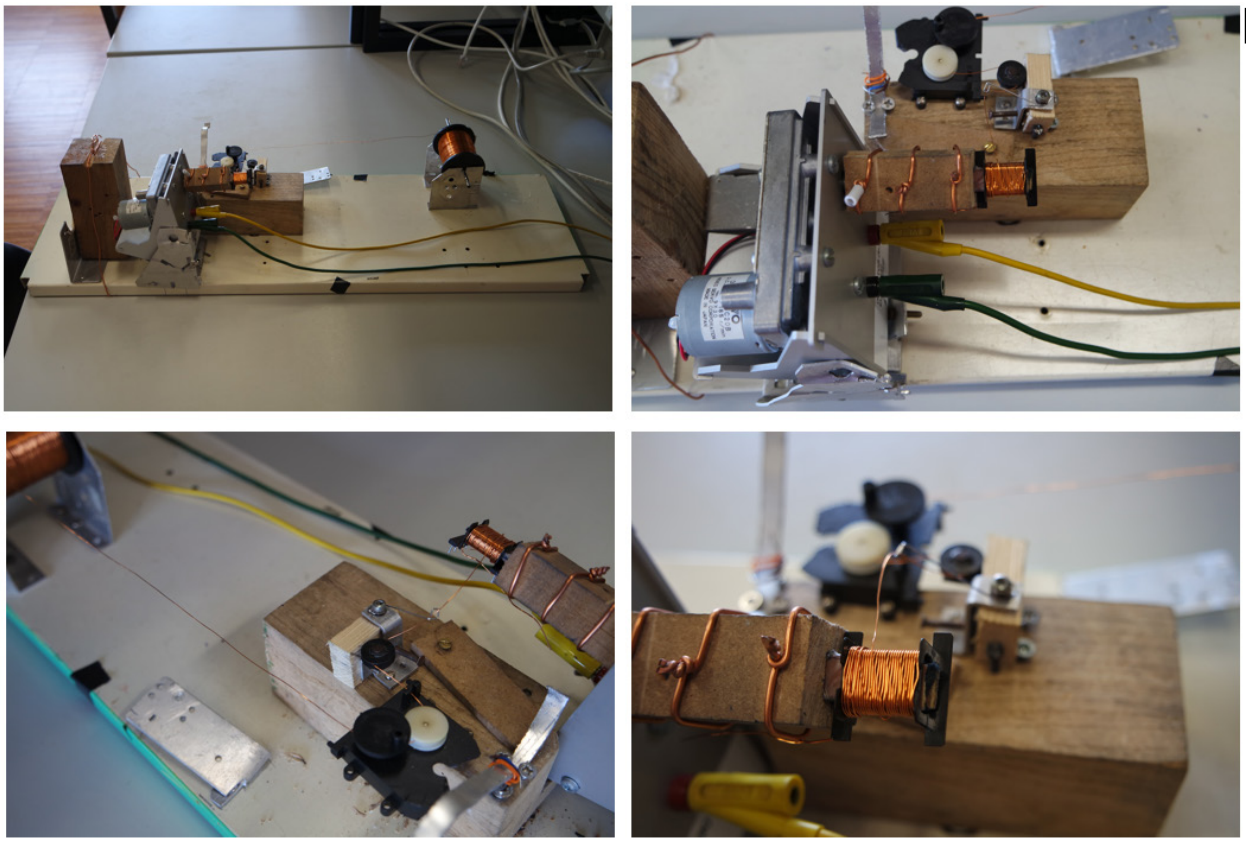

Fig. C. 3 - Coil winder prototype

For the AC winding a coil former, from the cores manufacturer was used. This coil former, for which the AC winding is placed around, as well as the rest of materials needed to assemble the variable inductor, are shown in the following two figures:

Fig. C. 4 - EFD 25 coil former

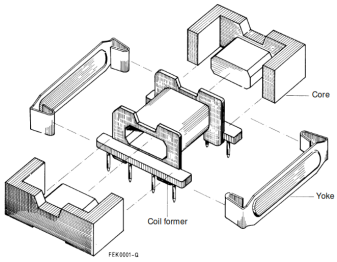

Fig. C. 5 – Core forming pieces provided by the core's manufacturer

For the control windings there is no coil former provided by any manufacturer, and therefore, for each control winding, a tiny coil former prototype had also to be built manually. This coil former was made using thin plastic sheets and glue and it is shown below:

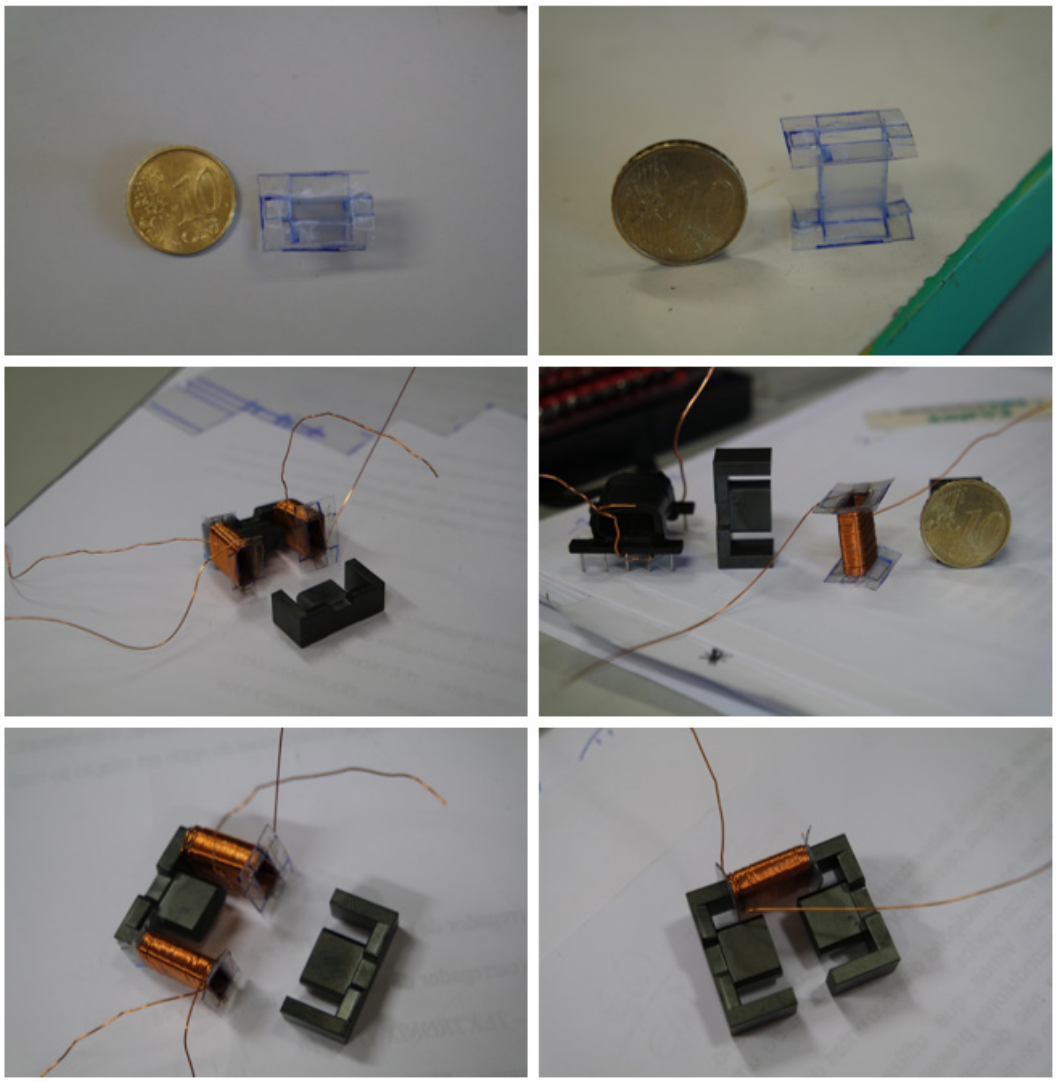

Fig. C. 6 - Control windings coil formers

After assembling all the pieces together the VI prototypes were concluded and a few pictures of them are presented as follows:

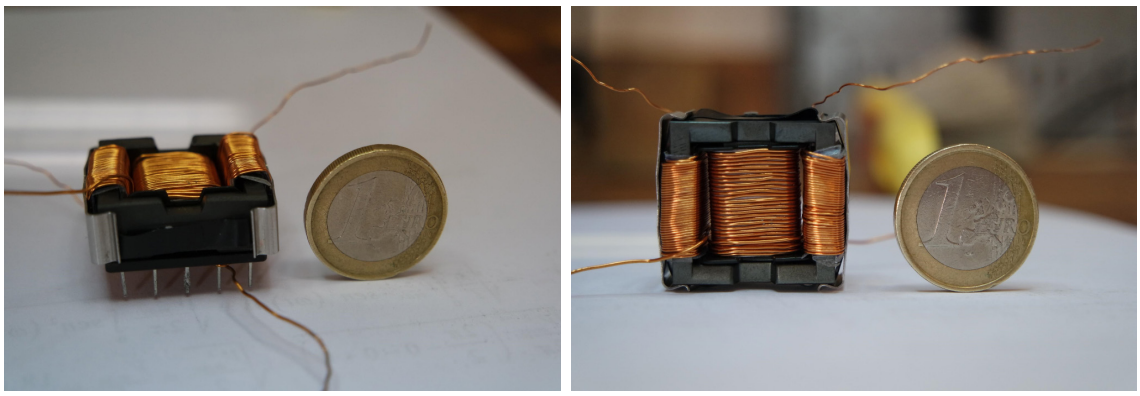

Fig. C. 7 - Variable Inductor prototype built

Relevant data regarding characteristics of the VI's windings are shown in Table K which is presented in next section.

C.3 – Driver Construction

Power Circuit – Components Selection

The components of the power circuit, shown in Fig. C. 8, were selected based in the maximum voltage or current they will have to sustain and on the laboratory availability. From the theoretical analysis of the converter addressed in section 4.3.1 both power Mosfets M_1 and M_2 and both diodes D_1 and D_2, will have to sustain the maximum value of the resonant current flowing through the resonant tank which can be obtained using the equation (4.21), recalled as follows:

$$I_{r_{\max}} = 4 \cdot I_{LEDs} \tag{6.23}$$

Using the previous equation and the maximum expected value of the LEDs average current of 0.35 A, then the maximum value that both Mosfets and Diodes have to support equals 1.4 A (4*0.35 A). From a simple circuit analysis, Mosfets have to sustain the value of the 48 V DC input voltage, so the commercial Mosfets IRF520 was selected. Regarding diodes once again, from the circuit analysis it is shown that they have to sustain a voltage value corresponding to V_{in}-V_{LEDs}. Therefore, considering the maximum output voltage to be the nominal lamp voltage of 64 V the diode will have to sustain 16 V (48-64 V). Subsequently, based on the previous conditions, the diodes D_1 and D_2 selected were Hyper-Fast Diodes BYC5D-500. These diodes have good performance characteristics so to avoid any slow reverse recovery time. The resonant and output capacitors of 0.47 µF and 10 µF, respectively, were selected to be film capacitors, due to their low ESR and high lifespan.

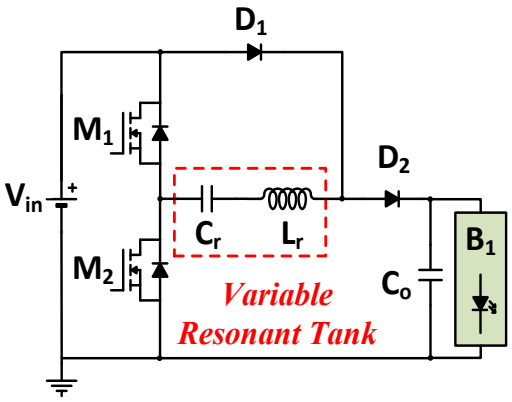

Fig. C. 8 - RSCC - Power Circuit

Mosfets Control – Design Procedure

The Mosfets control was provided by the IC[12] IR2153D using the following schematic:

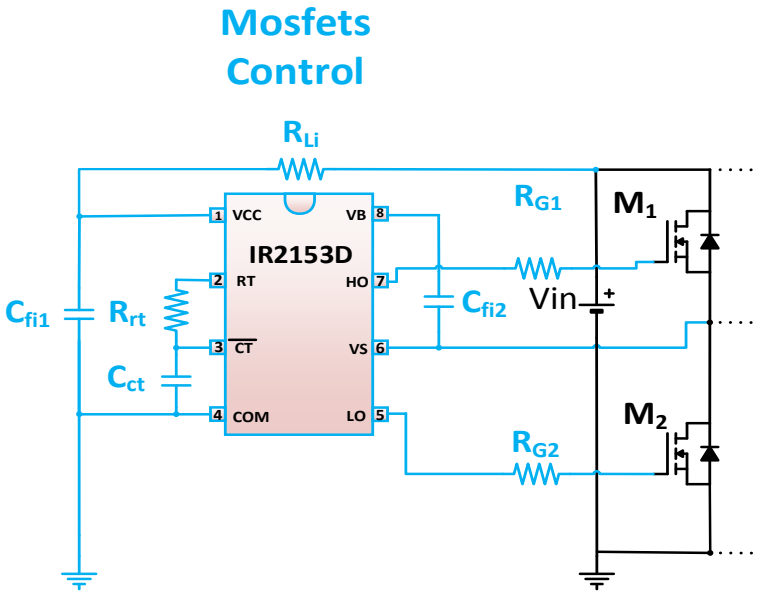

Fig. C. 9 - Mosfets Control

The IC IR2153D sets automatically an alternated 50% duty-cycle for each Mosfet switch and as a protection measure it ensures that both switches are never on the same state, i.e. ON state. Another advantage of this IC is that it does not require an external input low voltage source, i.e. 15 V input voltage, thus its V_{cc} pin (supply voltage pin) is directly connected, through the resistor R_{Li}, to the in voltage of the converter V_{in} (48 V). The resistor R_{Li} is responsible for limiting the input current supplied to the IC, which according to the manufacturer's datasheet is recommended to be 5 mA [136], thus its value can be calculated as follows:

[12] ***IC*** *– Integrated circuit*

$$R_{Li} = \frac{V_{in}}{I_{\text{supply}_{max}}} = \frac{48}{5*10^{-3}} = 9.6k\Omega \tag{6.24}$$

The capacitors C_{fi1} C_{fi2} were selected to have the commercial value of $1uF$ so to maintain a good voltage average level with low ripple for both IC supply voltage V_{cc} and high side floating supply voltage V_{BS}.

The timing resistor and capacitor, R_{rt} and C_{ct} were selected to provide the required oscillator frequency (switching frequency) which can be determined from the following equation and chart [136, 137]:

$$fs = \frac{1}{1.3863 * R_{rt} * C_{ct}} \tag{6.25}$$

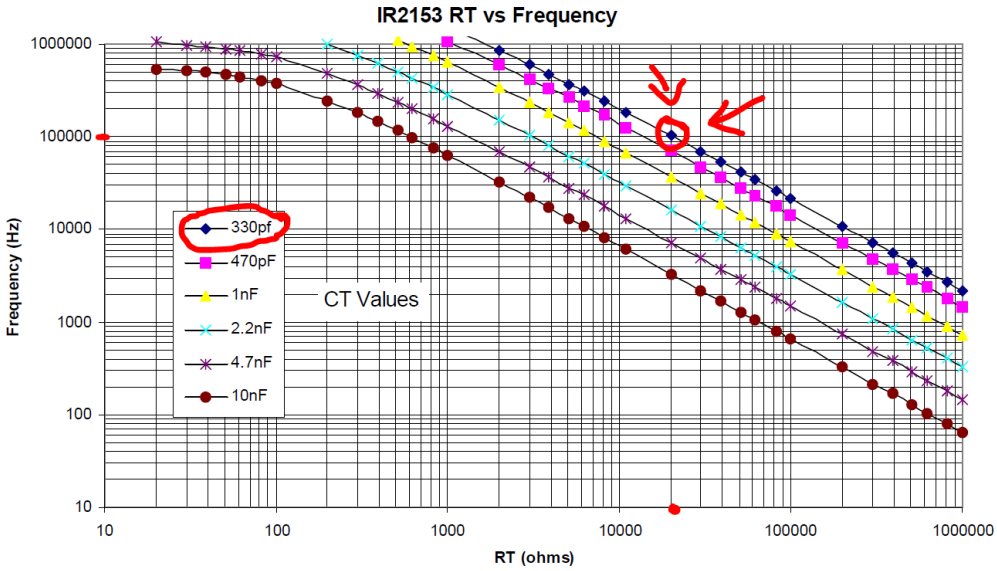

Fig. C. 10 - Timing resistor vs Frequency, adapted from [136]

The commercial value of 330 pF was selected for the timing capacitor. To obtain the required switching frequency of 100 kHz, one still needs to determine the value of the timing resistor, which was obtained from the previous equation and chart and equals 21,86 kΩ. A variable resistor was used to provide the required timing resistor. At last, the gate resistances R_{G1} and R_{G2} were selected to be 30 Ω, so to maintain a low amplitude of the negative voltage spikes that may appear on the V_s pin of the IR2153D [138].

Bias Winding Control

As mentioned and introduced in section 4.3.4, the output current control of the converter was provided through the control of the bias winding of the VI using the hardware and analogic controller proposed in [82]. The components used to assemble this controller, and the controller itself, are shown as follows:

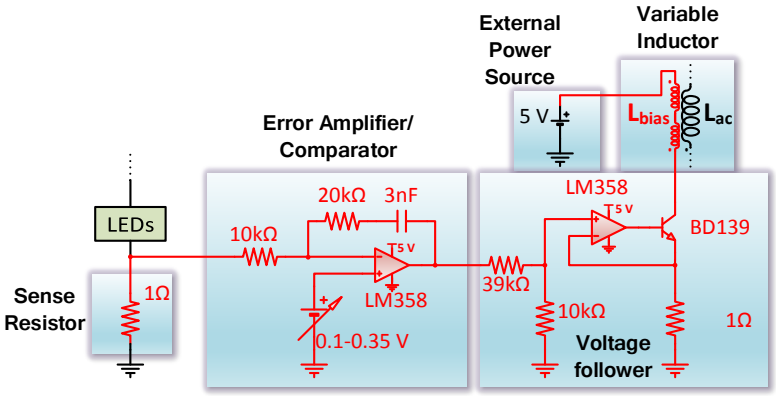

Fig. C. 11 - Voltage-controlled current source

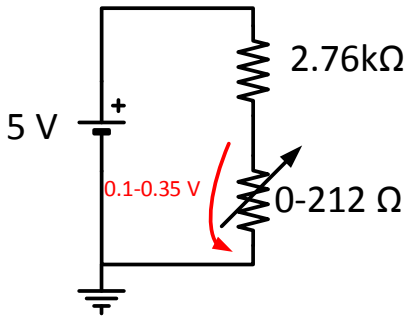

Fig. C. 12 - Current reference actuator

The output current reference, in the range of 100 mA to 350 mA, was generated using the circuit shown in Fig. C. 12.

The RSCC prototype was built on a perfboard, is shown and described below:

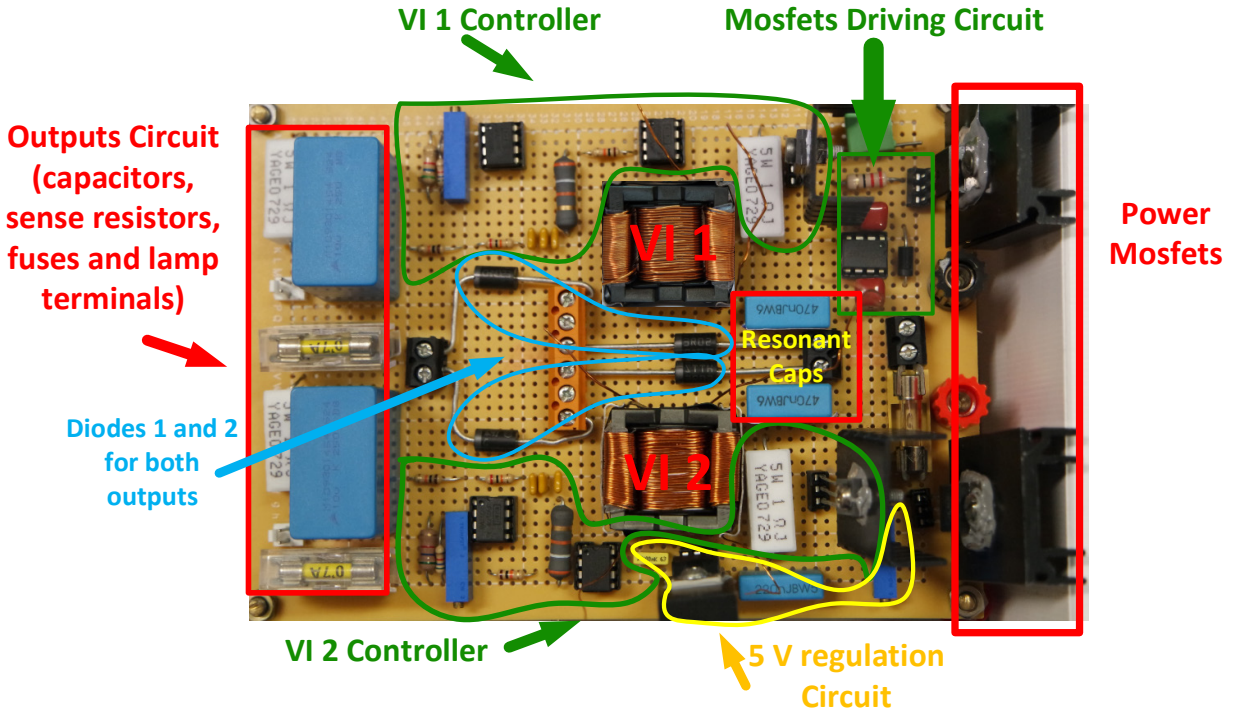

Fig. C. 13 - RSCC - Practical prototype implemented

C.3.1 – Final Assembly and Experimental Results

After assembling all parts, the experimental tests were carried out using an experimental setup as shown below:

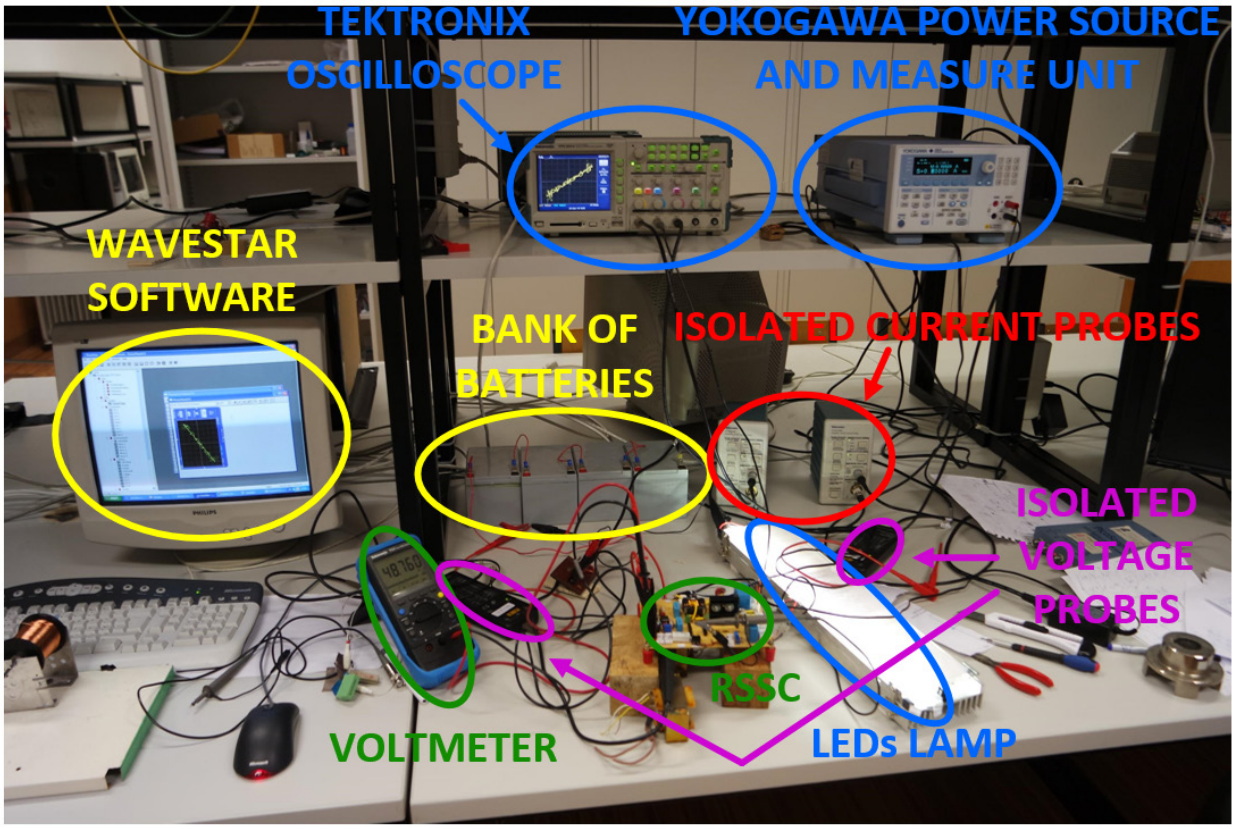

Fig. C. 14 - Final assembly and experimental tests setup

Several components and parameters have already been introduced, nevertheless in the following table are resumed the most relevant:

Table K –Prototype main parameters and components

Description	Specification
Input Voltage	$V_{in} = 48$ V
Switching frequency	100 kHz
Duty cycle	0.5
Switches	MOSFET IRF520, 9.2 A, 100 V, 0.27 Ω, N-channel
Diodes	BYC5D 500, 5 A, 500V
Resonant Capacitor	$C_r = 0.47$ µF, 100 V, film capacitor
Variable Inductor	$L_r = 40$ µH ~ 140 µH, $N_{ac} = 35$ turns, $0.63\ mm, R_{ac}\ at\ 100\ kHz \approx 0.3\ \Omega$ $N_{dc} = 2 * 71$ turns, $0.315\ mm, R_{dc}\ at\ 100\ kHz \approx$ 1.29 Ω EFD 25/13/9 - air gap $= 0{,}3 * 2\ mm$
Output Capacitor	$C_o = 10$ µF, 250 V, film capacitor
LED Branches (B_1)	2x20 Golden Dragon Plus 3.2 V, 350 mA, 5000 k,

Complementary experimental waveforms

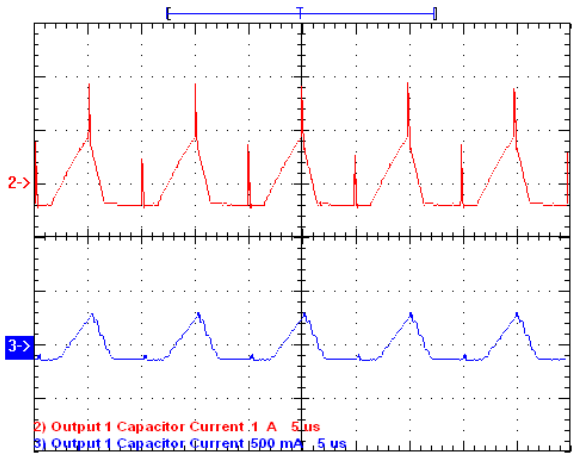

Fig. C. 15 – Output capacitor 1 current, at maximum dimming level and minimum dimming level, respectively, ch.2-1 A/div and ch.3-0.5 A/div respectively, 2.5 µs/div

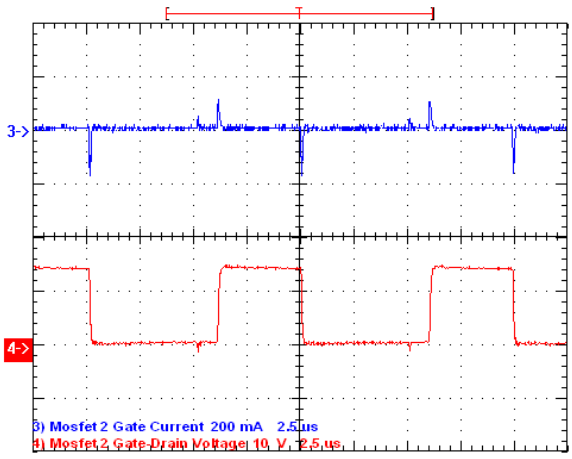

Fig. C. 16 - Mosfet 2 gate current and gate-source voltage, ch.3-200 mA/div and ch.4-10 V/div, respectively, 2.5 µs/div

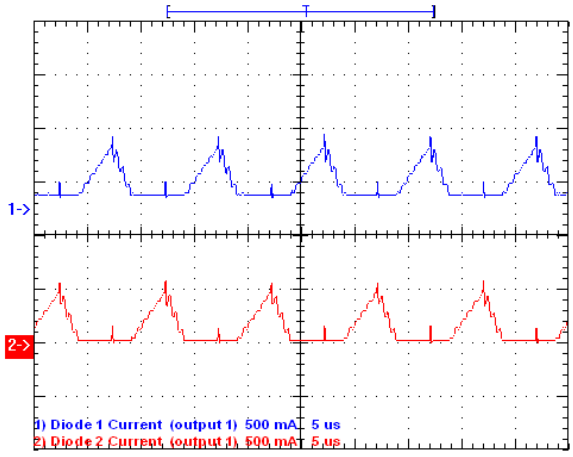

Fig. C. 17 – Diodes 1 and 2 current at minimum diming level conditions, blue and red curves, respectively, 0.5 A/div, 5 µs/div

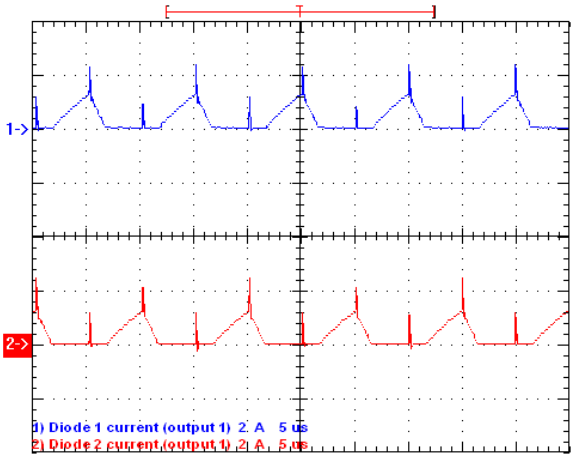

Fig. C. 18 - Diodes 1 and 2 current at maximum diming level conditions, blue and red curves, respectively, 0.5 A/div, 5 µs/div

C.4 – Lamp Illuminance Measurement

In order to estimate the luminous flux emitted by the LED lamp, which is required to confirm and validate the proposed dimming technique, an integrating sphere[13] should be used, however this device was not available in the laboratory, and thereby, a similar device for the same purpose, was built. It consists on a cubic box, in which its interior surface is coated with white

[13] ***Integrating Sphere*** *– is a device typically used for optical power measurement*

paper, fully isolated from external light sources and with a small orifice to house a lux meter photocell. The built prototype, an "integrating cube", is shown below:

Fig. C. 19 - "Integrating cube"

Fig. C. 20 - Lux meter LX-101[14]

The "integrating cube" is by no means a perfect replacement of the integrating sphere. Nevertheless, it was decided to build and use it because its main purpose is to account for the relative changes in the luminous flux emitted and not to particularly find the exact values of the luminous flux. In fact, luminous flux was not directly measured, instead it was measured the illuminance, with the lux meter shown in the previous figure.

[14] *This **lux meter** was lent for this work by courtesy of the professor Humberto Jorge by the "Laboratório de Gestão de Energia" of the Electrical and Computers Engineering Department from University of Coimbra*

As known, illuminance equals the luminous flux on a surface per unit area, i.e. lm/m^2. Therefore, assuming (with only little error possibility) that, for LEDs nominal current value, the luminous flux value is the one given by the manufacturer's datasheet a relation, C_i, which is constant and equals the equivalent surface area, between illuminance (E_v) and luminous flux (ϕ_v) can be obtained using the following equation:

$$C_i = \frac{E_v}{\phi_v} = \frac{8280[lux]}{101[lm] \cdot 40[LEDs]} = 2.0495 \tag{6.26}$$

where 8280 [*lux*] is the total illuminance measured with the lux meter at nominal lamp operation, 101 [*lm*] is the luminous flux value given by the manufacturer for a single LED at nominal conditions and 40 is the total LEDs number of the lamp. The results obtained (input power and illuminance) and calculated (luminous flux) are shown in the following table:

Average Lamp Input Power [W]	Illuminance [lux]	Luminous Flux [lm]
13,564	3240	1581
15,262	3600	1757
17,153	3960	1932
18,892	4220	2059
20,733	4540	2215
22,666	4840	2362
24,354	5150	2513
26,330	5460	2664
28,208	5760	2810
30,082	6040	2947
32,045	6300	3074
33,915	6540	3191
35,388	6800	3318
37,250	7040	3435
38,954	7260	3542
40,961	7500	3659
42,812	7680	3747
44,457	7920	3864
46,108	8080	3942
48,094	8280	4040

Appendix D – Fundamentals of Electromagnetism

Fundamentals of electromagnetism may be introduced by, at first, by invoking the Gauss's Law in its general form: this law states that the value (scalar) of the magnetic flux ϕ which crosses a surface S is related to the magnetic flux density as follows:

$$\phi = \int_s \vec{B} \cdot d\vec{S} \tag{6.27}$$

where the vector $\vec{B}$ is the surface density of the magnetic flux and $d\vec{S}$ is the area element or vector with the direction normal to the surface element dS and magnitude equal to the area of dS. In the case where the flux density is uniform and perpendicular to the whole surface area A, the relation (6.27) may be rewritten as follows:

$$\phi = BA \tag{6.28}$$

where B is the magnetic flux density. The next step is to relate linkage flux Ψ with the magnetic flux density. To do so we shall recall the *Faraday's Law*: a variable in time magnetic flux $\phi(t)$ crossing a winding, composed by a closed loop of wire, induces an inductive voltage[15] $v_i(t)$ in that wire and can be stated as follows:

$$v_i(t) = \frac{d\phi(t)}{dt} \tag{6.29}$$

If such winding has multiple and identical N turns, and if the flux varies at the same rate through each turn, the concept of total *flux linkage* Ψ shall be used. Basically, the flux linkage is N times larger than the flux crossing a single turn of the winding:

$$\Psi = N\phi \tag{6.30}$$

so the expression (6.29) may be redefined as follows:

$$v_i(t) = N\frac{d\phi(t)}{dt} = \frac{d\Psi(t)}{dt} \tag{6.31}$$

It's important to notice that in the previous equation the DC resistance of the winding is neglected, otherwise the sum of the term $R \cdot i(t)$ would have to be included in the right side of the equation.

---

[15] *The **inductive induced voltage** v_i is typically represented in literature by the symbol $\mathcal{E}$ preceded by a minus sign*

In terms of magnetic field intensity H, we shall introduce it by recalling Ampere's law in its general form: for any winding composed of a closed loop path with length l, the sum (integral) of the length elements times the magnetic field intensity vector equals the total current i flowing through that path times the number of turns N of the winding:

$$\oint_l \vec{H} \cdot d\vec{l} = Ni \tag{6.32}$$

Note that each term of the previous definition is equivalent to a source called magnetomotive force $\mathcal{F}$ (*mmf*). Another common way to state Ampere's law is as follows:

$$\oint_l \vec{B} \cdot d\vec{l} = \mu i \tag{6.33}$$

where μ is the permeability of the material/medium. Rearranging the equations (6.32) and (6.33) one may find the relation between B and H which results in the following equation:

$$B = \mu H \tag{6.34}$$

The flux produced in a magnetic medium/material by a *mmf* depends, of course, on the material's resistance which is so-called *reluctance,* $\mathcal{R}$ (the inverse of reluctance is called *permeance* $\mathcal{P}$). Essentially reluctance is a magnetic impedance, namely a measure of the opposition to flux within any region of a magnetic device. The mathematical and general definition of reluctance, considering a homogeneous material maybe be derived from the magnetomotive force definition as follows:

$$\mathcal{R} = \frac{\mathcal{F}}{\phi} = \frac{Hl}{BA} = \frac{l}{\mu A} \tag{6.35}$$

where l and A are the magnetic path length and constant cross-section of the material, respectively, and μ the permeability of the material. A simple look at the previous *reluctance* definition shows that this parameter is highly dependent on the type of the material and its shape/dimension.

Taking into account the equations (6.28), (6.34) and (6.35) the equation (3.1) may be easily rewritten as follows:

$$L = \frac{N^2}{\mathcal{R}} \tag{6.36}$$